TRAPPING INTERNAL WATER CLUSTERS AND HYDROGEN-BONDING NETWORKS IN PHOTOSYNTHETIC OXYGEN EVOLUTION

A Dissertation
Presented to
The Academic Faculty

by

Zhanjun Guo

In Partial Fulfillment
of the Requirements for the Degree
Doctor of Philosophy in the
School of Chemistry and Biochemistry

Georgia Institute of Technology
May 2018

TRAPPING INTERNAL WATER CLUSTERS AND HYDROGEN-BONDING NETWORKS IN PHOTOSYNTHETIC OXYGEN EVOLUTION

Approved by:

Dr. Bridgette A. Barry, Advisor
School of Chemistry and Biochemistry
Georgia Institute of Technology

Dr. Adegboyega K. Oyelere
School of Chemistry and Biochemistry
Georgia Institute of Technology

Dr. Raquel L. Lieberman
School of Chemistry and Biochemistry
Georgia Institute of Technology

Dr. Ingeborg Schmidt-Krey
School of Biology
Georgia Institute of Technology

Dr. Wendy L. Kelly
School of Chemistry and Biochemistry
Georgia Institute of Technology

Date Approved: Jan 3rd, 2018

ACKNOWLEDGEMENTS

I wish to thank all people who helped me during this Ph.D. process. Without their supports, I couldn't complete the program. I want to thank Dr. Bridgette A. Barry, my academic advisor, for her support and guidance through all those years. The Ph.D. training under her supervision makes me not only a better scientist, but also a better person. I want to thank my thesis committee members: Dr. Raquel L. Lieberman, Dr. Wendy L. Kelly, Dr. Adegboyega K. Oyelere and Dr. Ingeborg Schmidt-Krey, for all their supports and valuable comments and inputs during this journey. I would like to thank Dr. Mary E. Peek for her care and inspiration during the biochemistry laboratory courses. From her, I learned the biochemistry expertise outside my research fields to broaden my spectrum of skills. I want to thank Dr. Tina Dorr for BBY purification training; Dr. Adam Offenbacher for OTG-PSII purification training; Dr. Cynthia Pagba for laser alignment; Dr. James Keough for guidance with cyanobacteria purification and EPR and Dr. Brandon Polander for help with IR setup. I would like to thank Professor Barry's group member: Dr. Jiafeng Geng, Atlee Watson, Udita Brahmachari, Tyler McCaslin, Yusuf Uddin, Jiayuan He, Chichi Obi and Sara Konecny for their helps and useful comments on the projects. Especially thank to Udita Brahmachari for all the weekend hard-works, supports for the difficult situations and scientific (non-scientific) discussions. I would like to acknowledge my friends, Rui Chen, Dr. Siyuan Zhang, Xuejiao Lin, Dr. Jige Quan, Hongduo Zhou, Shuai Zhi, Dr. Dongchang Chen, Dr. Xuefeng Wang and others, for all the supports during this wonderful journey. Especially I want to thank Rui Chen for all the advices and supports that helps me through thick and thin. Last but not the least, I want to thank my sister Lijun Guo, brother-in-law

Xiaoshu Wang and my parents Shuzhen Ge and Liangqi Guo for all their love and supports during all those years. Without their supports, I wouldn't even be able to start my scientific career.

Any omission in this acknowledgment does not constitute a lack of gratitude.

TABLE OF CONTENTS

LIST OF TABLES

LIST OF FIGURES

LIST OF SYMBOLS AND ABBREVIATIONS

Å	angstrom
Abs	absorbance
ATP	adenosine triphosphate
AU	absorbance units
Ba PSII	barium reconstituted photosystem II
Ca PSII	calcium reconstituted photosystem II
CD PSII	calcium depleted photosystem II
Chl *a*	chlorophyll *a*
DD	double difference
DCBQ	2,6-dichloro-1,4-benzoquinone
DFT	density functional theory
EPR	electron paramagnetic resonance
E. coli	*Escherichia coli*
ENDOR	electron nuclear double resonance
HEPES	4-(2-hydroxyethyl)-1-piperazineethanesulfonic acid
FTIR	Fourier transform infrared
MES	2-(*N*-morpholino) ethanesulfonic acid
Mg PSII	magnesium reconstituted photosystem II
OEC	oxygen-evolving complex
OTG	*n*-octyl-beta-D-thioglucoside
Pheo *a*	pheophytin *a*

PSII	photosystem II
Q_A	plastoquinone acceptor (bound)
Q_B	plastoquinone acceptor (mobile)
QM/MM	quantum mechanical/molecular mechanical
SDS-PAGE	sodium dodecyl sulfate polyacrylamide gel electrophoresis
Sr PSII	strontium reconstituted photosystem II
T. elongatus	*Thermosynechococcus elongatus*
UV	ultraviolet
V	volt
XANES	X-ray absorption near edge spectroscopy
Y_D	tyrosine 160 of the D2 polypeptide
Y_Z	tyrosine 161 of the D1 polypeptide

Additional abbreviations are explained in the text.

CHAPTER 1. INTRODUCTION

1.1 Internal Water Cluster in Biological System

Proton transfer in aqueous environment has been the subject of numerous theoretical and experimental studies, since van Grotthus first proposed a proton-hopping mechanism.[1-3] The proton binds to a water molecule or delocalizes between several waters during the transfer process. Proton transfer plays an important catalyzing role during numerous reactions.

Unlike liquid water, proteins require well-organized structures, such as hydrogen-bonded networks of amino acid side chains and internal water, to quickly transfer protons, and eventually conduct reactions efficiently. Internal water has been shown to play either structural or functional roles in several enzymes. One of its important functional roles is to assist in the quick release of proton by acting either as proton acceptor or donor in membrane proteins, such as bacteriorhodopsin,[4-5] cytochrome c oxidase,[6-7] carbonic anhydrase,[8] and photosystem II[9-11].

Among various enzymes, bacteriorhodopsin provides an excellent model to investigate the function of internal water. Bacteriorhodopsin, a seven α-helical membrane protein, performs a photo-driven proton pump cycle.[5] High resolution crystal structure of bacteriorhodopsin and models based on this structure have identified several important water clusters functioning as proton acceptors and donors through the proton-pumping cycle (Figure 1.1A).[12] During the process, absorption of photon leads to protein conformational changes leading to proton transfer from one side of the protein to the other

via a well-ordered network of amino acid side chains and internal water clusters (Figure 1.1B). Various experimental methods including reaction induced FT-IR transient spectroscopy have been applied successfully to show involvement of internal water cluster during the proton transfer cycle.[13]

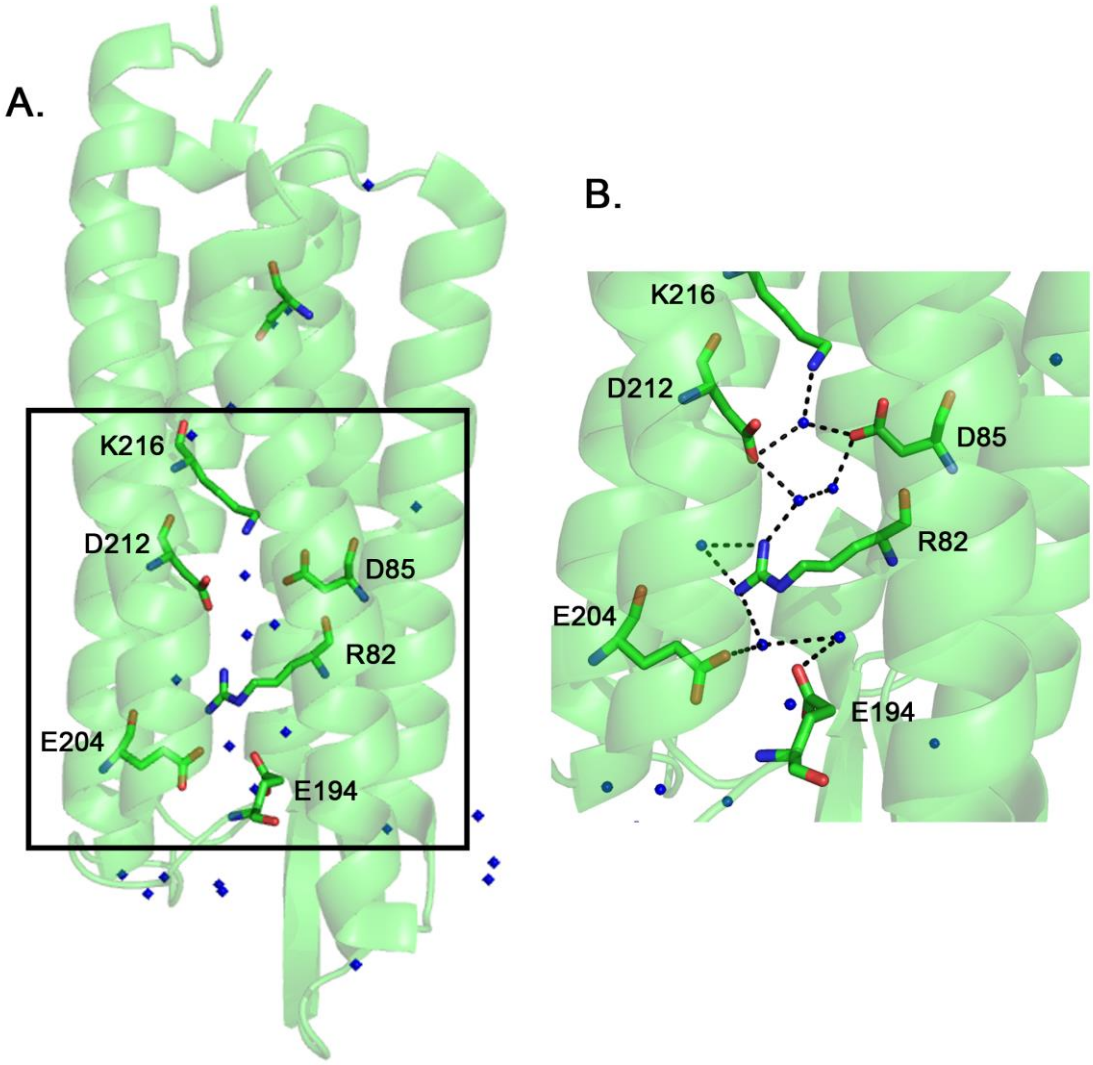

Figure 1.1 Proton transfer pathway in bacteriorhodopsin. (A) overview of bacteriorhodopsin structure, only important residues involved in proton pathway is shown. Blue sphere depicts water molecule. (B) zoomed view of proton transfer pathway involving amino acid sidechains and internal water clusters (black box region in (A)). PDB ID: 1C3W.[12] The figure was created using PyMol.

1.2 Photosynthesis

Photosynthesis is one of the most important reactions on earth. Through this reaction process, solar energy is used to reduce CO_2 and oxidize H_2O to yield carbohydrate and O_2 respectively by algae, green plant and cyanobacteria.[14] During the light reaction, the electrons generated from the water oxidation reaction are utilized to produce nicotinamide adenine dinucleotide phosphate(NADPH). A transmembrane proton gradient also develops during this reaction. These protons are ultimately used to generate adenosine triphosphate (ATP). The ATP and NADPH thereby generated are utilized during the Calvin cycle, also referred as the dark reaction, to produce carbohydrates.[14]

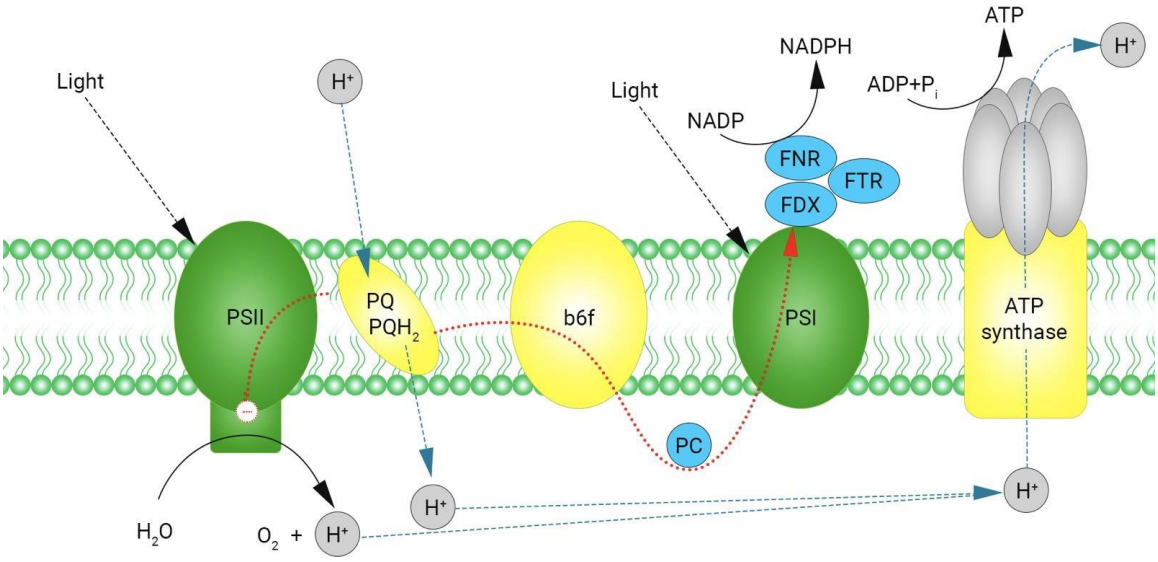

Figure 1.2 Schematic representation of the thylakoid membrane components: Photosystem II (PSII), Cytochrome b6f, Photosystem I (PSI), Protein translocating ATP synthase.[15] The blue dashed line shows the proton movement and the red shows the electron movement. Picture credit to Rui Chen.

In cyanobacterial cell, the reaction occours in the inner plasma membrane. In green plants, the site of photosynthesis is the chloroplast. Within the chloroplast, there are stacks of disclike sacs named thylakoids, which contain the enzyme required for oxygen

evolution.[16] The thylakoid membranes of cyanobacteria are more homogeneous compared to higher plants.[15] The light-driven process utilizes four multisubunit membrane- protein complexes: Photosystem II (PSII), Cytochrome b_6f, Photosytem I (PSI), and Protein translocating ATP synthase; shown in Figure 1.2.[15] After absorbing four photons of light, PSII oxidizes two molecules of water to generate oxygen and four protons are released to the lumen side. On the stroma side, two molecules of plastoquinone (PQ) are reduced to plastoquinol (PQH_2).[17-18] The PQH_2 migrates to cytochrome b_6f where it re-oxided to PQ through the reduction of plastocyanin (PC).[18] The electrons are transferred to light-excited PSI through PC.[17] Subsequently, ferredoxin is reduced by photo-exicted PSI and binds to ferredoxin:$NADP^+$ reductase (FNR) to generate NADPH from $NADP^+$.

1.3 Photosystem II

Photosystem II (PSII) is the site of photosynthetic oxidation of water and contains 17 transmembrane subunits and 3 extrinsic subunits. The structure of PSII was first revealed in studies of crystals using X-ray crystallography.[19] Studies using a X-ray laser have yielded "damage-free" crystallographic information.[20] Structures of spinach PSII are now available, as derived from cryo-electron microscopy.[21] There are four integral intrisinc subunits: CP43 and CP47, which are the chlorophyll binding proteins, and D1 and D2, which holds the redox active cofactors required for photo-induced water oxidation.[19-20] Other extrinsic polypetides, such as PsbO, PsbP and PsbQ, are also required for optimal oxygen evolution activity under physiological condition.[22] Removal of the PsbO subunit using $CaCl_2$ or urea treatment lowers the oxygen evolution activity, and high concentrations of Ca^{2+} and Cl^- are requried to restore the activity without rebinding the polypeptide.[23-27] In addition to these subunits, each monomer of In addition to these

subunits, each monomer of the enzyme also has 35 chlorophylls, 2 pheophytins, 11 β-carotenes, more than 20 lipids (Figure 1.3A).[20] During photosynethetic water oxidation, chlorophyll is excited by light. Following electron transfer to chlorophyl P680, the charge seperated state $P680^{+}$/ $Pheo^{-}$ is generated with the intermediate electron acceptor, pheophytin (Pheo). The $P680^{+}$/ $Pheo^{-}$ pair is quickly stablized by the reduction of $P680^{+}$ by Tyr161 of the D1 protein (Yz) and the oxidation of $Pheo^{-}$ by a quinone molecule (Q_A).[28] The oxidation of Yz generates a netural tyrosyl radical (Yz•), which is subsequentially reduced by the oxygen evolving complex (OEC) which contains a Mn_4CaO_5 cluster. Finally, Q_A is reduced by a second quinone molecule (Q_B). After two successive rounds of electron transfer along the reaction center, a doubly reduced plastoquinol (Q_B^{-2}) will be replaced by another fully oxidized quinone (Figure 1.3B).[29]

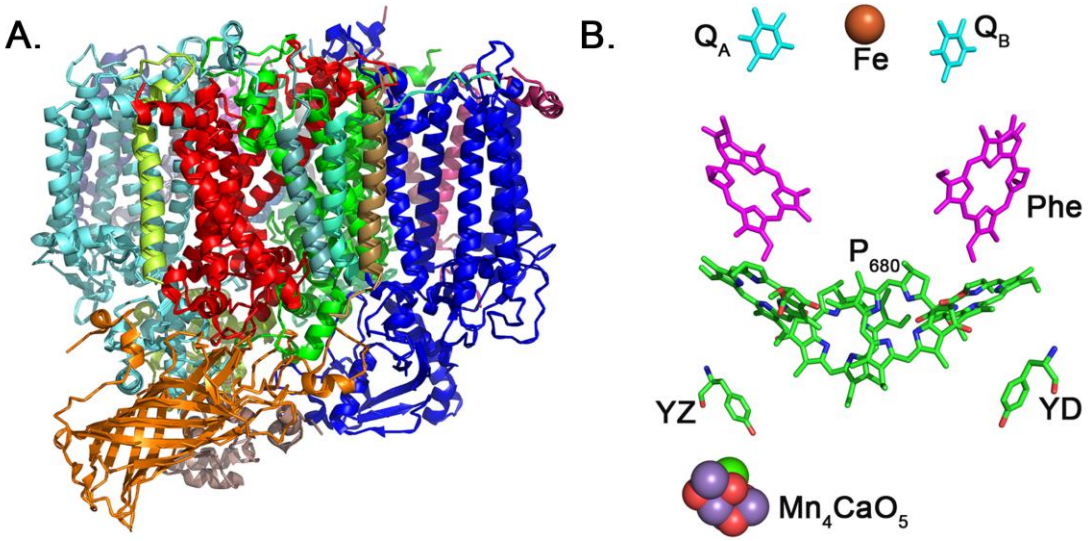

Figure 1.3 PSII and the redox active cofactors. (A) PSII structure, with subunits shown in different colors. D1 in red, D2 in green, CP43 in cyan, CP47 in blue and PsbO is shown in orange. PDB ID: 4UB6.[20] (B) PSII electron transfer pathway, In B, the phytyl tails are omitted. The figure was created using PyMol.

1.4 Oxygen Evovling Complex and S-state Transition

During photosynthetic water oxidation, the OEC (Figure 1.4A) oxidizes two molecules of water and generates four protons, four electrons and one molecule of oxygen. Within the processs, OEC cyles through 5 different oxidation states, named S_n states, where n= 0-4 (Figure 1.4B).[30] S_1 represents the dark- adapted state.[31-32] A single flash will advance S_1 to S_2 state, corresponding to the oxidation of one Mn (III) to Mn (IV) (see ref. 32, but also see ref. 33).[33-34] The second flahs advanes S_2 to S_3 state. Oxygen evolution occurrs during third flash accompanying the S_3 to $[S_4]$ to S_0 transition, where $[S_4]$ represents a transient intermediate state. Each S state transition has a temperature barrier.[35-36] Specifically, the S_1 to S_2 transition has a significantly lower temperature barrier compared to the other transitions. The half inhibition temperature for the S_1 to S_2 transition is 135 K. The S_2 to S_3, S_3 to S_0 and S_0 to S_1 transition barriers are 230 K, 235 K and 220 K, respectively.[36]

It has been proposed that in order for the water oxidation to be thermodynamically feasible, each S state transition will be coupled with a proton and electron release from the OEC.[37-38] Unlike other S state transitions, there is no net proton release detected in sucrose containing buffers during the S_1 to S_2 transition.[39] Recently, it has been proposed that internal water cluster acts as a proton acceptor and thereby forms a protonated water cluster at 190 K, 263 K and 283 K. This idea can effectively rationalize the failure to observe proton release during this transition (Figure 1.4B inset).[9-11]

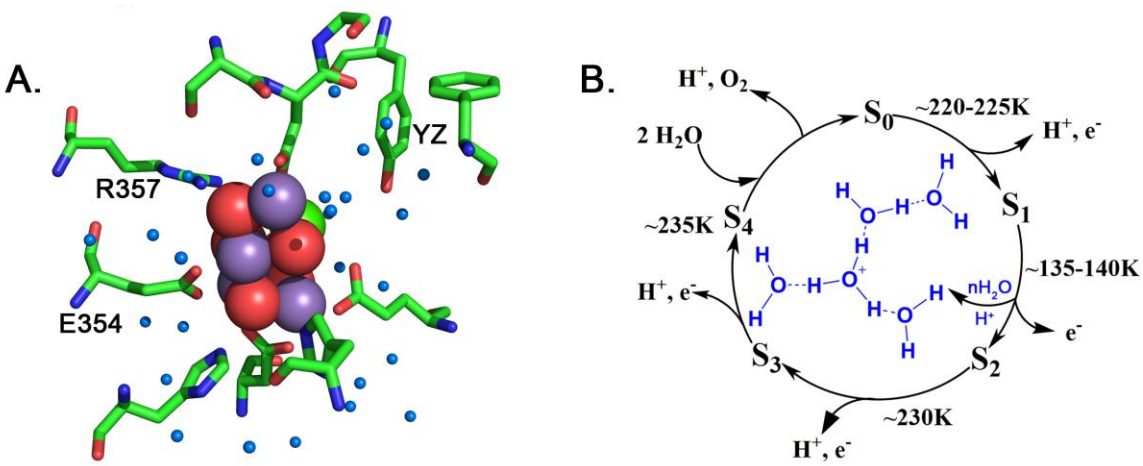

Figure 1.4 OEC and S-state cycle. (A) OEC and its ligand environment, PDB ID: 4UB6.[20] The figure was created using PyMol; (B) S-state cycle with half inhibition temperature and proton release pattern.[11] Protonation of a small water cluster during S_1 to S_2 transition is shown in inset. Manganese, purple; calcium, dark green; oxygen, red; water, blue.

The OEC contains one calcium which is essential for oxygen evolution. It has been proposed to bind and acitvate substrate water during the reaction process.[40-41] In the crystal structure, there are two water molecules bound to the calcium ion. Calcium can be removed and reconstituted back to restore the acitivity. Among various divalent ions, only strontium is able to reconstitute the oxygen evolving activity of PSII.[42] Removal of calcium or substitution of strontium doesn't have a significant impact on the local electronic structure of manganese ions.[43-44] Barium is an inhibitor of oxygen evolution activity.[45-46] Change of divalent ions from calcium to strontium/barium is expected to change the p*K*a of the bound waters[42], and consequently change the hydrogen-bonding interactions.[46]

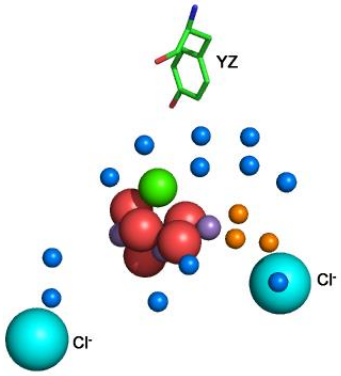

Figure 1.5 OEC and its local environment. Manganese, purple; calcium, dark green; oxygen, red; chloride, cyan; water, blue; proposed ammonia binding sites, orange. PDB ID: 4UB6.[20]

Ammonia is a substrate analog which effectively inhibits oxygen evolving activity. It is proposed to bind to two different locations, as assessed by different methods (Figure 1.5).[47-52] In one binding site of ammonia, it competes with chloride, an essential PSII cofactor. In the other binding site, ammonia competes with the substrate.[42] Ammonia is proposed to interrupt the hydrogen-bonding network around OEC.[11, 53] It has been shown that ammonia induce shifts in amide I carbonyl region of PSII, which is attributed to the weakening of hydrogen-bonding interaction.[53]

1.5 The S_2 State

The S_2 state has been extensively studies by various of experimental methods such as electron paramagnetic resonance (EPR), Fourier transform infra-red (FT-IR), UV-vis and X-ray absorption spectroscopies. Under native conditions, the EPR signal of S_2 state of spinach has two different forms: one multiline signal centered at g = 2 from a S_T = ½ form of OEC, which is the dominant signal of the two and the other signal centered at g = 4.1 from a S_T = $^5/_2$ form of OEC.[54-57] Different treatments, such as site-directed mutagensis,

calcium/strontium exchange, chloride anion exchange and cryo-protectant change, can shift the equilibrium in favor of one of these two forms.[57] Density functional theory (DFT) calculations, which incorporated the structural information from the high resolution crystal structures, have been applied to rationalize the spin isomers of S_2 state. According to the model, the two isomers are generated depending on which Mn is oxidized during the S_1 to S_2 transition (Figure 1.6).[58] The g = 2 signal originates from Mn4 being oxidized during the reaction, and the g = 4.1 signal from Mn1 being oxidized. The model has been compared to extended X-ray absorption fine structure (EXAFS) data. The differences between the Mn-Mn distances in EXAFS data has further proven the correlation of structural models with EPR data.[59] According to the quantum mechanics/ molecular mechanics (QM/MM) studies performed on the same structure models, the intercoversion of the two isoformers is thermodynamically allowed at room temperature. But it becomes very slow and almost negliglible at low temperature over the simulation time.[60]

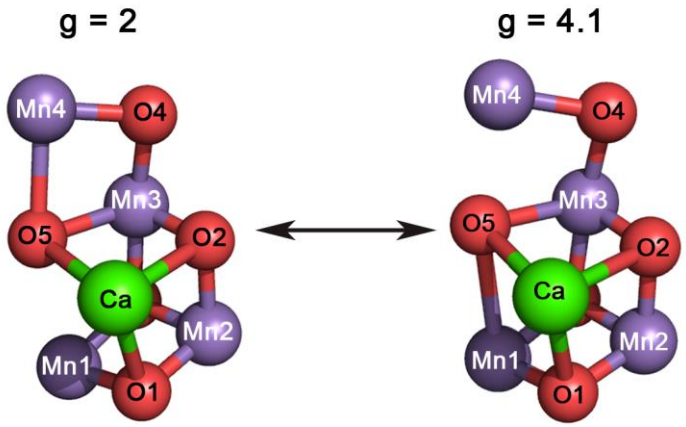

Figure 1.6 Schematic models for S_2 state spin isomers.[20, 58] PDB ID: 4UB6.[20] The figure was created using PyMol.

1.6 YZ and YD

YZ (D1-Y161) is an integral component for water oxidation. Following PSII's pseudo C2 symmetry, there is another redox-active tyrosine, YD (D2-Y160, Figure 1.3B), which is not required for photosynthetic water oxidation. YD is proposed to be important during the photoassembly of the OEC.[61] YZ and YD radical can be differentiated by their distinct lifetime and the microwave saturation properties. Solvent isotope exchange can also be used to distinguish between them. Differences in solvent isotope effect (SIE) has been attributed to different decay mechanisms of the tyrosyl radicals, i.e. YZ• decays with a pH-insensitive coupled electron and proton transfer (CPET) mechanism, while YD• decays via a proton first then electron transfer (PTET) pathway at low pH and CPET pathway at high pH.[62-65]

1.7 Electron Paramagnetic Resonance (EPR) Spectroscopy

EPR spectroscopy is a powerful technique to study unpaired electrons. In a system containing a single unpaired electron, the electron can exist in one of the two spin states with spin quantum numbers, +½ or -½, which will both have the same energy in the absence of an external magnetic field. When the magnetic field is applied, the energy levels will no longer degenerate and the difference in energy will be proportional to the strength of the magentic field (Equation 1.1).[66] In the equation, h is the Plank's constant; υ is the frequency; g is proportionality factor which is determined by the type of the magnetic center and its spin coupling parameters; β_e is the Bohr magneton and B_0 is the external magnetic field strength. The g-value is the slope of energy split. A free electron has a g-value of g_e = 2.002319.[67] The spin coupling between the electron and nuclei causes g-values of other radicals to deviate from that of the free electron. In addition to the g-value, the hyperfine interaction (A), which is determined by the interaction of the electron spin

with the nearby NMR active nuclei, is important for interpreting an EPR spectra. Both g-value and hyperfine coupling are dependent on the orientation.

Equation 1.1 $$\Delta E = h\upsilon = g\,\beta_e\,B_0 \quad (1)$$

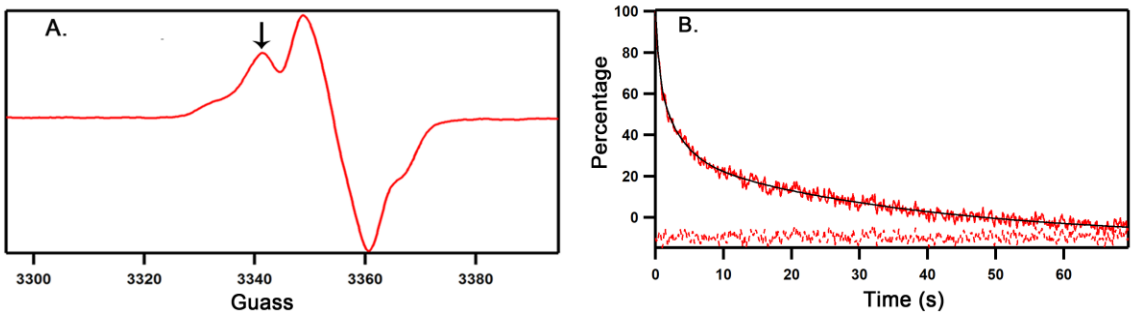

Figure 1.7 (A) EPR spectrum of $S_2YZ^{\bullet}$. Data were derived from Ca-PSII at pH 7.5 and 255 mM total chloride under continuous red illumination at 190 K. The g value is 2.004. The black arrow indicates the field position used to monitor $S_2YZ^{\bullet}$ decay kinetics in part B. (B) Transient $S_2YZ^{\bullet}$ kinetic data (red line) from the same condition as A, black line is the fitting and the bottom red dotted line is residual from the fitting. The transients were normalized to 100% at t = 0. In part A, the spectra were recorded with a microwave power of 0.639 mW. In part B, the microwave power was increased to 101.3 mW to saturate the $YD^{\bullet}$ signal.[46]

EPR spectroscopy has been extensively applied to study PSII.[68] The S_2 state multiline signal and its equilibrated g = 4.1 signal gives valuable insights into the OEC electronic structure in the early 1990s before the availability of the high resolution crystal structures.[54-55] Later, the similar multiline signal has been observed in the S_0 state. It provided evidence of the oxidation states sampled by OEC during the water oxidation reaction.[69] Conventional EPR spectroscopy is always accompanied by inhomogeneous broadening of the spectra. For this reason, other pulse and CW-EPR, such as electron spin echo envelope modulation (ESEEM) and electron nuclear double resonance spectroscopy (ENDOR), have been applied to study PSII.[47, 70] In addition to the EPR spectroscopic

investigation of the OEC, the technique has also been utilized to investigate the impact of S- state progression, local environment change and SIE on the tyrosyl radical decay process at cryogenic temperature (Figure 1.7).[46, 63-65]

1.8 Reaction Induced Fourier-Transform Infrared (RIFT-IR) Spectroscopy

Vibrational spectroscopy, such as infrared spectroscopy, probes the structural and environmental changes of functional groups. The frequency of vibration (υ) is determined by the reduced mass (μ), bond strength and bond angle (k, force constant) of the molecule (Equation 1.2) by the approximation of the classical harmonic oscillator. Molecules with more than two atoms have 3n – 6 vibrational modes (n is the number of the atoms in the molecule) and 3n – 5 modes if the molecule is linear.[71]

Equation 1.2

$$\upsilon = \frac{1}{2\pi}\sqrt{\frac{k}{\mu}} \qquad (2)$$

Due to the large number of overlapping vibrational modes, the IR spectrum of large biological molecules such as proteins will be extremely complex. In order to effectively interpret and assign such a complex vibrational spectrum, reaction-induced Fourier-transform infrared (RIFT-IR) spectroscopy can be utilized. The general principle is that the same sample will be used for two different states and the reaction is induced either electronically or photochemically. The two corresponding states will be ratioed to each other to get rid of the background from the protein, the difference spectrum will be the vibrational bands corresponding to the reaction-induced features (Figure 1.8). For the assignment of the bands, site-directed mutagenesis and isotopic labelling can be employed.

RIFT-IR has been applied to characterize the various proteins, such as bacteriorhodopsin, rhodopsin, phytochrome and photosystem II.[4, 72-73] PSII is an ideal system for the application of RIFT-IR since light absorption will drive the reaction.

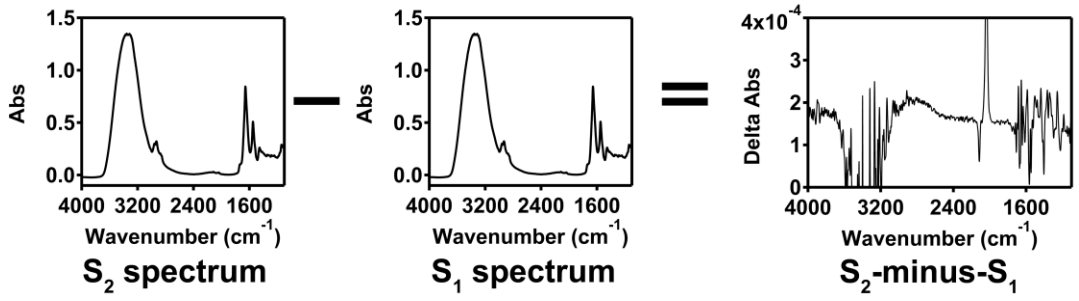

Figure 1.8 An example of RIFT-IR spectra, details could be found in ref [73].

1.9 Summary of the Thesis

Chapter 2 describes a cryogenic RIFT-IR study of internal water as a transient proton acceptor during the S_1 to S_2 transition in PSII. In this study, we have tested the hypothesis that the inability to observe proton release to bulk solvent in sucrose buffer during the S_1 to S_2 transition is due to the trapping of a proton by an internal water cluster. To test the hypothesis, we utilized the cryogenic RIFT-IR technique to accumulate the S_2 state and solvent isotope exchange into D_2O and $H_2{}^{18}O$ to assign the broad band centered at 2740/2900 cm^{-1}, which is sensitive to the chloride ion concentration, to a protonated water cluster. The water OH stretching bands were also identified. We further tested the band sensitivity to calcium depletion and strontium reconstitution and found out that the effects are pH dependent.

Chapter 3 presents a cryogenic EPR study of cationic effects on the YZ proton couple electron transfer (PCET) reaction in the S_2 state. During this research, we used

transient EPR spectroscopy to study the effect of calcium on the recombination reaction of tyrosyl radical in S_2 state ($S_2YZ•Q_A^-$) through calcium depletion, divalent cation substitution and ammonia addition. At 190K, the S state cycle is blocked at S_2 state. One additional laser flash (532 nm) will oxidize the YZ to YZ•, but YZ• is not able to oxidize OEC at this temperature and decays back via recombination with Q_A^-. The impact of cation substitution on $S_2YZ•Q_A^-$ decay is pH dependent. Ammonia and barium ion, which are water oxidation reaction inhibitors, slow down the reaction regardless of the pH. These results lead us to propose a two-pathway model, involving two competing proton donors, for the $S_2YZ•Q_A^-$ decay reaction.

Chapter 4 reports on hydrogen-bonding interactions and conformational dynamics of $S_2YZ•Q_A^-$ decay reaction. During this research, we utilized cryogenic RIFT-IR spectroscopy to investigate the effects of pH and different divalent cations on the recombination reaction of $S_2YZ•Q_A^-$. The half-life values obtained from chapter 3 was served as a theoretical basis for the RIFT-IR data collection design. Using calcium depletion, and strontium and barium reconstitution, we identify calcium, strontium, and barium-sensitive tyrosyl radical and singlet bands in the S_2 state. The frequencies of these bands are correlated with the expected pKa of metal-bound water and are indicative of a hydrogen bond interaction. The data also provide evidence that YZ singlet is hydrogen bonded to calcium-bound water. Analysis of the amide I region indicates that calcium restricts the backbone and dihedral angle distribution of YZ conforms, which are trapped in the S_2 state. These results indicate that a conformational change is linked to the YZ radical/singlet PCET reaction. They also indicate hydrogen bonding between calcium bound water and YZ, in both the radical and singlet states.

Chapter 5 summarizes all the results from previous chapters. And the future directions for each project have been discussed in there too.

1.10 References

1. Schuster, P.; Zundel, G.; Sandorfy, C., In *Hydrogen Bond; Recent Developments in Theory and Experiments*, North-Holland Publishing Company: Amsterdam, Netherlands, 1976.

2. Knight, C.; Voth, G. A., The Curious Case of the Hydrated Proton. *Acc. Chem. Res.* **2012,** *45* (1), 101-9.

3. Kulig, W.; Agmon, N., A 'Clusters-in-Liquid' Method for Calculating Infrared Spectra Identifies the Proton-Transfer Mode in Acidic Aqueous Solutions. *Nat. Chem.* **2013,** *5* (1), 29-35.

4. Kotting, C.; Gerwert, K., Proteins in Action Monitored by Time-Resolved FTIR Spectroscopy. *Chemphyschem* **2005,** *6* (5), 881-8.

5. Freier, E.; Wolf, S.; Gerwert, K., Proton Transfer via a Transient Linear Water-Molecule Chain in a Membrane Protein. *Proc. Natl. Acad. Sci. USA* **2011,** *108* (28), 11435-11439.

6. Seibold, S. A.; Mills, D. A.; Ferguson-Miller, S.; Cukier, R. I., Water Chain Formation and Possible Proton Pumping Routes in Rhodobacter Sphaeroides Cytochrome c Oxidase: A Molecular Dynamics Comparison of the Wild Type and R481K Mutant. *Biochemistry* **2005,** *44* (31), 10475-10485.

7. Xu, J.; Sharpe, M. A.; Qin, L.; Ferguson-Miller, S.; Voth, G. A., Storage of an Excess Proton in the Hydrogen-Bonded Network of the D-Pathway of Cytochrome c Oxidase: Identification of a Protonated Water Cluster. *J. Am. Chem. Soc.* **2007,** *129* (10), 2910-2913.

8. Silverman, D. N.; Mckenna, R., Solvent-Mediated Proton Transfer in Catalysis by Carbonic Anhydrase. *Acc. Chem. Res.* **2007,** *40* (8), 669-675.

9. Polander, B. C.; Barry, B. A., Detection of an Intermediary, Protonated Water Cluster in Photosynthetic Oxygen Evolution. *Proc. Natl. Acad. Sci. USA* **2013,** *110* (26), 10634-9.

10. Brahmachari, U.; Barry, B. A., Dynamics of Proton Transfer to Internal Water during the Photosynthetic Oxygen-Evolving Cycle. *J. Phys. Chem. B* **2016,** *120* (44), 11464-11473.

11. Guo, Z.; Barry, B. A., Cryogenic Trapping and Isotope Editing Identify a Protonated Water Cluster as an Intermediate in the Photosynthetic Oxygen-Evolving Reaction. *J. Phys. Chem. B* **2016,** *120* (34), 8794-8808.

12. Luecke, H.; Schobert, B.; Richter, H. T.; Cartailler, J. P.; Lanyi, J. K., Structure of Bacteriorhodopsin at 1.55 A Resolution. *J. Mol. Biol.* **1999,** *291* (4), 899-911.

13. Garczarek, F.; Wang, J. P.; El-Sayed, M. A.; Gerwert, K., The Assignment of the Different Infrared Continuum Absorbance Changes Observed in the 3000-1800-cm^{-1} Region during the Bacteriorhodopsin Photocycle. *Biophys. J.* **2004,** *87* (4), 2676-2682.

14. Arnon, D. I., Conversion of Light into Chemical Energy in Photosynthesis. *Nature* **1959,** *184* (4679), 10-21.

15. Voet, D. V. J., *Biochemistry 4th edition*. Wiley: 2011.

16. Nevo, R.; Charuvi, D.; Tsabari, O.; Reich, Z., Composition, Architecture and Dynamics of the Photosynthetic Apparatus in Higher Plants. *Plant J.* **2012,** *70* (1), 157-176.

17. Yocum, C., Structure and Function of Photosystem I and Photosystem II. *Annu. Rev. Plant Biol.* **2006,** *57*.

18. Baniulus, D., Structure-Function of the Cytochrome b6f Complex. *Photochem. & Photobiol.* **2008,** *84*.

19. Umena, Y.; Kawakami, K.; Shen, J. R.; Kamiya, N., Crystal Structure of Oxygen-Evolving Photosystem II at a Resolution of 1.9 A. *Nature* **2011,** *473* (7345), 55-60.

20. Suga, M.; Akita, F.; Hirata, K.; Ueno, G.; Murakami, H.; Nakajima, Y.; Shimizu, T.; Yamashita, K.; Yamamoto, M.; Ago, H.; Shen, J. R., Native Structure of Photosystem II at 1.95 A Resolution Viewed by Femtosecond X-Ray Pulses. *Nature* **2015,** *517* (7532), 99-103.

21. Wei, X. P.; Su, X. D.; Cao, P.; Liu, X. Y.; Chang, W. R.; Li, M.; Zhang, X. Z.; Liu, Z. F., Structure of Spinach Photosystem II-LHCII Supercomplex at 3.2 Angstrom Resolution. *Nature* **2016,** *534* (7605), 69-74.

22. Roose, J. L.; Frankel, L. K.; Mummadisetti, M. P.; Bricker, T. M., The Extrinsic Proteins of Photosystem II: Update. *Planta* **2016,** *243* (4), 889-908.

23. Bricker, T. M., Oxygen Evolution in the Absence of the 33 kDa Manganese-Stabilizing Protein. *Biochemistry* **1992,** *31* (19), 4623-4628.

24. Ono, T. A.; Inoue, Y., Mn-Preserving Extraction of 33-kDa, 24-kDa and 16-kDa Proteins from O2-Evolving PSII Particles by Divalent Salt-Washing. *Febs Lett.* **1983,** *164* (2), 255-260.

25. Miyao, M.; Murata, N., Role of the 33-kda Polypeptide in Preserving Mn in the Photosynthetic Oxygen-Evolution System and Its Replacement by Chloride-Ions. *Febs Lett.* **1984,** *170* (2), 350-354.

26. Miyao, M.; Murata, N., Effect of Urea on Photosystem-II Particles - Evidence for an Essential Role of the 33 kDa Polypeptide in Photosynthetic Oxygen Evolution. *Biochim. Biophys. Acta* **1984,** *765* (3), 253-257.

27. Kuwabara, T.; Miyao, M.; Murata, T.; Murata, N., The Function of 33-kDa Protein in the Photosynthetic Oxygen-Evolution System Studied by Reconstitution Experiments. *Biochim. Biophys. Acta* **1985,** *806* (2), 283-289.

28. Saito, K.; Rutherford, A. W.; Ishikita, H., Mechanism of Proton-Coupled Quinone Reduction in Photosystem II. *Proc. Natl. Acad. Sci. U.S.A.* **2013,** *110* (3), 954-9.

29. Muh, F.; Glockner, C.; Hellmich, J.; Zouni, A., Light-Induced Quinone Reduction in Photosystem II. *Biochim. Biophys. Acta* **2012,** *1817* (1), 44-65.

30. Kok, B.; Forbush, B.; Mcgloin, M., Cooperation of Charges in Photosynthetic O_2 Evolution: 1. A Linear 4-step Mechanism. *Photochem. Photobiol.* **1970,** *11* (6), 457-475.

31. Barry, B. A.; Cooper, I. B.; De Riso, A.; Brewer, S. H.; Vu, D. M.; Dyer, R. B., Time-Resolved Vibrational Spectroscopy Detects Protein-Based Intermediates in the Photosynthetic Oxygen-Evolving Cycle. *Proc. Natl. Acad. Sci. U.S.A.* **2006,** *103* (19), 7288-91.

32. Chen, J.; Barry, B. A., Ultraviolet resonance Raman microprobe spectroscopy of photosystem II. *Photochem Photobiol* **2008,** *84* (3), 815-8.

33. Haumann, M.; Grabolle, M.; Neisius, T.; Dau, H., The First Room-Temperature X-Ray Absorption Spectra of Higher Oxidation States of the Tetra-Manganese Complex of Photosystem II. *FEBS Lett.* **2002,** *512* (1-3), 116-120.

34. Kuzek, D.; Pace, R. J., Probing the Mn Oxidation States in the OEC. Insights from Spectroscopic, Computational and Kinetic Data. *Biochim. Biophys. Acta* **2001,** *1503* (1-2), 123-137.

35. Ioannidis, N.; Zahariou, G.; Petrouleas, V., Trapping of the S-2 to S-3 State Intermediate of the Oxygen-Evolving Complex of Photosystem II. *Biochemistry* **2006,** *45* (20), 6252-6259.

36. Ioannidis, N.; Zahariou, G.; Petrouleas, V., The EPR Spectrum of Tyrosine Z* and Its Decay Kinetics in O_2-Evolving Photosystem II Preparations. *Biochemistry* **2008,** *47* (24), 6292-6300.

37. Krishtalik, L. I., Energetics of Multielectron Reactions: Photosynthetic Oxygen Evolution. *Biochim. Biophys. Acta* **1986,** *849* (1), 162-171.

38. Linke, K.; Ho, F. M., Water in Photosystem II: Structural, Functional and Mechanistic Considerations. *Biochim. Biophys. Acta* **2014,** *1837* (1), 14-32.

39. Junge, W.; Haumann, M.; Ahlbrink, R.; Mulkidjanian, A.; Clausen, J., Electrostatics and Proton Transfer in Photosynthetic Water Oxidation. *Philos. T. Roy. Soc. B* **2002,** *357* (1426), 1407-1417.

40. Askerka, M.; Brudvig, G. W.; Batista, V. S., The O-2-Evolving Complex of Photosystem II: Recent Insights from Quantum Mechanics/Molecular Mechanics (QM/MM), Extended X-ray Absorption Fine Structure (EXAFS), and Femtosecond X-ray Crystallography Data. *Acc. Chem. Res.* **2017,** *50* (1), 41-48.

41. Siegbahn, P. E. M., Nucleophilic Water Attack is not a Possible Mechanism for O-O Bond Formation in Photosystem II. *Proc. Natl. Acad. Sci. USA* **2017,** *114* (19), 4966-4968.

42. Yocum, C. F., The Calcium and Chloride Requirements of the O_2 Evolving Complex. *Coordin. Chem. Rev.* **2008,** *252* (3-4), 296-305.

43. Lohmiller, T.; Shelby, M. L.; Long, X.; Yachandra, V. K.; Yano, J., Removal of Ca^{2+} from the Oxygen-Evolving Complex in Photosystem II Has Minimal Effect on the Mn_4O_5 Core Structure: A Polarized Mn X-ray Absorption Spectroscopy Study. *J. Phys. Chem. B* **2015,** *119* (43), 13742-54.

44. Koua, F. H. M.; Umena, Y.; Kawakami, K.; Shen, J. R., Structure of Sr-substituted Photosystem II at 2.1 Angstrom Resolution and Its Implications in the Mechanism of Water Oxidation. *Proc. Natl. Acad. Sci. USA* **2013,** *110* (10), 3889-3894.

45. Polander, B. C.; Barry, B. A., Calcium and the Hydrogen-Bonded Water Network in the Photosynthetic Oxygen-Evolving Complex. *J. Phys. Chem. Lett.* **2013,** *4* (5), 786-791.

46. Guo, Z.; Barry, B. A., Calcium, Ammonia, Redox-Active Tyrosine YZ, and Proton-Coupled Electron Transfer in the Photosynthetic Oxygen-Evolving Complex. *J. Phys. Chem. B* **2017,** *121* (16), 3987-3996.

47. Britt, R. D.; Zimmermann, J. L.; Sauer, K.; Klein, M. P., Ammonia Binds to the Catalytic Mn of the Oxygen-Evolving Complex of Photosystem II: Evidence by Electron-Spin Echo Envelope Modulation Spectroscopy. *J. Am. Chem. Soc.* **1989,** *111* (10), 3522-3532.

48. Boussac, A.; Rutherford, A. W.; Styring, S., Interaction of Ammonia with the Water Splitting Enzyme of Photosystem II. *Biochemistry* **1990,** *29* (1), 24-32.

49. Kim, D. H.; Britt, R. D.; Klein, M. P.; Sauer, K., The Manganese Site of the Photosynthetic Oxygen-Evolving Complex Probed by EPR Spectroscopy of Oriented Photosystem II Membranes: the g = 4 and g = 2 Multiline Signals. *Biochemistry* **1992,** *31* (2), 541-547.

50. Navarro, M. P.; Ames, W. M.; Nilsson, H.; Lohmiller, T.; Pantazis, D. A.; Rapatskiy, L.; Nowaczyk, M. M.; Neese, F.; Boussac, A.; Messinger, J.; Lubitz, W.; Cox,

N., Ammonia Binding to the Oxygen-Evolving Complex of Photosystem II Identifies the Solvent-Exchangeable Oxygen Bridge (μ-oxo) of the Manganese Tetramer. *Proc. Natl. Acad. Sci. USA* **2013,** *110* (39), 15561-15566.

51. Vinyard, D. J.; Askerka, M.; Debus, R. J.; Batista, V. S.; Brudvig, G. W., Ammonia Binding in the Second Coordination Sphere of the Oxygen-Evolving Complex of Photosystem II. *Biochemistry* **2016,** *55* (31), 4432-6.

52. Young, I. D.; Ibrahim, M.; Chatterjee, R.; Gul, S.; Fuller, F. D.; Koroidov, S.; Brewster, A. S.; Tran, R.; Alonso-Mori, R.; Kroll, T.; Michels-Clark, T.; Laksmono, H.; Sierra, R. G.; Stan, C. A.; Hussein, R.; Zhang, M.; Douthit, L.; Kubin, M.; de Lichtenberg, C.; Vo Pham, L.; Nilsson, H.; Cheah, M. H.; Shevela, D.; Saracini, C.; Bean, M. A.; Seuffert, I.; Sokaras, D.; Weng, T. C.; Pastor, E.; Weninger, C.; Fransson, T.; Lassalle, L.; Brauer, P.; Aller, P.; Docker, P. T.; Andi, B.; Orville, A. M.; Glownia, J. M.; Nelson, S.; Sikorski, M.; Zhu, D.; Hunter, M. S.; Lane, T. J.; Aquila, A.; Koglin, J. E.; Robinson, J.; Liang, M.; Boutet, S.; Lyubimov, A. Y.; Uervirojnangkoorn, M.; Moriarty, N. W.; Liebschner, D.; Afonine, P. V.; Waterman, D. G.; Evans, G.; Wernet, P.; Dobbek, H.; Weis, W. I.; Brunger, A. T.; Zwart, P. H.; Adams, P. D.; Zouni, A.; Messinger, J.; Bergmann, U.; Sauter, N. K.; Kern, J.; Yachandra, V. K.; Yano, J., Structure of Photosystem II and Substrate Binding at Room Temperature. *Nature* **2016,** *540* (7633), 453-457.

53. Polander, B. C.; Barry, B. A., A Hydrogen-Bonding Network Plays a Catalytic Role in Photosynthetic Oxygen Evolution. *Proc. Natl. Acad. Sci. USA* **2012,** *109* (16), 6112-6117.

54. Zimmermann, J. L.; Rutherford, A. W., Electron-Paramagnetic-Res Studies of the Oxygen-Evolving Enzyme of Photosystem II. *Biochim. Biophys. Acta* **1984,** *767* (1), 160-167.

55. Zimmermann, J. L.; Rutherford, A. W., Electron-Paramagnetic Resonance Properties of the S-2 State of the Oxygen-Evolving Complex of Photosystem II. *Biochemistry* **1986,** *25* (16), 4609-4615.

56. Steenhuis, J. J.; Barry, B. A., Protein and Ligand Environments of the S_2 State in Photosynthetic Oxygen Evolution: a Difference FT-IR Study. *J. Phys. Chem. B* **1997,** *101* (33), 6652-6660.

57. Pokhrel, R.; Brudvig, G. W., Oxygen-Evolving Complex of Photosystem II: Correlating Structure with Spectroscopy. *Phys. Chem. Chem. Phys.* **2014,** *16* (24), 11812-11821.

58. Pantazis, D. A.; Ames, W.; Cox, N.; Lubitz, W.; Neese, F., Two Interconvertible Structures that Explain the Spectroscopic Properties of the Oxygen-Evolving Complex of Photosystem II in the S2 State. *Angew. Chem. Int. Edit.* **2012,** *51* (39), 9935-9940.

59. Liang, W.; Latimer, M. J.; Dau, H.; Roelofs, T. A.; Yachandra, V. K.; Sauer, K.; Klein, M. P., Correlation between Structure and Magnetic Spin-State of the Manganese Cluster in the Oxygen-Evolving Complex of Photosystem-II in the S-2 State -

Determination by X-Ray-Absorption Spectroscopy. *Biochemistry* **1994,** *33* (16), 4923-4932.

60. Bovi, D.; Narzi, D.; Guidoni, L., The S-2 State of the Oxygen-Evolving Complex of Photosystem II Explored by QM/MM Dynamics: Spin Surfaces and Metastable States Suggest a Reaction Path Towards the S-3 State. *Angew. Chem. Int. Edit.* **2013,** *52* (45), 11744-11749.

61. Ananyev, G. A.; Sakiyan, I.; Diner, B. A.; Dismukes, G. C., A Functional Role for Tyrosine-D in Assembly of the Inorganic Core of the Water Oxidase Complex of Photosystem II and the Kinetics of Water Oxidation. *Biochemistry* **2002,** *41* (3), 974-980.

62. Jenson, D. L.; Evans, A.; Barry, B. A., Proton-Coupled Electron Transfer and Tyrosine D of Photosystem II. *J. Phys. Chem. B* **2007,** *111* (43), 12599-12604.

63. Jenson, D. L.; Barry, B. A., Proton-Coupled Electron Transfer in Photosystem II: Proton Inventory of a Redox Active Tyrosine. *J. Am. Chem. Soc.* **2009,** *131* (30), 10567-10573.

64. Keough, J. M.; Jenson, D. L.; Zuniga, A. N.; Barry, B. A., Proton Coupled Electron Transfer and Redox-Active Tyrosine Z in the Photosynthetic Oxygen-Evolving Complex. *J. Am. Chem. Soc.* **2011,** *133* (29), 11084-11087.

65. Keough, J. M.; Zuniga, A. N.; Jenson, D. L.; Barry, B. A., Redox Control and Hydrogen Bonding Networks: Proton-Coupled Electron Transfer Reactions and Tyrosine Z in the Photosynthetic Oxygen-Evolving Complex. *J. Phys. Chem. B* **2013,** *117* (5), 1296-1307.

66. Poole, C. P., *Electron Spin Resonance: A Comprehensive Treatise on Experimental Techniques*. Courier Corporation: 1996.

67. Weil, J. A.; Bolton, J. R., *Electron Paramagnetic Resonance: Elementary Theory and Practical Applications*. John Wiley & Sons: 2007.

68. Huber, M., Introduction to Magnetic Resonance Methods in Photosynthesis. *Photosynth. Res.* **2009,** *102* (2-3), 305-310.

69. Messinger, J.; Nugent, J. H. A.; Evans, M. C. W., Detection of an EPR multiline signal for the S-0 state in photosystem II. *Biochemistry* **1997,** *36* (37), 11055-11060.

70. Britt, R. D.; Peloquin, J. M.; Campbell, K. A., Pulsed and Parallel-Polarization EPR Characterization of the Photosystem II Oxygen-Evolving Complex. *Annu. Rev. Bioph. Biom.* **2000,** *29*, 463-495.

71. Wilson, E. B.; Decius, J. C.; Cross, P. C., *Molecular Vibrations: The Theory of Infrared and Raman Vibrational Spectra*. Courier Corporation: 2012.

72. Vogel, R.; Siebert, F., Vibrational Spectroscopy as a Tool for Probing Protein Function. *Curr. Opin. Chem. Biol.* **2000,** *4* (5), 518-523.

73. Barry, B. A.; Brahmachari, U.; Guo, Z., Tracking Reactive Water and Hydrogen-Bonding Networks in Photosynthetic Oxygen Evolution. *Acc. Chem. Res.* **2017,** *50* (8), 1937-1945.

CHAPTER 2. CRYOGENIC TRAPPING AND ISOTOPE EDITING IDENTIFY A PROTONATED WATER CLUSTER AS AN INTERMEDIATE IN THE PHOTOSYNTHETIC OXYGEN-EVOVLING REACTION

By

Zhanjun Guo and Bridgette A. Barry*

School of Chemistry and Biochemistry and Petit Institute for Bioengineering and Biosciences, Georgia Institute of Technology, Atlanta, GA 30332

Reprinted with permission from *The Journal of Physical Chemistry B*

Guo, Z. and Barry, B. A. Cryogenic Trapping and Isotope Editing Identify a Protonated Water Cluster as an Intermediate in the Photosynthetic Oxygen-Evolving Reaction. *J. Phys. Chem. B* **2016** *120* (34), 8794-8808

2.1 Abstract

Internal water is known to play a catalytic role in several enzymes. In photosystem II (PSII), water is the substrate. To oxidize water, the PSII Mn_4CaO_5 cluster or oxygen evolving center (OEC) cycles through five oxidation states, termed S_n states. As reaction products, molecular oxygen is released, and protons are transferred through a ~25 Å hydrogen-bonded network from the OEC to the thylakoid lumen. Previously, it was reported that a broad infrared band at 2880 cm^{-1} is produced during the S_1-to-S_2 transition and accompanies flash-induced, S state cycling at pH 7.5. Here, we report that when the S_2 state is trapped by continuous illumination under cryogenic conditions (190 K), an analogous 2740/2900 cm^{-1} band is observed. The frequency depended on the sodium chloride concentration. This band is unambiguously assigned to a normal mode of water by $D_2{}^{16}O$ and $H_2{}^{18}O$ solvent exchange. Its large, apparent $H_2{}^{18}O$ isotope shift, ammonia sensitivity, frequency, and intensity support assignment to a stretching vibration of a hydronium cation, H_3O^+, in a small, protonated internal water cluster, $nH_2O(H_3O^+)$. Water OH stretching bands, which may be derived from the hydration shell of the hydronium ion, are also identified. Using the 2740 cm^{-1} infrared marker, the results of calcium depletion and strontium reconstitution on the protonated water cluster are found to be pH dependent. This change is attributed to protonation of an amino acid side chain and a possible change in $nH_2O(H_3O)^+$ localization in the hydrogen-bonding network. These results are consistent with an internal water cluster functioning as a proton acceptor and an intermediate during the S_1-to-S_2 transition. Our experiments demonstrate the utility of this infrared signal as a novel functional probe in PSII.

2.2 Introduction

Since the von Grotthuss proton-hopping mechanism was proposed, many experimental and theoretical studies have focused on understanding proton migration in liquid water.[1-3] In comparison with an aqueous environment, proteins typically require ordered structures to transfer protons quickly and to conduct biological reactions efficiently.[4] Net proton release may go through a series of proton transfer steps involving hydrogen-bonded amino acid sidechains and internal water. A prototypical example is bacteriorhodopsin, which conducts light-induced trans-membrane proton transfer through the use of protonable amino acid side chains and internal water.[5-7] Internal water clusters may assist in the facile release of protons and function either as acceptors or donors.[8-11]

In oxygenic photosynthesis, photosystem II (PSII) catalyzes the oxidation of water and the reduction of quinone. PSII is a multi-subunit membrane protein, and in current cyanobacterial PSII X-ray structures, each monomer contains at least 20 subunits. There are 17 intrinsic and 3 extrinsic polypeptides.[12-13] With photoexcitation, a charge separation between the primary electron donor P_{680} and a bound quinone molecule (Q_A or Q_B) is generated. P_{680}^+ oxidizes a tyrosine residue, YZ (Y161-D1 subunit), and subsequently YZ· oxidizes the oxygen evolving complex (OEC).[14] PSII also contains a more stable tyrosine radical, YD· (Y160-D2 subunit),[15] which is ~20 Å from the OEC, a Mn_4CaO_5 metal cluster (Figure 2.1A). In plants, two extrinsic subunits, PsbP (24 kDa) and PsbQ (18 kDa), regulate the affinity for calcium and chloride.[16] These two subunits are not present in the current PSII X-ray structures, which derive from cyanobacterial PSII.[13] There are other distinctions in subunit composition when plants and cyanobacterial PSII are compared.[17-18]

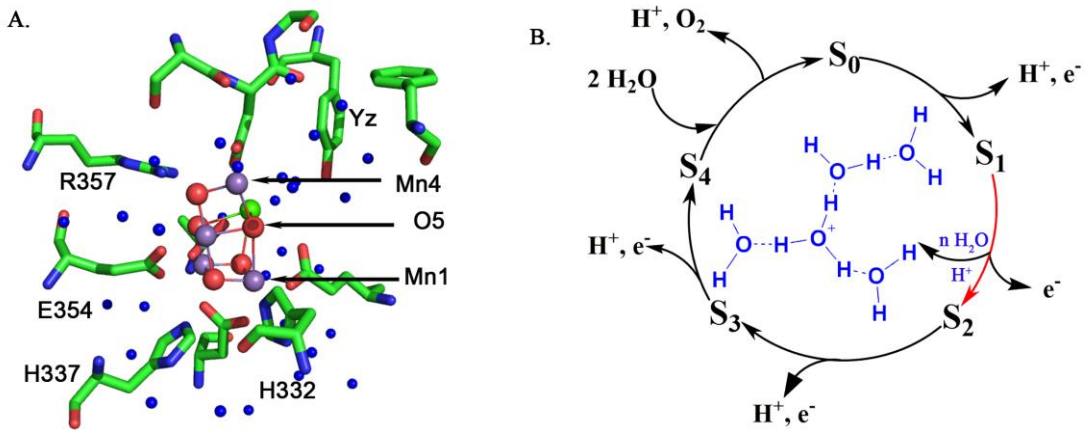

Figure 2.1 Photosynthetic water oxidation and protonation of an internal, water cluster. (A) X-ray crystallographic structure of the OEC (PDB ID: 4UB6), including selected, nearby amino acids: D1: Y161, Ser169, Asp170, Gly171, Phe182, His332, His337, Asp342, Ala344 and CP43-R357. Water molecules (shown in blue) within 8 Å of OEC are also shown. Oxygen ions are red, the calcium ion is green, and manganese are magenta.[13] (B) S-state cycle of the photosynthetic reaction, showing proton trapping on internal water and electron release on the S_1 to S_2 transition.[19-20] The red arrow, which represents the S_1-to-S_2 transition, is the only transition allowed under the experimental conditions employed here. B, inset: a water cluster acts as a transient proton acceptor during the S_1-to-S_2 transition to form a $nH_2O(H_3O^+)$ cluster, where n is depicted as 5. For the S_2 state, OH stretching bands, assignable to the hydrating water shell, nH2O, are detected here, as well as a stretching vibration of the H_3O^+ core.

To oxidize water, the OEC cycles through 5 different oxidation states, named S_n states (Figure 2.1B). A short, single flash advances the dark-adapted, stable sample (S_1 state) to the S_2 state, which corresponds to a Mn oxidation reaction.[21-24] On subsequent flashes, the O-O bond forms, and oxygen is released during S_3-to-S_0 transition. During the cycle, the calcium ion plays an essential role[25] and has been proposed to bind and activate a substrate water molecule.[26-28] In the X-ray structures, calcium binds water molecules that are in contact with an extensive hydrogen bonding network, which leads to the lumenal surface.[13] This extensive network may constitute the proton transport pathway from the metal cluster to the lumen. It has been suggested that D61 in the D1 polypeptide, which is

a component of this pathway (Figure 2.2), plays a direct role in proton transfer.[29-30] Of divalent ions, only strontium reconstitutes activity.[25, 31] Chloride is also required for activity under physiological conditions,[32] and may also play a role in proton transfer.[25, 32-34]

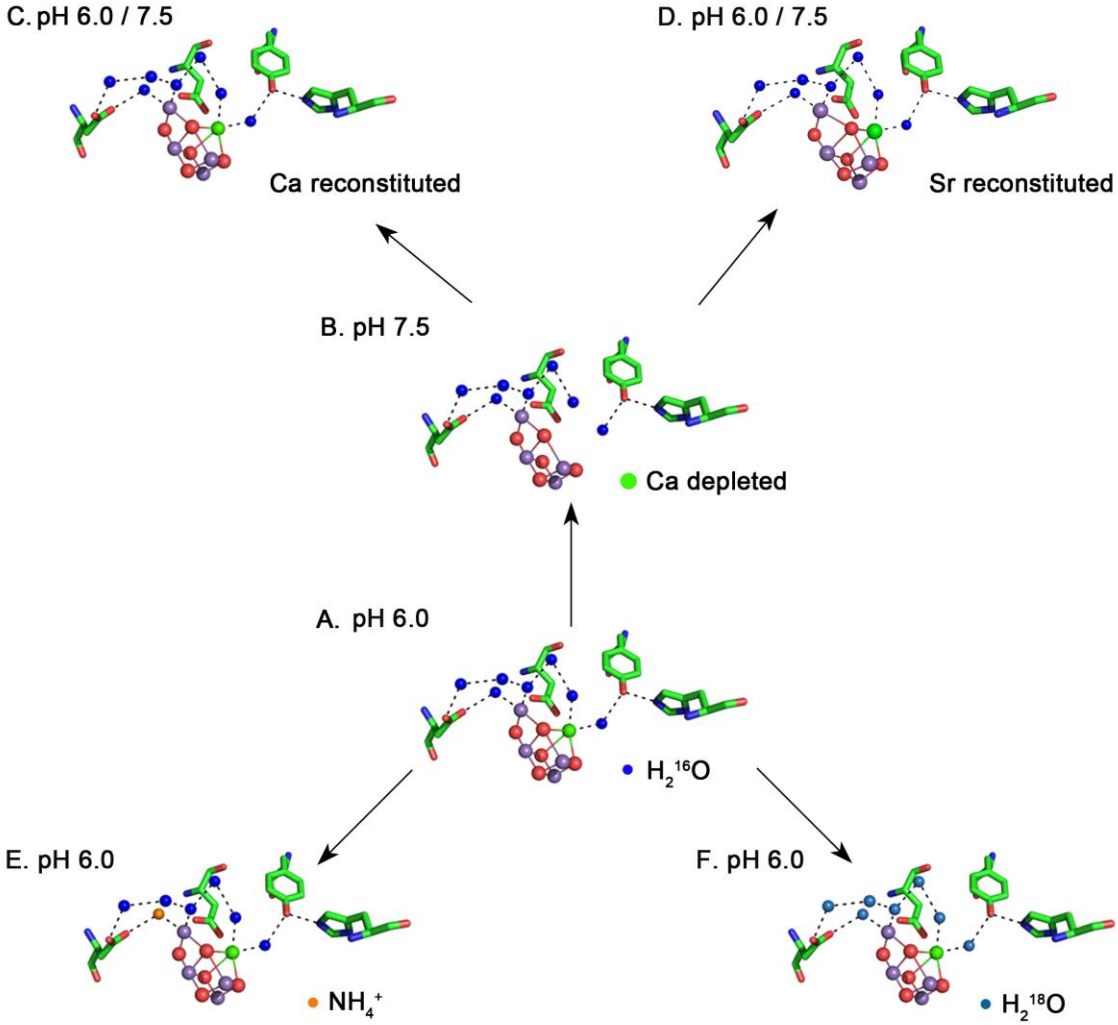

Figure 2.2 Schematic of experimental strategy. A portion of the OEC is shown, including YZ (Y161-D1), His190-D1, D170D1, and D61-D1 (PDB ID: 4IL6 for strontium PSII; PDB ID: 4UB6 for calcium PSII).[13, 31] $H_2{}^{16}O$ is represented by blue spheres; $H_2{}^{18}O$ is represented by dark blue spheres; ammonia is represented by orange spheres. In the metal cluster, calcium/strontium is shown in green, manganese ions are shown in magenta, and oxygens are shown in red. The depiction of the structural effects caused by calcium depletion and ammonia treatment are

speculative. In (A), native PSII is resuspended in $H_2{}^{16}O$ at pH 6.0, SMN buffer. In (B), PSII is calcium depleted (CD) at pH 7.5, SHN buffer. In (C), CD PSII is transferred in $H_2{}^{16}O$ buffer to pH 6.0 or 7.5, measurements are performed, and then calcium is reconstituted in $H_2{}^{16}O$ at pH 6.0 or 7.5. In (D), PSII is strontium reconstituted in $H_2{}^{16}O$ at pH 6.0 or 7.5. In (E), native PSII is treated with ammonia in $H_2{}^{16}O$ pH 6.0. In (F), native PSII is exchanged into $H_2{}^{18}O$, pH 6.0.

It has been proposed that each OEC oxidation is linked with a water deprotonation event to make the reactions thermodynamically feasible.[35-36] Unlike the other S state transitions (Figure 2.1B), the S_1-to-S_2 transition is not coupled with a net proton release to the lumen in sucrose-containing buffers and therefore has been proposed to lead to positive charge accumulation.[20] Recently, an internal water cluster has been suggested to be an internal proton acceptor during the S_1-to-S_2 transition at pH 7.5 (Figure 2.1B, inset). The experiments were conducted at temperatures of 263 K and 283 K, during which the entire S state cycle can be completed (Figure 2.1B).[37] By serving as transient storage for the substrate proton, the existence of such a protonated, internal water cluster rationalizes the failure to observe proton release to the bulk during this transition. Depending on the location of the protonated water cluster, this protonation event could lead to an apparent accumulation of positive charge on the OEC. Notably, this infrared signal is expected to act as a marker for proton transfer and to exhibit frequency shifts as a result of changes in the size of the protonated water cluster.[37-38] Thus, this infrared signal provides a novel and incisive way to monitor internal proton transfer events in PSII.

Here, we show that a cationic water infrared signal, originating from a small protonated water cluster, $n(H_2O)(H_3O^+)$, can be detected under cryogenic conditions when the S_2 state is formed under continuous illumination. This experiment establishes that oxidation of the cluster is associated with proton transfer to an internal acceptor, even under

cryogenic conditions. Also, for the first time, we identify OH stretching modes of water(s), which are candidates to derive from the hydration shell of the hydronium ion. Interestingly, the intensity of the hydronium ion signal is shown to depend on calcium occupancy at pH 7.5, but not at pH 6.0. In addition, strontium reconstitution is found to support the signal at pH 6.0, but the signal is not detected at pH 7.5 in strontium-reconstituted PSII. This divalent ion and pH dependence, which is shown to be associated with a hydrogen-bonding change in the peptide backbone, rationalizes functional differences previously reported.

2.3 Material and Methods

To obtain highly purified and active preparations, PSII was prepared from market spinach using Triton-X 100, generating PSII membranes, and then purified further with octylthioglucoside (OTG).[39-40] After purification, samples were resuspended in SMN buffer (400 mM sucrose, 50 mM 2-(N-morpholino)ethanesulfonic acid (MES)-NaOH pH 6.0, 15 mM NaCl), flash frozen in liquid nitrogen, and then transferred to a -70°C freezer. The average oxygen evolution rate of the preparation (termed native, Figure 2.2A) was $\geq$900 μmol O_2 (mg chl·hr)$^{-1}$ at pH 6.0 and was measured by a protocol previously described.[41] Recrystallized 2,6-dichloro-1,4-benzoquinone (DCBQ, Sigma, St. Louis, MO, 0.5mM) and potassium ferricyanide ($K_3[Fe(CN)_6$) were used as electron acceptors at concentrations of 1 mM. Immediately before the measurement, a stock solution (100 mM) of recrystallized DCBQ was dissolved in ethanol, and a stock solution (100 mM) of potassium ferricyanide was dissolved in water. In some experiments, the inhibitor, 3-(3,4-dichlorophenyl)-1,1-dimethylurea (DCMU, Serva, Islandia, NY) was made up as a 10 mM stock solution in ethanol.[42] DCMU was employed under assay conditions at a concentration of 10 μM.

Table 1 Steady-state, light-induced oxygen evolution activity[1] in calcium-depleted, calcium-reconstituted, and strontium-reconstituted PSII

O_2 Evolution Assay Buffer	pH of Sample	Sample Description	Oxygen Evolution Rate
SMN, pH 6.0	6.0	CD[2]	460 ± 80
		Ca reconstituted[3]	690 ± 50
		CD with 10mM EGTA[4]	470 ± 60
		Sr reconstituted[5]	580 ± 40
	7.5	CD[2]	310 ± 30
		Ca reconstituted[3]	600 ± 40
		CD with 10mM EGTA[4]	320 ± 50
SHN, pH 7.5	6	CD[2]	380 ± 80
		Ca reconstituted[3]	700 ± 110
		CD with 10mM EGTA[4]	390 ± 30
	7.5	CD[2]	350 ± 60
		Ca reconstituted[3]	620 ± 90
		CD with 10mM EGTA[4]	260 ± 130
		Sr reconstituted[5]	530 ± 20

[1]Oxygen evolution rates: μmole O_2 (mg chl·hr)$^{-1}$. The activity of native (control) PSII preparations was ≥ 900 μmole O_2 (mg chl·hr)$^{-1}$. A negative PSII control, containing 10 μM of the inhibitor, DCMU, gave 140 ± 20 μmole O_2 (mg chl·hr)$^{-1}$. The SMN buffer contained 400 mM sucrose, 50 mM MES-NaOH, pH 6.0, 15 mM NaCl. The SHN buffer contained 400 mM sucrose, 50 mM HEPES-NaOH, pH 7.5, 15 mM NaCl. See Methods for additional details.
[2]Calcium-depleted PSII (CD) generated at pH 7.5 by 10 mM EGTA treatment.
[3]Calcium-reconstituted PSII generated by addition of 20 mM $CaCl_2$ from a buffered stock either at pH 6.0 or pH 7.5.
[4]EGTA added to oxygen evolution assay buffer from a buffered stock at pH 7.5.
[5]Strontum-reconstituted PSII generated by addition of 20 mM $SrCl_2$ from a buffered stock either at pH 6.0 or pH 7.5.

To deplete calcium, the native PSII sample (Figure 2.2A), which had been isolated, frozen, and stored at pH 6.0, was transferred to pH 7.5 (Figure 2.2B). This procedure has been shown to deplete extrinsic subunits.[43-45] SDS gel electrophoresis was used to confirm the CD samples, used here, were depleted of the PsbP and PsbQ extrinsic polypeptides (data not shown). The calcium-depleted (CD) sample was generated by treatment with 10 mM ethylene glycol tetraacetic acid (EGTA) at pH 7.5 in SHN buffer (400 mM sucrose, 50 mM 4-(2-hydroxyethyl)-1-piperazineethanesulfonic acid (HEPES)-NaOH pH 7.5, 15 mM NaCl) (Figure 2.2B).[46] A calcium-reconstituted sample was produced by pelleting and resuspending the CD sample either in SMN or SHN buffer without EGTA (residual carry over EGTA, estimated as 0.75 mM). This step was followed by the addition of 20 mM $CaCl_2$ from a 3 M buffered $CaCl_2$ stock (either in SHN or SMN) (Figure 2.2C).[46] Strontium reconstitution at pH 6.0 or pH 7.5 was performed by addition of 20 mM strontium from a 3 M strontium chloride buffered stock at the appropriate pH (Figure 2.2D). The results of oxygen evolution assays are shown in Table 1.

In some experiments, ammonia was used as an inhibitor (Figure 2.2E).[47-48] When employed, NH_4Cl (200 mM) was added from 3 M buffered NH_4Cl stock in SMN buffer. Previous experiments have shown that ammonia is an inhibitor of this PSII preparation,

either at pH 6.0 or pH 7.5.[49] The concentration of chloride was keep constant in all controls and was adjusted to 255 mM by additions from a 3 M buffered NaCl stock in SMN or SHN buffer.

Table 2 Steady-state, light-induced oxygen evolution activity[1] in ammonia-treated and control PSII

Sample condition	Without addition	20 mM Ca^{2+} and 155 mM Cl^-
No ammonia, Positive Control[2]	100% ± 10%	100% ± 10%
Plus ammonia, Negative Control[3]	18% ± 5%	80% ± 3%
Ammonia added and removed Sample[4]	53% ± 10%	89% ± 5%

[1]Oxygen evolution rates (μmole O_2/mg chl·hr) normalized to the rate of a native PSII preparation, assayed at pH 6.0. See Methods for more details. The assay buffer was SMN buffer, which contains 400 mM sucrose, 50 mM MES-NaOH pH 6.0, 15 mM NaCl. Calcium was added by addition of $CaCl_2$ from buffered stock at pH 6.0, and chloride was added from $CaCl_2$ and NaCl buffered stocks at pH 6.0.
[2]The PSII sample was incubated with 200 mM NaCl at pH 6.0 on ice for 40 min. After the 40 min incubation, the sample were centrifuged and resuspended into SMN buffer three times.
[3]The PSII sample was incubated with 200 mM NH_4Cl at pH 6.0 on ice for 40 min. After the 40 min incubation, the sample were centrifuged and resuspended into SMN buffer with 200 mM NH_4Cl three times.

[4]The PSII sample was incubated with 200 mM NH_4Cl at pH 6.0 on ice for 40 min. After the 40 min incubation, the sample were centrifuged and resuspended into SMN buffer three times.

In order to test for the reversibility of ammonia inhibition under our conditions, steady state oxygen evolution activity was monitored (Table 2). Two PSII samples were incubated with 200 mM NH_4Cl at pH 6.0 on ice for 40 min. As a positive control, a third PSII sample was incubated with 200 mM NaCl at pH 6.0 under the same conditions, but without ammonia. After the 40 min incubation, the positive control and an ammonia-containing sample were centrifuged and resuspended into SMN buffer three times. Another ammonia-containing sample was maintained in 200 mM NH_4Cl under the same conditions (negative control). Rates were normalized to the positive control, which did not require additional calcium and chloride in the assay buffer for activity (Table 2). The addition of ammonia decreased the rate to 18%; this rate recovered to 80% under illumination in the presence of calcium and chloride. Calcium chloride dependence is expected because the higher chloride concentration causes loss of the PsbP and PsbQ subunits in this preparation (data not shown). Also, ammonia inhibition is expected to be reversible under high continuous illumination, because the higher S states have a short lifetime.[48] When the sample was washed to remove ammonia before the assay (remaining ammonia, estimated as 1.6 mM), the rate recovered to 53% in the absence of calcium chloride and to 90% under illumination in the presence of calcium and chloride. This experiment indicates that ammonia inhibition is reversible either by washing (centrifugation/resuspension) or at high continuous light intensity, as expected.[48-49]

Reaction-induced FT-IR (RIFT-IR) difference spectroscopy of the S_1-to-S_2 transition was performed at 190 K and pH 6.0 or pH 7.5 using an infrared cryostat.[50-51] A PSII sample was thawed and pelleted. The sample was resuspended in the appropriate

buffer. Potassium ferricyanide was added from a 100 mM or 1 M freshly prepared buffered stock solution (either SHN or SMN buffer in $H_2{}^{16}O$ or $D_2{}^{16}O$) to give a final concentration of 7 mM. The sample was then centrifuged at 50,000 x g for 10 min to produce a pellet. Buffer exchange was accomplished by an additional resuspension in $H_2{}^{16}O$, $D_2{}^{16}O$ or $H_2{}^{18}O$ SMN buffer (Figure 2.2F).

The pelleted sample, which was never dehydrated, was spread on a CaF_2 window, and then sandwiched with a second CaF_2 window. The RIFT-IR sample was wrapped with parafilm to prevent dehydration during the experiment. At room temperature, the ratio of the water OH stretching band (3380 cm^{-1}) to the amide II band (1550 cm^{-1}) was ~3. In comparing native, calcium-depleted, calcium-reconstituted, strontium-reconstituted, and ammonia-treated samples, the chloride concentration was maintained at 255 mM. In comparing the $H_2{}^{16}O$, $D_2{}^{16}O$, and $H_2{}^{18}O$ exchanged samples, the chloride concentration was maintained at 15 mM. When necessary, the chloride concentration was increased by addition of NaCl from a buffered 3M stock solution (3 M in SMN or SHN buffer in $H_2{}^{16}O$).

Parameters for FT-IR spectroscopy were: 8 cm^{-1} spectral resolution; four levels of zero filling; Happ-Genzel apodization function; 60 KHz mirror speed; and Mertz phase correction. A 3 x 50 mm, 3-12 μM anti-reflection coated germanium window (Edmund Optics, Barrington, NJ) was used to block illumination of the sample by the internal He-Ne laser of the spectrometer. The sample was pre-flashed with a single 532 nm laser flash (40 mJ/cm^2) and dark-adapted for 20 min to generate 100% of the S_1 state. After the dark-adaption period, the sample was cooled to 190 K. Following six 15 second scans (corresponding to the S_1 state), an external 0.1 mJ He-Ne laser (633 nm, Melles Griot, Carlsbad, CA*)* was used to illuminate the sample for 90 sec. After illumination, six 15

second scans were collected (corresponding to the S_2 state). Difference spectra were constructed by ratio of two 15 second scans, one recorded in the dark immediately before the 633 nm laser illumination (S_1) and the second recorded in the dark 75 seconds after laser illumination ended (S_2). The difference spectra were normalized to an amide II intensity of 0.5 AU. In some experiments, samples were annealed at room temperature and then subjected to another round of data acquisition. See Figure Legends for more information. All the difference spectra with a total absorbance of less than 1.5×10^{-3} in the amide region and 1.0×10^{-3} at 3150 cm^{-1} were averaged to give the final data set.

The half-inhibition temperature of the S_1-to-S_2 transition is 100 K, while the half inhibition temperatures of the other transitions are 225-235K (Figure 2.1B).[19] Thus, at 190 K, the S_1-to-S_2 transition is permitted but the S_2-to-S_3 transition is blocked, and the S_2 state is trapped after 633 nm illumination. Previously, the half-life time of the recombination of $S_2YZ\cdot Q_A^-$ has been determined to be ~4.5 s at pH 6.0 at 190 K. The spectra presented here were accumulated 75 s after red light illumination. At 75 s, YZ· has fully decayed.[52] Thus, YZ· and its proton donors will not make a contribution to the spectra recorded here. Also, at 190 K, the Q_A^- to Q_B transition is blocked.[53] Therefore, the PSII contributors to the RIFT-IR spectra reported here are $S_2Q_A^-$-to-S_1Q_A. An additional contribution from the slowly decaying tyrosyl radical, YD·, is also expected.[54-55]

Previously, our group has employed cryogenic RIFT-IR spectroscopy to study the S_1-to-S_2 transition.[50-51] In that work, glycerol-containing buffers were employed to make an optical glass, and data were recorded under continuous illumination. Those spectra exhibit some frequency shifts and line broadening compared to the data reported here.

Those differences are attributed to the use of glycerol and to homogenous broadening in spectra recorded under illumination.[56]

2.4 Results

2.4.1 Isolation of PSII, Calcium Depletion, and Calcium Reconstitution.

The average oxygen evolution rate of the PSII preparations employed here was $\geq$900 µmol O_2 (mg chl·hr)$^{-1}$, as isolated and assayed at pH 6.0. Calcium is required for steady state oxygen evolution activity, and procedures that remove calcium are known to decrease the oxygen evolution rate of PSII.[57] To test the efficacy of the calcium depletion/reconstitution method employed here at two pH values, we present the oxygen evolution activity measurements in Table 1. Activity measurements were conducted either with a pH 6.0 or a pH 7.5 assay buffer. Residual oxygen activity in CD PSII was found to be similar when assays were performed at pH 6.0 and 7.5 (Table 1). When EGTA was added to the assay buffer during the oxygen evolution measurement, there was no significant change, either at pH 6.0 or 7.5 (Table 1). This indicates that all chelatable calcium has been removed from PSII; EGTA is an effective calcium chelator in the absence of the extrinsic subunits.[57-58] The oxygen evolution assays in Table 1are consistent with depletion of calcium in approximately half the PSII centers. This is in qualitative agreement with results obtained previously using other methods of calcium removal. For example, atomic absorption measurements showed that a method, employing 2 M NaCl treatment under illumination, depleted 40% of PSII calcium.[57]

Importantly, in the calcium depletion method employed here, there was no significant difference in residual oxygen evolution rate between the pH 6.0 and pH 7.5

samples (Table 1). These data indicate that the efficacy of calcium removal is similar at the two pH values. Oxygen evolution rates in all calcium-reconstituted preparations increased relative to the CD preparation (Table 1). Based on previous work, it is expected that 79% of the control rate will be restored.[57] As shown in Table 1, the extent of calcium reconstitution did not depend on the pH of the assay buffer or on the pH of the sample during the reconstitution step. Note that calcium depletion using the 2 M NaCl method was previously reported to give lower reconstituted rates, compared to the method employed here, for this type of PSII preparation.[46]

2.4.2 The 3100-2100 cm^{-1} Region of the RIFT-IR Spectrum and the Hydronium Cation Stretching Vibration.

In Figure 2.3A, the 3100-2100 cm^{-1} region of the reaction-induced FT-IR (RIFT-IR) spectrum, associated with the S_1-to-S_2 transition at 190 K at pH 7.5, is presented. As observed, the production of the S_2 state is associated with a broad signal at 2740 cm^{-1}, which is positive in the S_2-minus-S_1 spectrum. The spectrum shown in Figure 3A, acquired after continuous illumination, exhibits a significant improvement in baseline (Figure 2.3, bottom traces) compared to laser flash illumination at higher temperature.[37] Given the improvement in baseline, the 2740 cm^{-1} frequency in Figure 2.3A is congruent with the frequency previously reported for the S_2 signal at higher temperature (2880 cm^{-1}).[37]

At pH 6.0 and 190 K, the 2740 cm^{-1} S_2 absorptive signal was also observed (Figure 2.3D). Removal of the OEC with alkaline Tris,[59] which eliminates oxygen evolution activity, also eliminated the 2740 cm^{-1} signal (data not shown). This effect of alkaline Tris

supports the conclusion that the infrared band arises from the OEC and the functional Mn_4CaO_5 cluster and not from Q_A^-, YZ·, or YD·.

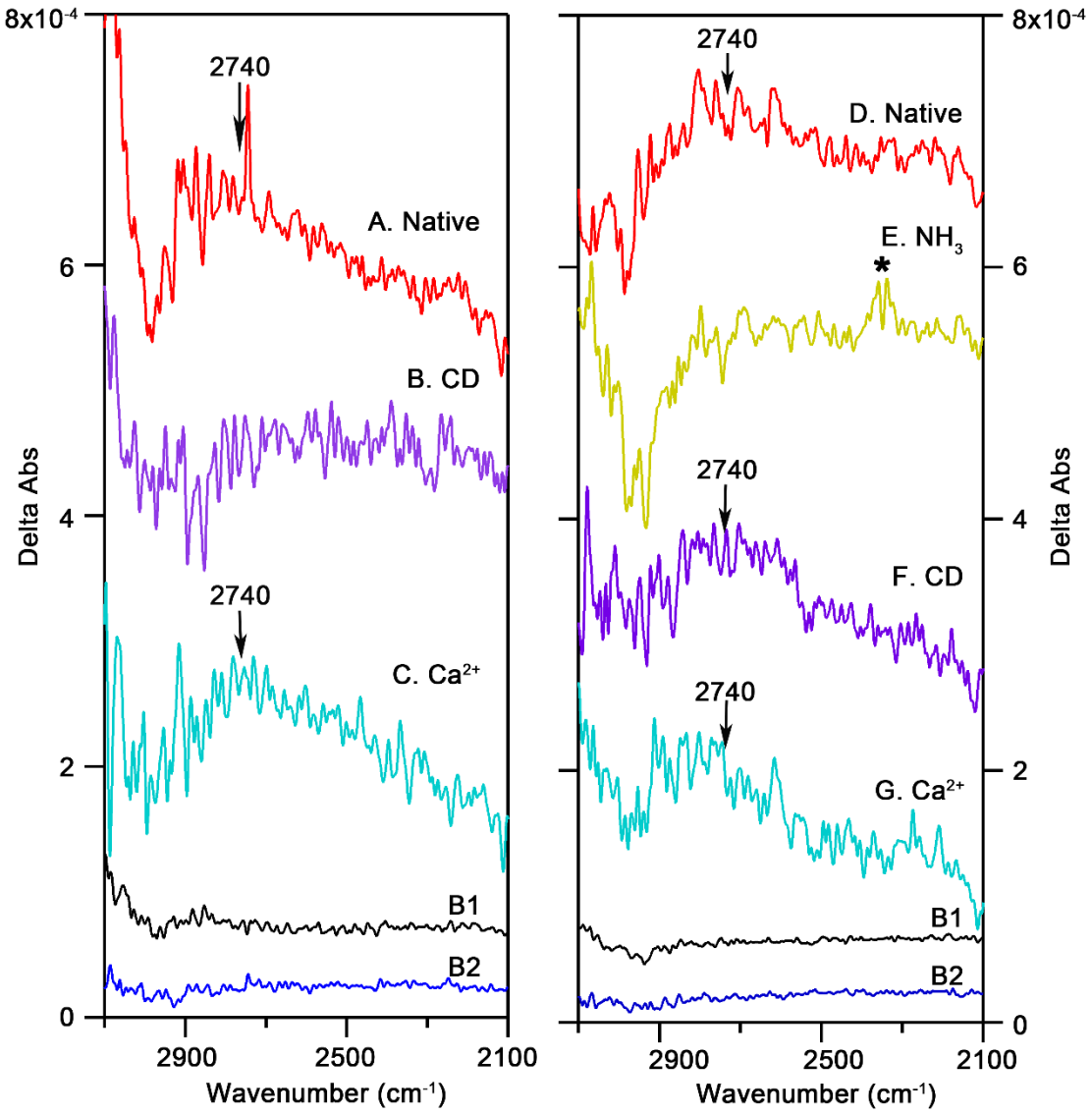

Figure 2.3 Reaction-induced FT-IR spectra (3100-2100 cm^{-1}) at 190 K, reflecting the S_1-to-S_2 transition and the effects of pH, ammonia treatment, calcium depletion and calcium reconstitution. The total chloride concentration was 255 mM. In the left panel, all samples were in pH 7.5 buffer. In (A) PSII (red), in (B) CD PSII (purple), and in (C) calcium-reconstituted PSII (cyan). In the right panel, all samples were in pH 6.0 buffer. In (D) PSII (red), in (E) PSII was treated with 200 mM ammonia; in (F) CD PSII (purple), and in (G), calcium-reconstituted PSII (cyan). (B1) is a baseline (S_1-minus-S_1) from dark-adapted PSII (black), and (B2) is a baseline (S_2-minus-S_2) after red-light illumination of PSII (blue). Spectra are averages of 5 (A), 3 (B), 5 (C),

6 (D), 7 (E), 5 (F) and 5 (G) samples. The spectral features induced by illumination are significant relative to dark-minus-dark controls (B1 and B2). Spectra are offset along the y axis for presentation purposes. The asterisk marks a contribution from CO_2.

To explore the origin of the pH 6.0 2740 cm^{-1} infrared signal in more detail, experiments were performed with the inhibitor, ammonia (Figure 2.2E). Manganese is oxidized during the S_1-to-S_2 transition in ammonia-treated PSII.[48, 60] Ammonia binds at two sites in the OEC.[30, 48, 60-61] At one of these binding sites, chloride competes with ammonia. The other binding site is the putative substrate-binding site. In addition to other modes of inhibition,[30, 47-48, 62-63] ammonia treatment has been shown to interrupt hydrogen bonding to OEC peptide carbonyl groups.[49] There is no evidence that ammonia treatment changes the spectroscopic properties of Q_A/Q_A^- or YD/YD•; these redox cofactors are relatively distant from the Mn_4CaO_5 cluster.[13]

Figure 2.3 presents a comparison of S_2-minus-S_1 RIFT-IR spectra at 190 K acquired from control (Figure 2.3D) and ammonia-treated (Figure 2.3E) PSII samples. As observed in Figure 2.3, addition of ammonia decreased the intensity of the 2740 cm^{-1} band at pH 6.0. Changes in the mid-infrared region were also observed (data not shown). Note that the effect of ammonia on oxygen evolution activity was reversible, as expected (see Methods and Table 2). In previous work, ammonia was reported to decrease in the intensity of the pH 7.5 signal at a higher temperature, 263 K.[37] The spectrum presented here shows that a similar ammonia effect is obtained at pH 6.0 and 190 K. This result supports assignment of the 2740 cm^{-1} band to the internal, hydrogen bonding network in the OEC.

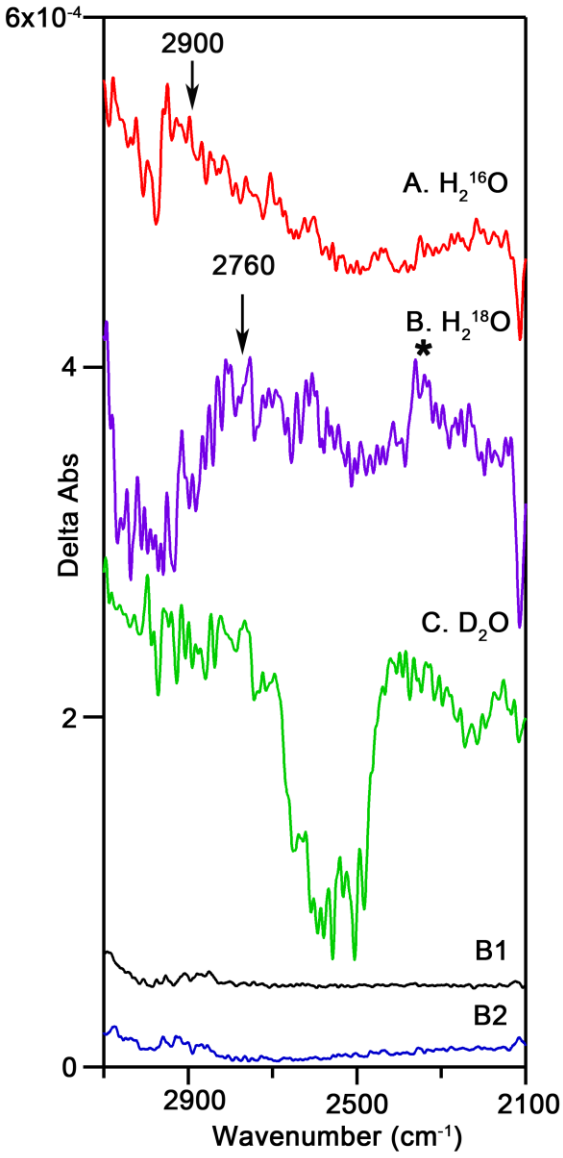

Figure 2.4 Reaction-induced FT-IR spectra (3100-2100 cm^{-1}) at 190 K, reflecting the S_1-to-S_2 transition and the effects of $D_2{}^{16}O$ and $H_2{}^{18}O$ buffer exchange. In (A) PSII in $H_2{}^{16}O$ buffer, in (B) PSII in $H_2{}^{18}O$ buffer and in (C) PSII in $D_2{}^{16}O$ buffer. (B1) is a baseline (S_1-minus-S_1) from dark-adapted PSII (black), and (B2) is a baseline (S_2-minus-S_2) after red-light illumination of PSII (blue). The total chloride concentration was 15 mM. Compared to samples employed in Figure 2.3, these samples were pelleted and resuspended an additional time in order to facilitate exchange. In addition, samples were annealed at room temperature, and four sets of data were obtained per sample. The four data sets were indistinguishable, given the signal to noise. Annealing had no effect on the PSII preparation as judged by steady state activity measurements[41] or gel electrophoresis.[64] Spectra are average of 11 (A), 6(B), and 14 (C) data sets. Spectra are offset along the y axis for presentation purposes. The asterisk marks a contribution from CO_2.

To determine the origin of the 2740 cm^{-1} band, solvent isotope exchange was employed at pH 6.0. Figure 2.4A present data on a PSII control in $H_2{}^{16}O$ buffer; a positive 2,900 cm^{-1} band was observed. The shift in band frequency, from 2740 cm^{-1} in Figure 2.3D to 2900 cm^{-1} in Figure 2.4A, is attributable to the difference in sodium chloride concentration in the two experiments (255 mM and 15 mM, respectively). This shift in frequency is further documented in Figure 2.5, in which the band shift can be seen in individual date sets, before the final average is performed. Chloride has previously been proposed to influence proton release.[29, 65] We attribute this NaCl-induced frequency shift to a change in electrostatic interactions in the proton exit pathway.

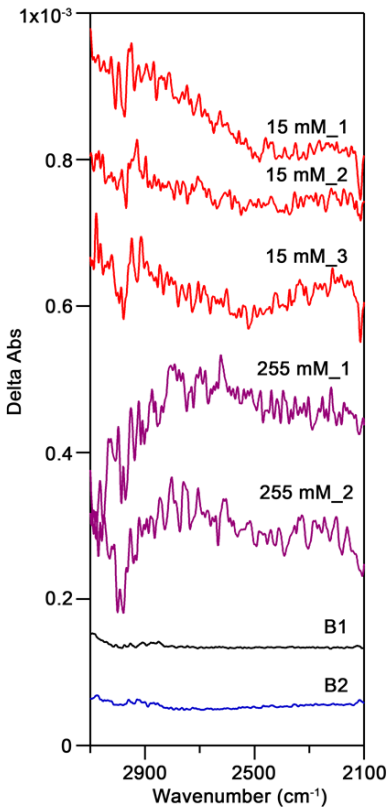

Figure 2.5 NaCl concentration effects on the RIFT-IR spectra of the S_1-to-S_2 transition (3100-2100 cm^{-1}). Data were recorded at 190 K from native PSII (in pH

6.0, SMN buffer) at the total chloride concentration shown (either 15 mM chloride or 255 mM chloride). Each replicate shown above is the average of 3 or 4 trials; the trials were chosen randomly from the total data set. (B1) is a baseline (S_1-minus-S_1) from dark-adapted PSII (black), and (B2) is a baseline (S_2-minus-S_2) after red-light illumination of PSII (blue). Spectra are offset along the y axis for presentation purposes. See Methods for details.

When exchanged into $D_2{}^{16}O$ buffer, the broad 2,900 cm^{-1} feature was eliminated (Figure 2.4C) presumably due to a shift into a region dominated by bulk $D_2{}^{16}O$ absorption. When exchanged into $H_2{}^{18}O$ buffer (Figure 2.4F), the broad 2,900 cm^{-1} band shifted down 140 cm^{-1} to 2760 cm^{-1} (Figure 2.4B). The results of these $D_2{}^{16}O$ and $H_2{}^{18}O$ solvent exchange experiments unambiguously support assignment of the 2740 cm^{-1} band to a vibrational mode of water. In the 2900 cm^{-1} spectral region, the most likely assignment of a water band is to a hydronium ion stretching mode in a small protonated water cluster, $nH_2O(H_3O^+)$.[37-38, 66]

As the next step, PSII samples were calcium-depleted (Figure 2.2B). This treatment inhibits oxygen evolution, disrupts hydrogen-bonding interactions in the OEC (Figure 2.1A), and leads to a substantial change in the mid-IR region of the S_2-minus-S_1 spectrum at pH 7.5.[46] There is no evidence that calcium removal changes the spectroscopic properties of Q_A/Q_A^-[67] or YD/YD•. As shown, at pH 7.5, calcium depletion eliminated the broad signal at 2740 cm^{-1}, observed at 255 mM chloride (Figure 2.3B). A similar result was reported at 263 K.[37] At pH 7.5, calcium reconstitution (Figure 2.2C) was observed to restore the signal (Figure 2.3C). However, at pH 6.0, calcium depletion/reconstitution (Figure 2.2C) did not alter the intensity of the 2740 cm^{-1} band (compare Figure 2.3F and G), although oxygen evolution assays provide evidence for a similar calcium depletion efficacy at pH 6.0 and 7.5 (Table 1). We conclude that calcium is not necessary for

observation of the 2740 cm^{-1} band of $nH_2O(H_3O^+)$ at pH 6.0, but is required for the formation or retention of the band at pH 7.5.

2.4.3 The 1800-1150 cm^{-1} Region of the RIFT-IR Spectrum, and Hydrogen Bonding to OEC Peptide Carbonyl Groups.

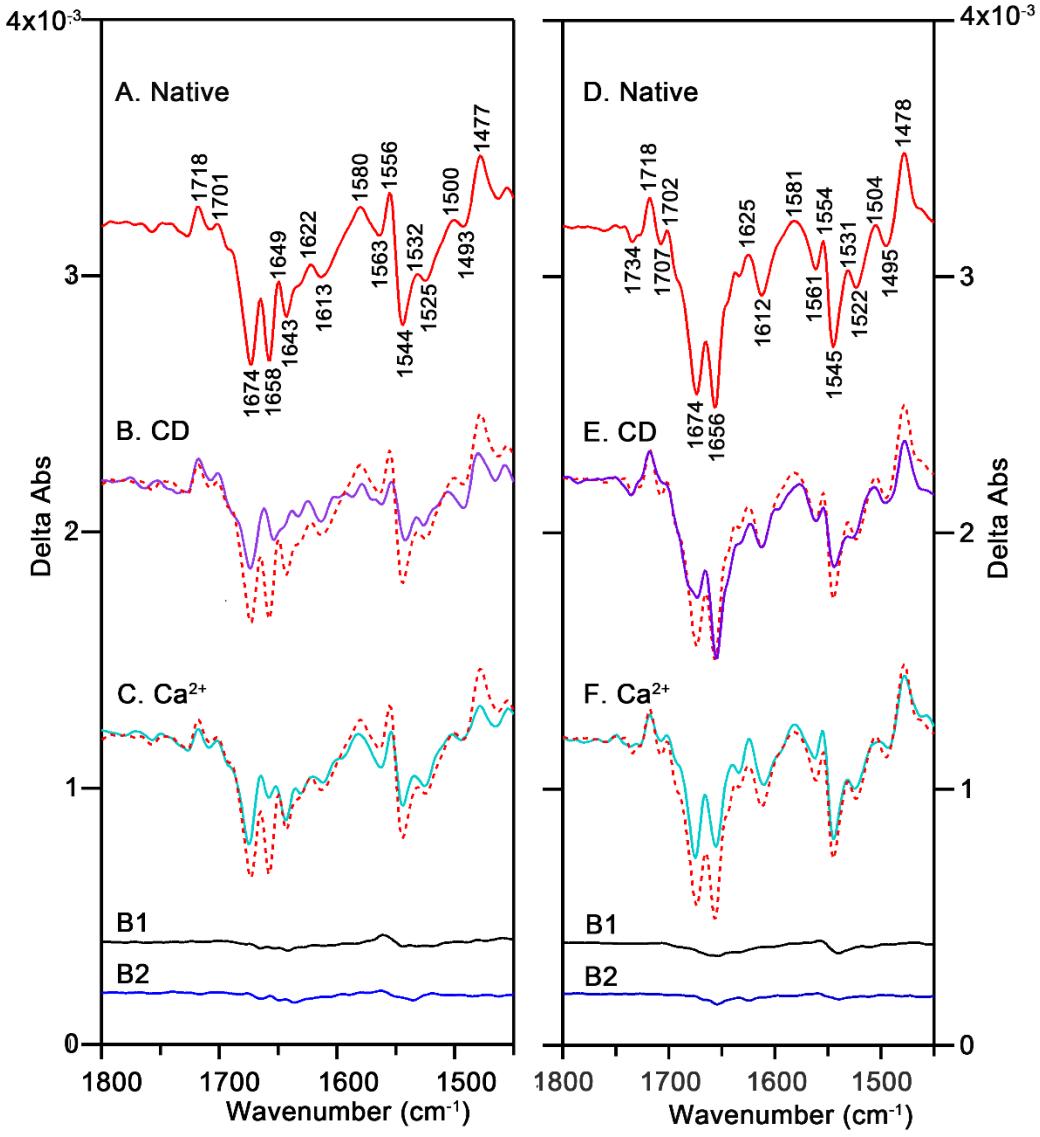

Figure 2.6 Reaction-induced FT-IR spectra (1800-1450 cm^{-1}) at 190 K, reflecting the S_1-to-S_2 transition and the effects of pH, calcium depletion and calcium reconstitution. The total chloride concentration was 255 mM. In the left panel, samples were in pH 7.5 buffer. In (A, solid and B, C dashed) PSII (red), in (B) CD

PSII (purple), and in (C) calcium-reconstituted PSII (cyan). In the right panel, samples were in pH 6.0 buffer. In (D, solid and E, F, dashed) PSII (red), in (E) CD PSII (purple), and in (F) calcium-reconstituted PSII (cyan). (B1) is a baseline (S_1-minus-S_1) from dark-adapted PSII (black), and (B2) is a baseline (S_2-minus-S_2) after red-light illumination of PSII (blue). Spectra are averages of 5 (A), 3 (B), 5 (C), 6 (D), 5 (E), and 5 (F) samples. The spectral features induced by illumination are significant relative to dark-minus-dark controls (B1 and B2). Spectra are offset along the y axis for presentation purposes.

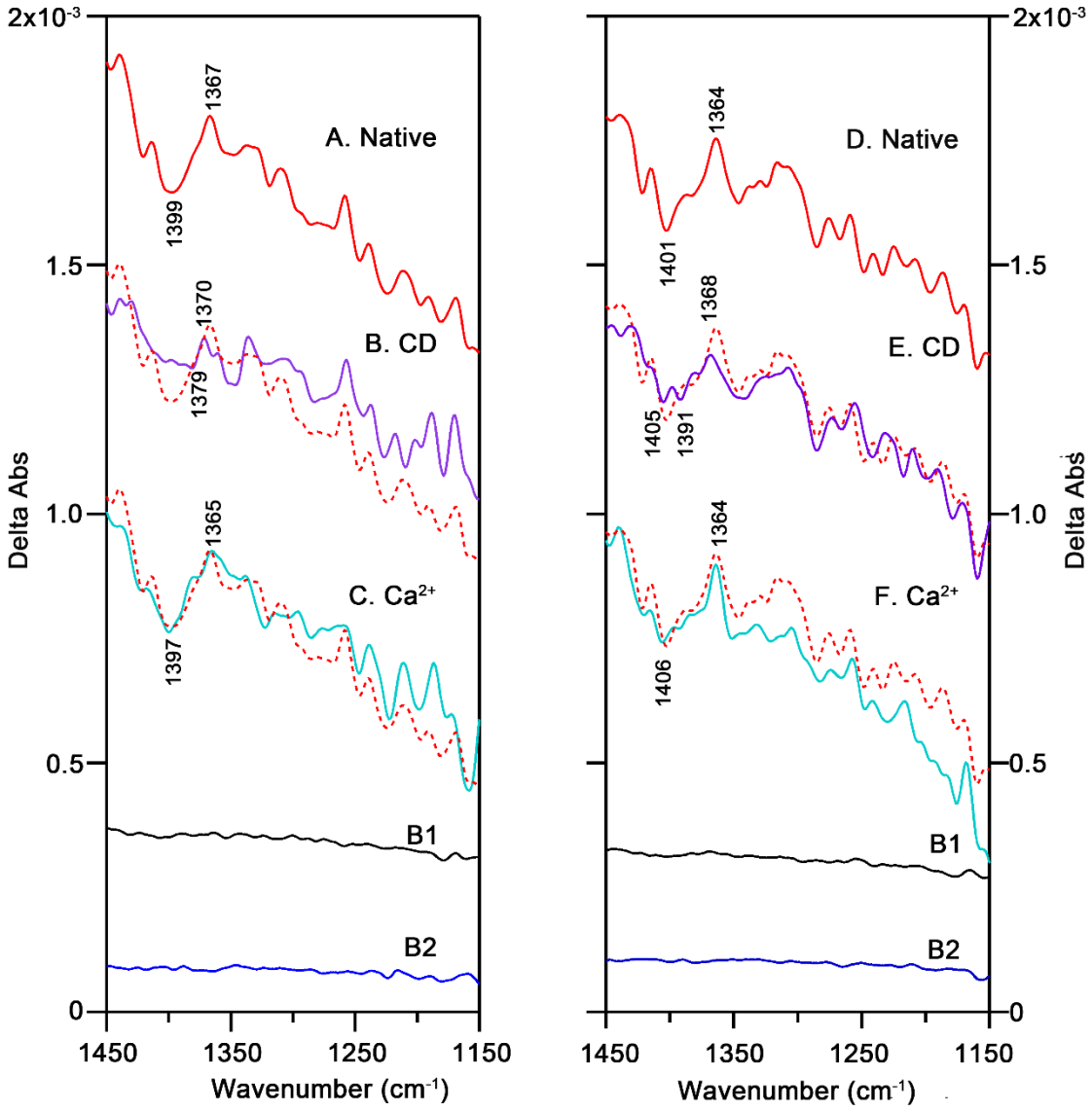

Figure 2.7 Reaction-induced FT-IR spectra (1450-1150 cm^{-1}) at 190 K, reflecting the S_1-to-S_2 transition and the effects of pH, calcium depletion and calcium reconstitution. The total chloride concentration was 255 mM. In the left panel, samples were in pH 7.5 buffer. In (A, solid and B, C dashed) PSII (red), in (B) CD

PSII (purple), and in (C) calcium-reconstituted PSII (cyan). In right panel, all samples were in pH 6.0 buffer. In (D, solid and E, F dashed) PSII (red), in (E) CD PSII (purple), and in (F) calcium-reconstituted PSII (cyan). (B1) is a baseline (S_1-minus-S_1) from dark-adapted PSII (black), and (B2) is a baseline (S_2-minus-S_2) after red-light illumination of PSII (blue). Spectra are averages of 5 (A), 3 (B), 5 (C), 6 (D), 5 (E), and 5 (F) samples. Spectra are offset along the y axis for presentation purposes.

To define this pH difference, we turned our attention to the mid-infrared region of the spectrum. A comparison of the 1800-1150 cm^{-1} regions at pH 6.0 and 7.5 in native PSII is presented in Figure 2.6A and Figure 2.7A. To summarize some of the previous vibrational assignments in this region, Q_A absorbs at 1650 cm^{-1}, as assessed by UV Raman[68] and RIFT-IR spectroscopy.[69] Q_A^- absorbs at 1482 cm^{-1}, as assessed by isotopic labeling and RIFT-IR spectroscopy.[69-70] In PSII samples that do not contain phosphate and formate, YD radical absorbs at 1473-1477 cm^{-1}, depending on the pH.[55, 71-72] The proton donor/acceptor, His189-D2, for YD gives rise to spectral contributions in the 3350-3250 cm^{-1} region, reflecting the strongly hydrogen-bonded imidazole/imidazolium cation and the effects of proton transfer from protonated histidine to tyrosyl radical.[54] Bands at ~1365/1405 cm^{-1} have been attributed to carboxylate ligand contributions, perturbed by oxidation of manganese during the S_1-to-S_2 transition. This assignment was based on depletion of calcium at pH 3.[73] However, it was also reported that there was no significant change in those bands when EGTA was used to remove calcium.[74] Supporting a carboxylate assignment for some of the bands in the 1710 and 1390 cm^{-1} regions, the DE170D1 mutation was shown to alter these regions of the 190 K S_2-minus-S_1 spectrum.[75] Other possible assignments of infrared bands throughout the 1700-1150 cm^{-1} region are to amide (amide I, II, and III) vibrational modes, which are altered by hydrogen bonding and secondary structural changes during the S state transition.[49]

As shown in Figure 2.6B and E, depletion of calcium altered the amide I (1650 cm^{-1}) and amide II (1550 cm^{-1}) regions of the spectrum, either at pH 6.0 or 7.5. The frequencies and intensities of these bands are expected to be sensitive to backbone hydrogen-bonding interactions.[46, 74] Reconstitution of calcium partially restored the amide II region either at pH 6.0 or 7.5 (Figure 2.6C and F). Reconstitution-induced changes in the amide I region were also observed. Observation of spectral changes induced by calcium depletion supports the interpretation that EGTA-treatment is effective in calcium removal. The majority of the spectrum recovered with calcium reconstitution. Lack of complete restoration at 1658 cm^{-1} may be attributable to a small change in water structure after calcium reconstitution, because water has an overlapping OH bending mode in this region.

At both pH values, calcium depletion decreased intensity at 1397/1365 or 1406/1364 cm^{-1} (Figure 2.7B and E), although the extent of the change was greater at pH 7.5 (Figure 2.7B). At both pH values, calcium reconstitution restored intensity and frequency in this region (Figure 2.7C and F). Taken together, these observations agree with previous reports[46, 73-74] and are consistent with calcium-induced alterations in the hydrogen-bonding network at both pH values.

To summarize, calcium removal is efficacious at pH 6.0 and 7.5, as assessed either by oxygen assays (Table 1) or the mid-infrared region of the spectrum (Figure 2.6 and Figure 2.7). However, as discussed above, calcium depletion at pH 6.0 did not significantly alter 2740 cm^{-1} band intensity, while calcium depletion at pH 7.5 did disrupt the 2740 cm^{-1} band. We conclude that generation or retention of the 2740 cm^{-1} signal depends on occupancy at the calcium site at pH 7.5, but calcium is not required to form the signal at pH 6.0.

Note that when pH 6.0 and 7.5 mid-infrared regions are compared to each other, the spectra are distinct. An additional amide I feature is observed at 1649 (positive) and 1643 (negative) cm^{-1} (compare Figure 2.6A and C) at pH 7.5. This band is not observed at pH 6.0. Instead, there was increased intensity at 1625 (positive)/1612 (negative) cm^{-1} in the pH 6.0 spectrum. Other distinctions are also observed in relative intensities in the 1674-1658 and 1580-1550 cm^{-1} regions. This result suggests that pH titration produces distinct hydrogen bonding environments in the OEC. In this pH range, this is likely due to protonation of amino acid side chains, such as histidine, in the hydrogen bonding network.

2.4.4 The 3700-3550 cm^{-1} Region of the RIFT-IR Spectrum, Reflecting the Hydrating Water Shell and OH Stretching Modes of Water.

In gas phase studies of $nH_2O(H_3O^+)$ clusters, the vibrational spectrum of water molecules in the first coordination shell (nH_2O) of the hydronium core $(H_3O)^+$ was defined.[38] Those "dangling" first shell water molecules had OH stretching vibrations in the 3600 cm^{-1} region. The intensity of these bands relative to the intensity of the hydronium stretching vibration was relatively low. Therefore, protonation of the internal water cluster in PSII may give rise to differential features, due to frequency shifts of water OH stretching bands in the 3600 cm^{-1} region.

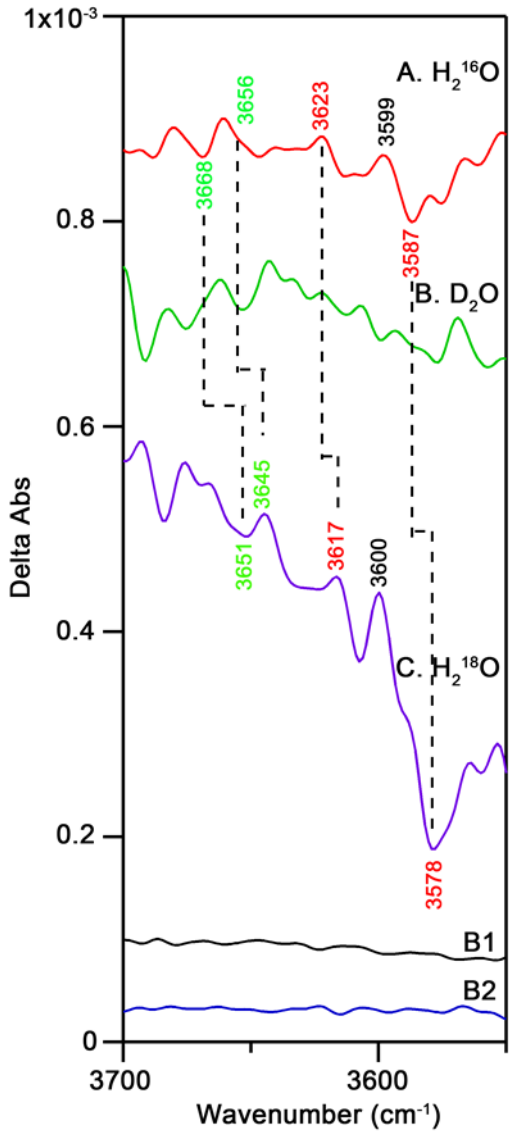

Figure 2.8 Reaction-induced FT-IR spectra (3700-3550 cm^{-1}) at 190 K, reflecting the S_1-to-S_2 transition and the effects of $D_2{}^{16}O$ and $H_2{}^{18}O$ buffer exchange. In (A) PSII in $H_2{}^{16}O$ buffer, in (B) PSII in $D_2{}^{16}O$ buffer, and in (C) PSII in $H_2{}^{18}O$ buffer. (B1) is a baseline (S_1-minus-S_1) from dark-adapted PSII (black), and (B2) is a baseline (S_2-minus-S_2) after red-light illumination of PSII (blue). The total chloride concentration was 15 mM. Spectra are average of 11 (A), 6 (B) and 14 (C) data sets. See Figure 2.4 legend for additional details. Spectra are offset along the y axis for presentation purposes.

To investigate whether such a hydrating water shell contributes to the S_1-to-S_2 spectrum, the effects of $D_2{}^{16}O$ and $H_2{}^{18}O$ exchange on the 3700-3550 cm^{-1} region were

investigated. These data are shown in Figure 2.8. The control, native PSII (Figure 2.8A), was maintained at a chloride concentration of 15 mM, and the sample was buffered at pH 6.0. In Figure 2.8A, bands are observed throughout the 3700 to 3550 cm^{-1} region, which are significant relative to the baseline (Figure 2.8, B1 and B2). With $D_2{}^{16}O$ exchange, OH bands of water are expected to decrease in intensity and shift out of this spectral region to ~2500 cm^{-1}. With $H_2{}^{18}O$ exchange, OH bands of water are expected to exhibit a small ~10 cm^{-1} shift.[76]

In Figure 2.8, three bands are candidates to be assigned to water(s) OH stretching modes, based on criteria described above. These candidates are negative 3668 (green label), positive 3623 (red label), and negative 3587 (red label) cm^{-1}. These bands were not observed in Tris-washed PSII, supporting assignment to the OEC (data not shown). These bands shifted out of this spectral region when $H_2{}^{16}O$ and $D_2{}^{16}O$ samples were compared (Figure 2.8A and B), and exhibited small shifts to 3651 (17 cm^{-1}), 3617 (6 cm^{-1}), and 3578 cm^{-1} (9 cm^{-1}) with $H_2{}^{18}O$ solvent exchange. A positive band, observed at 3645 cm^{-1} in $H_2{}^{18}O$ buffer, may originate at positive 3656 cm^{-1} (shoulder, green label), corresponding to an isotope shift of 11 cm^{-1}. This experiment definitively assigns these bands to the OH stretching vibration of water molecules in the OEC. Note that other, small, D_2O induced spectral changes were also observed in this region.

Figure 2.9 presents the effect of pH 6.0 ammonia treatment, calcium depletion, and calcium reconstitution on this 3700-3550 cm^{-1} region. In generating Figure 2.9, experiments were conducted at pH 6.0, but at a higher sodium chloride concentration, compared to Figure 2.8. This is necessary for comparison to the ammonia experiment, in which chloride is the counterion. Note that the addition of sodium chloride had an effect

on the background in this region, but the frequencies of the observed bands were similar at the two sodium chloride concentrations.

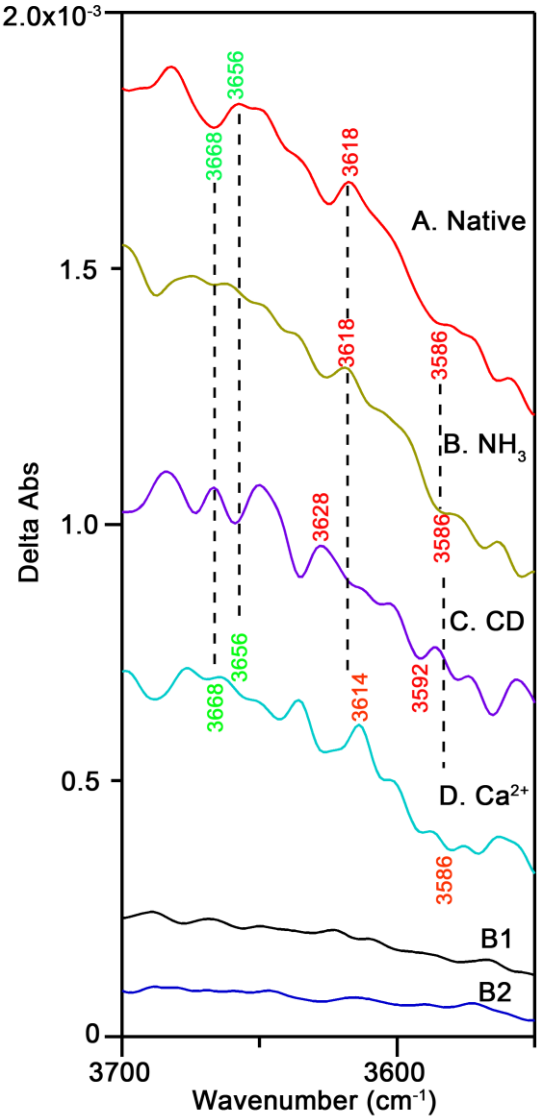

Figure 2.9 Reaction-induced FT-IR spectra (3700-3550 cm^{-1}) at 190 K, reflecting the S_1-to-S_2 transition and the effects of ammonia treatment, calcium depletion, and calcium reconstitution at pH 6.0. The total chloride concentration was 255 mM. In (A) PSII (red), in (B) PSII were treated with 200 mM ammonia, in (C) CD PSII (purple), and in (D) calcium-reconstituted PSII (cyan). (B1) is a baseline (S_1-minus-S_1) from dark-adapted PSII (black), and (B2) is a baseline (S_2-minus-S_2) after red-light illumination of PSII (blue). Spectra are averages of 6 (A), 7 (B), 5 (C), and 5 (D) samples. As shown, the spectral features induced by illumination are significant relative to dark-minus-dark controls (B1 and B2). Spectra are offset along the y axis for presentation purposes.

The 3668 cm^{-1} and 3656 cm^{-1} bands, observed at 15 mM sodium chloride, were also observed at 255 mM sodium chloride with the same frequencies (Figure 2.9A, green labels, native PSII). The intensities of these bands decreased with ammonia addition (Figure 2.9B, green). Therefore, these bands may arise from OH stretching modes in the ammonia-sensitive $nH_2O(H_3O^+)$ cluster. The frequencies/intensities of these bands were altered by removal of calcium at pH 7.5 (data not shown). Interesting, changes in this region (3668/3656 cm^{-1}) are observed with calcium depletion at pH 6.0 (Figure 2.9C), although this treatment did not alter the hydronium ion stretching band at 2740 cm^{-1} (Figure 2.3B). However, spectral changes observed with calcium depletion could be due to overlap with new spectral bands, which are shifted into this region with calcium depletion. Reconstitution of calcium altered frequencies and intensities, but did not completely restore the original spectrum (Figure 2.9D, green).

Analogs of the 3623 and 3587 cm^{-1} bands, discussed at 15 mM sodium chloride, were also observed at 255 mM chloride, with positions slightly shifted to 3618/3586 cm^{-1} (Figure 2.9A, red labels). The band positions were not altered by addition of ammonia at pH 6.0 (Figure 2.9B, red labels). The lack of ammonia sensitivity reveals that these bands are not likely to be linked to protonation of the internal water cluster. The frequencies of these bands appeared to be sensitive to calcium depletion and reconstitution. We conclude that these OEC water bands contribute to the S_2-minus-S_2 spectrum due to distinct perturbative mechanism, which is discussed below.

2.4.5 The effect of Strontium Reconstitution on the 3100-2100 cm^{-1} Region.

Strontium reconstitution is known to support oxygen evolution.[25] The X-ray structure of strontium-reconstituted PSII reveals no large ligation changes, but small changes in

hydrogen bonding with water were reported.[31] Such changes are expected due to the larger ionic radius of strontium and the higher pK_a of strontium-bound water.[25] To investigate the effect of strontium on the 2740/2900 cm^{-1} band and the $nH_2O(H_3O^+)$ cluster, we reconstituted strontium, instead of calcium, into CD PSII. As expected,[57] strontium-reconstituted PSII exhibited increased activity compared to CD PDII. In strontium-reconstituted PSII, >80% of the calcium-reconstituted oxygen evolution rate was obtained (Table 1).

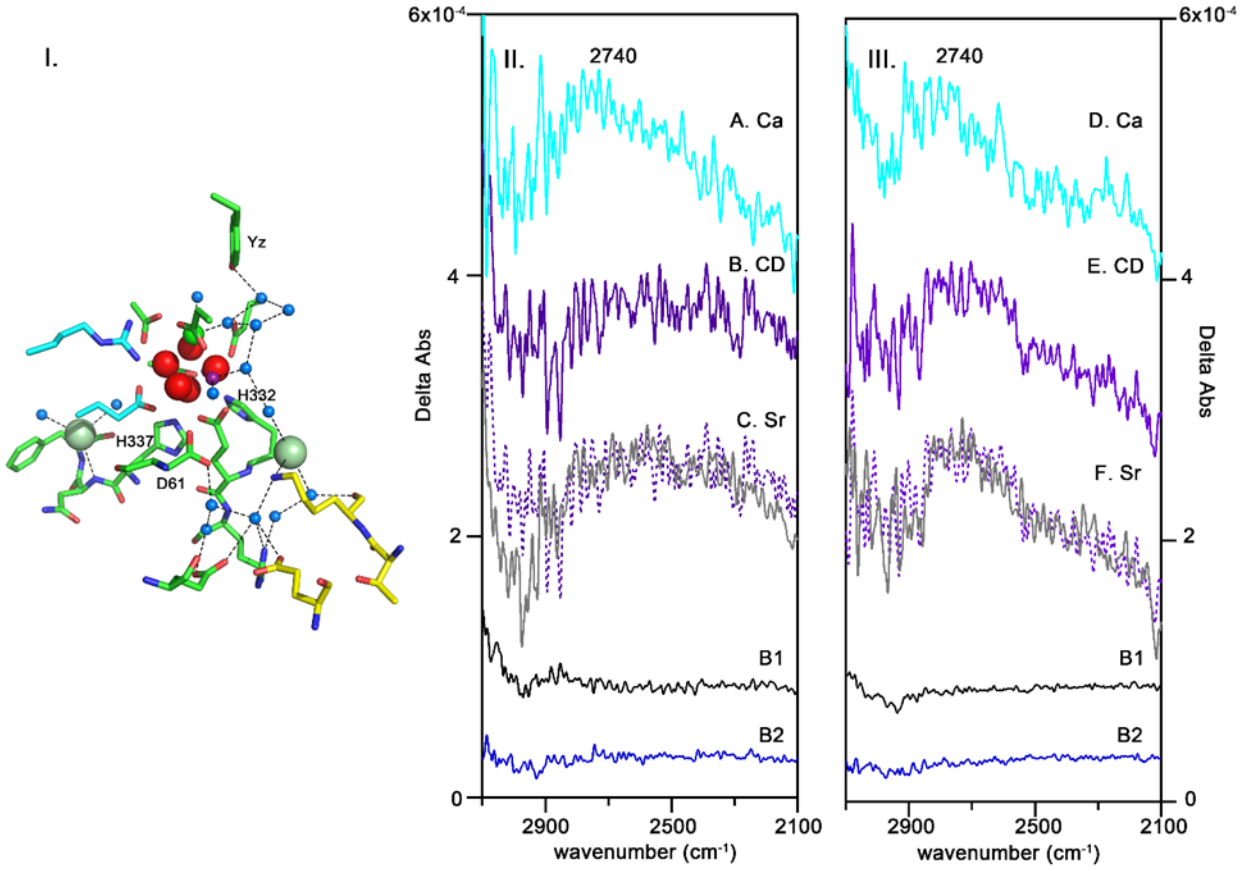

Figure 2.10 Panel (I): Proposed proton exit pathway in photosystem II.[12] The selected amino acids shown are: D1: Tyr161, Asp170, Glu189, His332, Glu333, Arg334, His337, Asn338, Phe339, Asp342, Ala344; CP43: E354, R357; D2: Glu312, Thr316, Lys317. Also, shown are two chloride ion (pale green), selected water molecules (blue), oxygens (red), calcium (green), and manganese (magenta, PDB ID: 4UB6).[13] Panel (II and III): Reaction-induced FT-IR spectra (3100-2100 cm^{-1}) at 190 K, reflecting the

S_1-to-S_2 transition and the effects of calcium reconstitution (A and D), calcium depletion (B and E), and strontium reconstitution (C and F). The total chloride concentration was 255 mM. In panel II, all samples were in pH 7.5 buffer. In (A) calcium-reconstituted PSII (cyan), in (B, solid and C, dotted) CD PSII (purple), and in (C) strontium-reconstituted PSII (grey). In panel III, all samples were in pH 6.0 buffer. In (D) calcium-reconstituted PSII (cyan), in (E, solid and F, dotted) CD PSII (purple), and in (F) strontium-reconstituted PSII (grey). (B1) is a baseline (S_1-minus-S_1) from dark-adapted PSII (black), and (B2) is a baseline (S_2-minus-S_2) after red-light illumination of PSII (blue). Spectra are averages of 5 (A), 3 (B), 5 (C), 5 (D), 5 (E) and 8 (F) samples. The spectral features induced by illumination are significant relative to dark-minus-dark controls (B1 and B2). Spectra are offset along the y axis for presentation purposes.

Figure 2.10C, panel II shows that strontium reconstitution at pH 7.5 does not support the observation of the 2740 cm^{-1} band, which is decreased in intensity in CD PSII (Figure 9B, panel II) and supported by calcium reconstitution at this pH (Figure 2.10A, panel II). However, at pH 6.0, neither calcium depletion (Figure 2.10E, panel III) nor strontium replacement (Figure 2.10F, panel III) altered the hydronium ion infrared signal, compared to the calcium-reconstituted sample (Figure 2.10D, panel III). This observation is in agreement with previous results. For example, it was reported that, at pH 6.0, strontium supports a broad 2900-2200 cm^{-1} band associated with the S_1-to-S_2 transition at 283 K.[77] On the other hand, at pH 7.5, strontium reconstitution did not support detection of the 2880 cm^{-1} band at 263 K.[78] This pH dependence suggests a possible pH-induced change in the localization of the protonated water cluster, as discussed below.

2.5 Discussion

Previously, water has been proposed to participate in internal proton transfer reactions in proteins, such as bacteriorhodopsin,[5-7] cytochrome c oxidase[9, 11] and carbonic anhydrase.[10] In bacteriorhodopsin, infrared spectroscopy has provided an incisive probe of water dynamics.[5-7]

Here, we use infrared spectroscopy to provide new information concerning the role of internal water in PSII proton transfer. Previously, we detected a new infrared signal from an internal, protonated water cluster in the PSII S_2 state under conditions in which S state cycling can occur.[37] In the work reported here, we show that this S_2 signal can also be photoaccumulated under cryogenic conditions as a broad, absorptive 2740/2900 cm^{-1} band. We unambiguously assign this band to a normal mode of water through the use of $D_2{}^{16}O$ and $H_2{}^{18}O$ solvent exchange. Gas phase studies have shown that the asymmetric stretch of the hydronium core (H_3O^+) can absorb in the ~2900-2700 cm^{-1} region. Moreover, the frequency is known to be cluster size dependent.[38] The closest frequency match, when comparing this work to those gas phase studies, is to a cluster size of 4 or 5. The large $H_2{}^{18}O$-induced shift, reported here, can be rationalized if changes in protonated water cluster size accompany $H_2{}^{18}O$ exchange. For example, for gas phase water clusters with sizes of 4-8, an increase in H_3O^+ stretching frequency was associated with an increase in cluster size.[38] Therefore, we interpret the large, apparent isotope shift as support for the assignment to a protonated water cluster. Similarly, the significant frequency shift, from 2740 to 2900 cm^{-1}, observed with changes in ionic strength, is attributable to an effect of electrostatic interactions on cluster size and a change in localization in the network. Previously, it has been shown that ionic strength alters carbonyl frequencies in FT-IR experiments, attributable to hydrogen bonding changes in the OEC network.[49]

The assignment of the 2900/2740 cm^{-1} bands to a protonated water cluster is also supported by comparison to infrared studies of bacteriorhodopsin. In bacteriorhodopsin, protons are transferred across the bacterial membrane in response to light absorption. An internal hydrogen-bonded water network has been proposed to participate in proton

transfer.[5-7] A broad infrared band between 2750 and 2540 cm^{-1} has been observed and has been proposed to derive from a water cluster, which acts as a transient proton transfer wire.[79] Theoretical simulations have supported this interpretation of the spectrum and the role of water in the proton transfer process.[7]

The assignment of the PSII 2740/2900 cm^{-1} band to the asymmetric stretch of a protonated water cluster is preferred over an assignment to a hydrogen bonded water molecule or to a proton prolarizability band. The frequency and isotope shift of the band are not consistent with assignment to a hydrogen bonded water molecule.[80] For example, in matrix isolation studies and the infrared predissociation spectrum, it was shown that hydrogen bonded water dimers exhibit downshifted OH stretching frequencies, but still absorb in the 3700-3500 cm^{-1} region.[81-83] Also, if the 2740 cm^{-1} band arises from a hydrogen bonded water molecule, $H_2{}^{18}O$ shifts of only ~10 cm^{-1} are expected.[76] Similarly, the observation of the large $H_2{}^{18}O$ isotope shift in our experiments is not consistent with assignment to a proton polarizability band.[84]

Using this 2740 cm^{-1} infrared marker, we report new information concerning proton transfer and the S_2 state of the photosynthetic water oxidizing cycle. The S_2 state can be trapped under illumination at 190 K. Other S state transitions are blocked at this temperature, but the S_2 state is formed with oxidation of the metal cluster and transfer of an electron to Q_A.[53] Our results demonstrate that proton transfer to an internal water cluster occurs at 190 K and must be tightly linked to the oxidation of the metal cluster. Therefore, we propose that the protonated water cluster is an intermediate in the S_1-to-S_2 reaction. Water ligands or hydroxide ligands are candidates to serve as the proton donor to the

internal water cluster under these conditions,[24, 27] but the proton could also originate from an oxidation-induced pK_a shift of an amino acid side chain.

In the crystal structure of cyanobacterial PSII, two water molecules, W1 and W2, are bound to manganese, and 2 water molecules, W3 and W4 are bound to calcium. PSII X-ray structures[12-13] also reveal extensive hydrogen bonded networks, involving water and amino acid side chains, which link these water molecules to the thylakoid lumen (Figure 2.10, panel I). These potential proton transfer pathways include chloride ions. Interestingly, the S_2 state has been proposed to have two structural forms that are associated with two different EPR signals. In the open form, O5 binds to Mn4 and gives rise to a S_2 multiline signal. In the closed form, O5 shifts to Mn1, producing a g=4.1 EPR signal.[23-24] The two forms are predicted to be nearly isoenergetic and can be interconverted by a variety of treatments.

Ammonia is a substrate water analog and has been shown to be an inhibitor of this PSII preparation either at pH 6.0 or pH 7.5.[49] Ammonia binds to two sites in PSII, one of which competes with chloride[47] and one of which is assumed to be the substrate-binding site.[48, 60, 63] Ammonia binding to the non-chloride sensitive site modifies the S_2 multiline signal, but the modification is detected only at temperatures over 190 K.[48, 60] Ammonia binding to the chloride-dependent site has been reported to stabilize the g=4.1 signal.[30, 48, 85] In RIFT-IR spectroscopy on PSII, frequency shifts of peptide carbonyl group were observed with ammonia treatment. These frequency shifts occur both at 190 K (this work, data not shown) and at 263 K.[49] In the experiments reported here, addition of ammonia disrupts the 190 K 2740 cm^{-1} signal. The disruption of the 2740 cm^{-1} band is attributed to an alteration in amide hydrogen bonding, which destabilizes the protonated water cluster.

This interpretation supports assignment of the 2740 cm^{-1} infrared band to the internal water-containing network. The effect of increasing sodium chloride is also consistent with the assignment to a small, protonated water cluster in an internal network, which is altered by ionic strength. A detailed analysis of the ionic strength-induced change awaits future studies.

RIFT-IR spectroscopy in the 3600 cm^{-1} region can be complicated by contributions from water vapor and potential, high absorption from bulk water. In this region, published S_2-minus-S_1 spectra from different laboratories exhibit differences in frequency and intensity, which have previously been discussed and attributed to differences in humidity and preparation type in different laboratories.[84] In published work from other groups, samples were dehydrated and then rehydrated.[80] These treatments may disrupt the native water network. Also, some experimental protocols involved multiple loops to cycle PSII at higher temperatures, which can lead to PSII damage.[80]

In our experiments, we use highly hydrated samples that have never been dehydrated. We also document a sensitivity to ionic strength, which must be controlled in comparing results. In addition, spectra are constructed from data acquired after continuous illumination, improving the baseline in the 3600 cm^{-1} spectral region. A temperature of 190 K was employed. As a result of solvent exchange under these conditions, bands at negative 3668, positive 3623, and negative 3587 cm^{-1} are assigned here to OH stretching modes of OEC water. A positive 3656 (shoulder) cm^{-1} band is also a candidate to be assigned to OEC water. Of these, one negative/positive pair is sensitive to ammonia (3668/3656 cm^{-1}), while the other positive/negative pair is not sensitive to ammonia treatment at 190 K (3623/3587 cm^{-1}). We assign the 3668/3656 cm^{-1} bands to OH stretching bands, which may be derived

from the hydrating shell of the hydronium cation. This is the first report of frequencies of OH stretching modes, which arise from nH_2O in the $nH_2O(H_3O^+)$ cluster. These bands were not observed at higher temperature in our earlier report.[37] The other OH stretching pair must arise from one or more additional water molecules, perturbed via a distinct mechanism during this transition. Note that bands arising from water(s) are expected to be strongly coupled, representing OH atomic displacements of multiple water molecules.[7]

To compare to previous S_2-minus-S_1 spectral assignments in the 3600 cm^{-1} region, bands at ~3618 and ~3585 cm^{-1} have been assigned to an "active" water in PSII, which is perturbed by a change in hydrogen bonding during the S_1-to-S_2 transition.[86] The band at ~3663 cm^{-1} has been previously assigned to a water molecule near a chloride ion, on the basis of site directed mutagenesis.[84] It has been suggested previously that a positive 3658 cm^{-1} band may arise from water near Q_A^-.[87] The OEC-derived bands, assigned here on the basis of sensitivity to ammonia, Tris, and calcium depletion, could overlap such a band from a Q_A^- water.[87]

Our experiments show that proton transfer to water occurs either at pH 6.0 or 7.5 during the S_1-to-S_2 transition. This is significant because this pH change alters PSII activity,[45] but the structural reasons for these effects are not understood. Thermophilic cyanobacterial structures were determined at pH 6.5.[12-13] Under illumination, the plant lumen is acidic due to trans-thylakoid proton transfer.[88] High pH has been reported to decrease the affinity for chloride and thus slow the rate of the S state transitions.[45, 89] The binding affinities of the PsbP and PsbQ subunits also decrease at pH 7.5.[43-44] The detailed pH dependence of S state transition has been investigated by various techniques such as oscillation of oxygen yield,[90-91] flash-induced fluorescence,[91] and EPR[92-95] spectroscopy.

It was reported that induction of S_2 multiline EPR signal is pH independent.[92] Additional experiments concluded that the S_1-to-S_2 transition efficiency is independent of pH from 4.1-8.4.[94-95] It was reported that the probability of double hits is pH-independent while the miss parameter is strongly influenced by pH and is minimal at neutral pH.[90-91] Additional studies concluded that there were two distinct effects on PSII at high pH. One is reversible due to chloride displacement, and the other is irreversible due to loss of Mn.[90, 93] Note that irreversible loss of Mn does not occur under the pH 7.5 conditions employed here, as documented by the similar rates of oxygen evolution after pH 7.5 and 6.0 incubation (Table 1). Previously, the reversible effect of high pH treatment was attributed to protonation/deprotonation of amino acid residues that are essential for the catalytic cycle.

Our experiments document a pH-dependent calcium effect, which is likely to be caused by such protonation/deprotonation events. Calcium binds water in the hydrogen bonding network in the X-ray structure and is required for oxygen evolution activity. Both EPR and EXAFS studies suggest that the overall structure of OEC remains the same after calcium removal.[96-98] Based on the PSII structure, the expectation is that calcium depletion will disrupt hydrogen-bonding interactions in a proton transfer network. For example, it has been proposed that a water/bridging oxo ligand protonation event will occur when calcium is removed.[99]

Our results show that the effect of calcium on protonation or retention of the $nH_2O(H_3O^+)$ cluster is pH dependent. Calcium is not required to observe the 2740 cm^{-1} band at pH 6.0, but is required at pH 7.5. This difference could be caused either by a failure to form the cluster or by faster decay of the protonated cluster at pH 7.5. Such differences between the pH 6.0 and 7.5 samples are likely due to protonation of an amino acid residue

at pH 6.0. In the pH range employed, protonation of a histidine side chain would be a likely trigger for this change in the pathway. A candidate for this histidine is His337 in the D1 polypeptide (Figure 2.10, panel I). This histidine has been proposed to sample either a positively charged imidazolium cation or a neutral imidazole state during S state cycling.[99] Alternatively, the protonable group could be a carboxylate with a high pK_a. It has been proposed that during S_1-to-S_2 transition, a partial proton transfer occurs to D1-D61.[29] At this time, it is not known if the protonation of the internal water cluster is related to this putative aspartate protonation event. These hypotheses will be tested in future work.

The sensitivity of the $nH_2O(H_3O)^+$ band to strontium replacement at pH 7.5 is also notable, especially given the insensitivity of the band to calcium depletion and strontium replacement at pH 6.0. This observation suggests that the hydronium ion may localize in different parts of the hydrogen-bonded network at the two pH values. In this interpretation, the calcium-associated water molecules play an important role in interactions at pH 7.5, but are less critical to formation or stabilization of the hydronium ion at pH 6.0. Importantly, the amide regions of the RIFT-IR spectra presented here support the conclusion that there is a pH-induced conformational change in the OEC, which may also be caused by a side chain protonation event. This change could lead to an alteration in the localization of $nH_2O(H_3O^+)$ in the proton exit pathway.

2.6 Conclusions

Our experiments provide evidence that an internal water cluster acts as an intermediate and transiently stores a proton during the S_1-to-S_2 reaction. This protonation is observed at 190 K and at two different pH values. These data give new insight into the mechanism of OEC proton release, which must be carefully controlled to move the proton efficiently over the

~25 Å from the metal cluster to the lumen. Our experiments demonstrate the utility of the infrared signal as a probe of the protonation state of the $nH_2O(H_3O^+)$ cluster and emphasize the importance of calcium, pH, and internal water in proton transfer.

2.7 References

1. Schuster, P.; Zundel, G.; Sandorfy, C., In *Hydrogen Bond; Recent Developments in Theory and Experiments*, North-Holland Publishing Company: Amsterdam, Netherlands, 1976.

2. Knight, C.; Voth, G. A., The Curious Case of the Hydrated Proton. *Acc. Chem. Res.* **2012,** *45* (1), 101-9.

3. Kulig, W.; Agmon, N., A 'Clusters-in-Liquid' Method for Calculating Infrared Spectra Identifies the Proton-Transfer Mode in Acidic Aqueous Solutions. *Nat. Chem.* **2013,** *5* (1), 29-35.

4. Mohammed, O. F.; Pines, D.; Dreyer, J.; Pines, E.; Nibbering, E. T., Sequential Proton Transfer Through Water Bridges in Acid-Base Reactions. *Science* **2005,** *310* (5745), 83-86.

5. Garczarek, F.; Wang, J. P.; El-Sayed, M. A.; Gerwert, K., The Assignment of the Different Infrared Continuum Absorbance Changes Observed in the 3000-1800-cm^{-1} Region during the Bacteriorhodopsin Photocycle. *Biophys. J.* **2004,** *87* (4), 2676-2682.

6. Garczarek, F.; Gerwert, K., Functional Waters in Intraprotein Proton Transfer Monitored by FTIR Difference Spectroscopy. *Nature* **2006,** *439* (7072), 109-12.

7. Wolf, S.; Freier, E.; Cui, Q.; Gerwert, K., Infrared Spectral Marker Bands Characterizing a Transient Water Wire Inside a Hydrophobic Membrane Protein. *J. Chem. Phys.* **2014,** *141* (22), 22D524.

8. Kotting, C.; Gerwert, K., Proteins in Action Monitored by Time-Resolved FTIR Spectroscopy. *Chemphyschem* **2005,** *6* (5), 881-8.

9. Seibold, S. A.; Mills, D. A.; Ferguson-Miller, S.; Cukier, R. I., Water Chain Formation and Possible Proton Pumping Routes in Rhodobacter Sphaeroides Cytochrome c Oxidase: A Molecular Dynamics Comparison of the Wild Type and R481K Mutant. *Biochemistry* **2005,** *44* (31), 10475-10485.

10. Silverman, D. N.; Mckenna, R., Solvent-Mediated Proton Transfer in Catalysis by Carbonic Anhydrase. *Acc. Chem. Res.* **2007,** *40* (8), 669-675.

11. Xu, J.; Sharpe, M. A.; Qin, L.; Ferguson-Miller, S.; Voth, G. A., Storage of an Excess Proton in the Hydrogen-Bonded Network of the D-Pathway of Cytochrome c Oxidase: Identification of a Protonated Water Cluster. *J. Am. Chem. Soc.* **2007,** *129* (10), 2910-2913.

12. Umena, Y.; Kawakami, K.; Shen, J. R.; Kamiya, N., Crystal Structure of Oxygen-Evolving Photosystem II at a Resolution of 1.9 A. *Nature* **2011,** *473* (7345), 55-60.

13. Suga, M.; Akita, F.; Hirata, K.; Ueno, G.; Murakami, H.; Nakajima, Y.; Shimizu, T.; Yamashita, K.; Yamamoto, M.; Ago, H.; Shen, J. R., Native Structure of Photosystem II at 1.95 A Resolution Viewed by Femtosecond X-Ray Pulses. *Nature* **2015,** *517* (7532), 99-103.

14. Barry, B. A., Proton Coupled Electron Transfer and Redox Active Tyrosines in Photosystem II. *J. Photochem. Photobiol. B* **2011,** *104* (1-2), 60-71.

15. Barry, B. A.; Babcock, G. T., Tyrosine Radicals Are Involved in the Photosynthetic Oxygen-Evolving System. *Proc. Natl. Acad. Sci. USA* **1987,** *84* (20), 7099-103.

16. Roose, J. L.; Frankel, L. K.; Mummadisetti, M. P.; Bricker, T. M., The Extrinsic Proteins of Photosystem II: Update. *Planta* **2016,** *243* (4), 889-908.

17. Patzlaff, J. S.; Barry, B. A., Pigment Quantitation and Analysis by HPLC Reverse Phase Chromatography: A Characterization of Antenna Size in Oxygen-Evolving Photosystem II Preparations from Cyanobacteria and Plants. *Biochemistry* **1996,** *35* (24), 7802-7811.

18. Wei, X. P.; Su, X. D.; Cao, P.; Liu, X. Y.; Chang, W. R.; Li, M.; Zhang, X. Z.; Liu, Z. F., Structure of Spinach Photosystem II-LHCII Supercomplex at 3.2 Angstrom Resolution. *Nature* **2016,** *534* (7605), 69-74.

19. Styring, S.; Rutherford, A. W., Deactivation Kinetics and Temperature Dependence of the S-State Transitions in the Oxygen-Evolving System of Photosystem II Measured by EPR Spectroscopy. *Biochim. Biophys. Acta* **1988,** *933* (2), 378-387.

20. Junge, W.; Haumann, M.; Ahlbrink, R.; Mulkidjanian, A.; Clausen, J., Electrostatics and Proton Transfer in Photosynthetic Water Oxidation. *Philos. T. Roy. Soc. B* **2002,** *357* (1426), 1407-1417.

21. Nelson, N.; Yocum, C. F., Structure and Function of Photosystems I and II. *Annu. Rev. Plant Biol.* **2006,** *57*, 521-565.

22. Dau, H.; Zaharieva, I.; Haumann, M., Recent Developments in Research on Water Oxidation by Photosystem II. *Curr. Opin. Chem. Biol.* **2012,** *16* (1-2), 3-10.

23. Cox, N.; Pantazis, D. A.; Neese, F.; Lubitz, W., Biological Water Oxidation. *Acc. Chem. Res.* **2013,** *46* (7), 1588-96.

24. Siegbahn, P. E., Water Oxidation Mechanism in Photosystem II, Including Oxidations, Proton Release Pathways, O-O Bond Formation and O_2 Release. *Biochim. Biophys. Acta* **2013,** *1827* (8-9), 1003-19.

25. Yocum, C. F., The Calcium and Chloride Requirements of the O_2 Evolving Complex. *Coordin. Chem. Rev.* **2008,** *252* (3-4), 296-305.

26. Vrettos, J. S.; Stone, D. A.; Brudvig, G. W., Quantifying the Ion Selectivity of the Ca^{2+} Site in Photosystem II: Evidence for Direct Involvement of Ca^{2+} in O_2 Formation. *Biochemistry* **2001,** *40* (26), 7937-45.

27. Sproviero, E. M.; Gascon, J. A.; McEvoy, J. P.; Brudvig, G. W.; Batista, V. S., Quantum Mechanics/Molecular Mechanics Study of the Catalytic Cycle of Water Splitting in Photosystem II. *J. Am. Chem. Soc.* **2008,** *130* (11), 3428-3442.

28. Ugur, I.; Rutherford, A. W.; Kaila, V. R., Redox-Coupled Substrate Water Reorganization in the Active Site of Photosystem II: The Role of Calcium in Substrate Water Delivery. *Biochim. Biophys. Acta* **2016,** *1857* (6), 740-8.

29. Amin, M.; Vogt, L.; Szejgis, W.; Vassiliev, S.; Brudvig, G. W.; Bruce, D.; Gunner, M. R., Proton-Coupled Electron Transfer During the S-State Transitions of the Oxygen-Evolving Complex of Photosystem II. *J. Phys. Chem. B* **2015,** *119* (24), 7366-7377.

30. Vinyard, D. J.; Askerka, M.; Debus, R. J.; Batista, V. S.; Brudvig, G. W., Ammonia Binding in the Second Coordination Sphere of the Oxygen-Evolving Complex of Photosystem II. *Biochemistry* **2016**.

31. Koua, F. H. M.; Umena, Y.; Kawakami, K.; Shen, J. R., Structure of Sr-substituted Photosystem II at 2.1 Angstrom Resolution and Its Implications in the Mechanism of Water Oxidation. *Proc. Natl. Acad. Sci. USA* **2013,** *110* (10), 3889-3894.

32. Olesen, K.; Andreasson, L. E., The Function of the Chloride Ion in Photosynthetic Oxygen Evolution. *Biochemistry* **2003,** *42* (7), 2025-2035.

33. Homann, P. H., Chloride and Calcium in Photosystem II: from Effects to Enigma. *Photosynth. Res.* **2002,** *73* (1-3), 169-175.

34. Pokhrel, R.; McConnell, I. L.; Brudvig, G. W., Chloride Regulation of Enzyme Turnover: Application to the Role of Chloride in Photosystem II. *Biochemistry* **2011,** *50* (14), 2725-2734.

35. Krishtalik, L. I., Energetics of Multielectron Reactions: Photosynthetic Oxygen Evolution. *Biochim. Biophys. Acta* **1986,** *849* (1), 162-171.

36. Linke, K.; Ho, F. M., Water in Photosystem II: Structural, Functional and Mechanistic Considerations. *Biochim. Biophys. Acta* **2014,** *1837* (1), 14-32.

37. Polander, B. C.; Barry, B. A., Detection of an Intermediary, Protonated Water Cluster in Photosynthetic Oxygen Evolution. *Proc. Natl. Acad. Sci. USA* **2013,** *110* (26), 10634-9.

38. Headrick, J. M.; Diken, E. G.; Walters, R. S.; Hammer, N. I.; Christie, R. A.; Cui, J.; Myshakin, E. M.; Duncan, M. A.; Johnson, M. A.; Jordan, K. D., Spectral Signatures of Hydrated Proton Vibrations in Water Clusters. *Science* **2005,** *308* (5729), 1765-1769.

39. Berthold, D. A.; Babcock, G. T.; Yocum, C. F., A Highly Resolved, Oxygen-Evolving Photosystem-II Preparation from Spinach Thylakoid Membranes: EPR and Electron-Transport Properties. *Febs. Lett.* **1981,** *134* (2), 231-234.

40. Mishra, R. K.; Ghanotakis, D. F., Selective Extraction of CP 26 and CP 29 Proteins without Affecting the Binding of the Extrinsic Proteins (33, 23 and 17 kDa) and the DCMU Sensitivity of a Photosystem-II Core Complex. *Photosyn. Res.* **1994,** *42* (1), 37-42.

41. Barry, B. A., Tyrosyl Radicals in Photosystem II. *Methods Enzymol.* **1995,** *258*, 303-19.

42. Mattoo, A. K.; Pick, U.; Hoffmanfalk, H.; Edelman, M., The Rapidly Metabolized 32,000-Dalton Polypeptide of the Chloroplast Is the Proteinaceous Shield Regulating Photosystem-II Electron-Transport and Mediating Diuron Herbicide Sensitivity. *Proc. Natl. Acad. Sci. USA* **1981,** *78* (3), 1572-1576.

43. Kuwabara, T.; Murata, N., Quantitative Analysis of the Inactivation of Photosynthetic Oxygen Evolution and the Release of Polypeptides and Manganese in the Photosystem II Particles of Spinach Chloroplasts. *Plant Cell Physiol.* **1983,** *24* (4), 741-747.

44. Vass, I.; Koike, H.; Inoue, Y., High pH Effect on S-State Turnover in Chloroplasts Studied by Thermoluminescence. Short-Time Alkaline Incubation Reversibly Inhibits S_3-to-S_4 Transition. *Biochim. Biophys. Acta* **1985,** *810* (3), 302-309.

45. Schiller, H.; Dau, H., Preparation Protocols for High-Activity Photosystem II Membrane Particles of Green Algae and Higher Plants, pH Dependence of Oxygen Evolution and Comparison of the S_2-State Multiline Signal by X-band EPR Spectroscopy. *J. Photochem. Photobiol. B* **2000,** *55* (2-3), 138-144.

46. Polander, B. C.; Barry, B. A., Calcium and the Hydrogen-Bonded Water Network in the Photosynthetic Oxygen-Evolving Complex. *J. Phys. Chem. Lett.* **2013,** *4* (5), 786-791.

47. Sandusky, P. O.; Yocum, C. F., The Mechanism of Amine Inhibition of the Photosynthetic Oxygen Evolving Complex. *Febs. Lett.* **1983,** *162* (2), 339-343.

48. Boussac, A.; Rutherford, A. W.; Styring, S., Interaction of Ammonia with the Water Splitting Enzyme of Photosystem II. *Biochemistry* **1990,** *29* (1), 24-32.

49. Polander, B. C.; Barry, B. A., A Hydrogen-Bonding Network Plays a Catalytic Role in Photosynthetic Oxygen Evolution. *Proc. Natl. Acad. Sci. USA* **2012,** *109* (16), 6112-6117.

50. Steenhuis, J. J.; Barry, B. A., A Difference Infrared Study of Protein Structural Changes in the Photosynthetic Water-Oxidizing Complex. *J. Am. Chem. Soc.* **1996,** *118* (47), 11927-11932.

51. Steenhuis, J. J.; Barry, B. A., Protein and Ligand Environments of the S_2 State in Photosynthetic Oxygen Evolution: a Difference FT-IR Study. *J. Phys. Chem. B* **1997,** *101* (33), 6652-6660.

52. Keough, J. M.; Jenson, D. L.; Zuniga, A. N.; Barry, B. A., Proton Coupled Electron Transfer and Redox-Active Tyrosine Z in the Photosynthetic Oxygen-Evolving Complex. *J. Am. Chem. Soc.* **2011,** *133* (29), 11084-11087.

53. de Paula, J. C.; Innes, J. B.; Brudvig, G. W., Electron Transfer in Photosystem II at Cryogenic Temperatures. *Biochemistry* **1985,** *24* (27), 8114-20.

54. Kim, S.; Liang, J.; Barry, B. A., Chemical Complementation Identifies a Proton Acceptor for Redox-Active Tyrosine D in Photosystem II. *Proc. Natl. Acad. Sci. USA* **1997,** *94* (26), 14406-14411.

55. Kim, S. Y.; Ayala, I.; Steenhuis, J. J.; Gonzalez, E. T.; Barry, B. A., Infrared Spectroscopic Identification of the C-O Stretching Vibration Associated with the Tyrosyl Z Center Dot and D Center Dot Radicals in Photosystem II. *Biochim. Biophys. Acta* **1998,** *1364* (3), 337-360.

56. Halverson, K. M.; Barry, B. A., Sucrose and Glycerol Effects on Photosystem II. *Biophys. J.* **2003,** *85* (2), 1317-1325.

57. Ghanotakis, D. F.; Babcock, G. T.; Yocum, C. F., Calcium Reconstitutes High Rates of Oxygen Evolution in Polypeptide Depleted Photosystem II Preparations. *Febs. Lett.* **1984,** *167* (1), 127-130.

58. Smith, G. L.; Miller, D. J., Potentiometric Measurements of Stoichiometric and Apparent Affinity Constants of EGTA for Protons and Divalent Ions Including Calcium. *Biochim. Biophys. Acta* **1985,** *839* (3), 287-299.

59. Yamamoto, Y.; Tamura, N.; Nishimura, M., Release of Polypeptides from Highly Active O_2 - Evolving Photosystem II Preparation by this Treatment. *Febs. Lett.* **1981,** *133* (2), 265-268.

60. Britt, R. D.; Zimmermann, J. L.; Sauer, K.; Klein, M. P., Ammonia Binds to the Catalytic Mn of the Oxygen-Evolving Complex of Photosystem II: Evidence by Electron-Spin Echo Envelope Modulation Spectroscopy. *J. Am. Chem. Soc.* **1989,** *111* (10), 3522-3532.

61. Kim, D. H.; Britt, R. D.; Klein, M. P.; Sauer, K., The Manganese Site of the Photosynthetic Oxygen-Evolving Complex Probed by EPR Spectroscopy of Oriented Photosystem II Membranes: the g = 4 and g = 2 Multiline Signals. *Biochemistry* **1992,** *31* (2), 541-547.

62. Navarro, M. P.; Ames, W. M.; Nilsson, H.; Lohmiller, T.; Pantazis, D. A.; Rapatskiy, L.; Nowaczyk, M. M.; Neese, F.; Boussac, A.; Messinger, J.; Lubitz, W.; Cox, N., Ammonia Binding to the Oxygen-Evolving Complex of Photosystem II Identifies the Solvent-Exchangeable Oxygen Bridge (μ-oxo) of the Manganese Tetramer. *Proc. Natl. Acad. Sci. USA* **2013,** *110* (39), 15561-15566.

63. Oyala, P. H.; Stich, T. A.; Debus, R. J.; Britt, R. D., Ammonia Binds to the Dangler Manganese of the Photosystem II Oxygen-Evolving Complex. *J. Am. Chem. Soc.* **2015,** *137* (27), 8829-8837.

64. Piccioni, R.; Bellemare, G.; Chua, N. H., Methods of Polyacrylamide Gel Electrophoresis in the Analysis and Preparation of Plant Polypeptides. In *Methods in chloroplast molecular biology*, North-Holland Publishing Company: Amsterdam, Netherlands, 1982.

65. Haumann, M.; Drevenstedt, W.; Hundelt, M.; Junge, W., Photosystem II of Green Plants. Oxidation and Deprotonation of the Same Component (Histidine?) on S_1-to-S_2 in Chloride-Depleted Centers as on S_2-to-S_3 in Controls. *Biochim. Biophys. Acta* **1996,** *1273* (3), 237-250.

66. Wang, H.; Agmon, N., Protonated Water Dimer on Benzene: Standing Eigen or Crouching Zundel? *J. Phys. Chem. B* **2015,** *119* (6), 2658-67.

67. Khan, S.; Sun, J. S.; Brudvig, G. W., Cation Effects on the Electron-Acceptor Side of Photosystem II. *J. Phys. Chem. B* **2015,** *119* (24), 7722-8.

68. Chen, J.; Yao, M. D.; Pagba, C. V.; Zheng, Y.; Fei, L. P.; Feng, Z. C.; Barry, B. A., Directly Probing Redox-Linked Quinones in Photosystem II Membrane Fragments via UV Resonance Raman Scattering. *Biochim. Biophys. Acta* **2015,** *1847* (6-7), 558-564.

69. Razeghifard, M. R.; Kim, S.; Patzlaff, J. S.; Hutchison, R. S.; Krick, T.; Ayala, I.; Steenhuis, J. J.; Boesch, S. E.; Wheeler, R. A.; Barry, B. A., In Vivo, in Vitro, and Calculated Vibrational Spectra of Plastoquinone and the Plastosemiquinone Anion Radical. *J. Phys. Chem. B* **1999,** *103* (44), 9790-9800.

70. Kim, S.; Patzlaff, J. S.; Krick, T.; Ayala, I.; Sachs, R. K.; Barry, B. A., Isotope-Based Discrimination between the Infrared Modes of Plastosemiquinone Anion Radicals and Neutral Tyrosyl Radicals in Photosystem II. *J. Phys. Chem. B* **2000,** *104* (41), 9720-9727.

71. Bernard, M. T.; Macdonald, G. M.; Nguyen, A. P.; Debus, R. J.; Barry, B. A., A Difference Infrared Study of Hydrogen-Bonding to the Z-Center-Dot Tyrosyl Radical of Photosystem II. *J. Biol. Chem.* **1995,** *270* (4), 1589-1594.

72. Kim, S. Y.; Barry, B. A., Vibrational Spectrum Associated with the Reduction of Tyrosyl Radical D-Center Dot in Photosystem II: a Comparative Biochemical and Kinetic Study. *Biochemistry* **1998,** *37* (39), 13882-13892.

73. Noguchi, T.; Ono, T.; Inoue, Y., Direct-Detection of a Carboxylate Bridge between Mn and Ca2+ in the Photosynthetic Oxygen-Evolving Center by Means of Fourier-Transform Infrared-Spectroscopy. *Biochim. Biophys. Acta* **1995,** *1228* (2-3), 189-200.

74. Kimura, Y.; Hasegawa, K.; Ono, T., Characteristic Changes of the S_2/S_1 Difference FTIR Spectrum Induced by Ca^{2+} Depletion and Metal Cation Substitution in the Photosynthetic Oxygen-Evolving Complex. *Biochemistry* **2002,** *41* (18), 5844-5853.

75. Steenhuis, J. J.; Hutchison, R. S.; Barry, B. A., Alterations in Carboxylate Ligation at the Active Site of Photosystem II. *J. Biol. Chem.* **1999,** *274* (21), 14609-14616.

76. Kandori, H.; Shichida, Y., Direct Observation of the Bridged Water Stretching Vibrations inside a Protein. *J. Am. Chem. Soc.* **2000,** *122* (47), 11745-11746.

77. Nakamura, S.; Ota, K.; Shibuya, Y.; Noguchi, T., Role of a Water Network around the Mn4CaO5 Cluster in Photosynthetic Water Oxidation: A Fourier Transform Infrared Spectroscopy and Quantum Mechanics/Molecular Mechanics Calculation Study. *Biochemistry* **2016,** *55* (3), 597-607.

78. Polander, B. C.; Barry, B. A., Calcium, Strontium, and Protein Dynamics during the S_2 to S_3 Transition in the Photosynthetic Oxygen-Evolving Cycle. *J. Phys. Chem. Lett.* **2013,** *4* (19), 3356-3362.

79. Freier, E.; Wolf, S.; Gerwert, K., Proton Transfer via a Transient Linear Water-Molecule Chain in a Membrane Protein. *Proc. Natl. Acad. Sci. USA* **2011,** *108* (28), 11435-11439.

80. Noguchi, T., FTIR Detection of Water Reactions in the Oxygen-Evolving Centre of Photosystem II. *Philos. T. Roy. Soc. B* **2008,** *363* (1494), 1189-1194.

81. Tursi, A. J., Matrix-Isolation Study of Water Dimer in Solid Nitrogen. *J. Chem. Phys.* **1970,** *52* (3), 1521-1528.

82. Page, R. H.; Frey, J. G.; Shen, Y. R.; Lee, Y. T., Infrared Predissociation Spectra of Water Dimer in a Supersonic Molecular-Beam. *Chem. Phys. Lett.* **1984,** *106* (5), 373-376.

83. Coker, D. F.; Miller, R. E.; Watts, R. O., The Infrared Predissociation Spectra of Water Clusters. *J. Chem. Phys.* **1985,** *82* (8), 3554-3562.

84. Debus, R. J., Evidence from FTIR Difference Spectroscopy That D1-Asp61 Influences the Water Reactions of the Oxygen-Evolving Mn4CaO5 Cluster of Photosystem II. *Biochemistry* **2014,** *53* (18), 2941-55.

85. Beck, W. F.; Brudvig, G. W., Binding of Amines to the O_2-Evolving Center of Photosystem II. *Biochemistry* **1986,** *25* (21), 6479-6486.

86. Noguchi, T.; Sugiura, M., Structure of an Active Water Molecule in the Water-Oxidizing Complex of Photosystem II as Studied by FTIR Spectroscopy. *Biochemistry* **2000,** *39* (36), 10943-10949.

87. Hou, L. H.; Wu, C. M.; Huang, H. H.; Chu, H. A., Effects of Ammonia on the Structure of the Oxygen-Evolving Complex in Photosystem II As Revealed by Light-Induced FTIR Difference Spectroscopy. *Biochemistry* **2011,** *50* (43), 9248-9254.

88. Kramer, D. M.; Sacksteder, C. A.; Cruz, J. A., How Acidic Is the Lumen? *Photosynth. Res.* **1999,** *60* (2-3), 151-163.

89. Lindberg, K.; Vanngard, T.; Andreasson, L. E., Studies of the Slowly Exchanging Chloride in Photosystem-II of Higher-Plants. *Photosynth. Res.* **1993,** *38* (3), 401-408.

90. Messinger, J.; Renger, G., Analyses of pH-Induced Modifications of the Period Four Oscillation of Flash-Induced Oxygen Evolution Reveal Distinct Structural Changes of the Photosystem II Donor Side at Characteristic pH Values. *Biochemistry* **1994,** *33* (36), 10896-905.

91. Christen, G.; Seeliger, A.; Renger, G., P680(+)* Reduction Kinetics and Redox Transition Probability of the Water Oxidizing Complex as a Function of pH and H/D Isotope Exchange in Spinach Thylakoids. *Biochemistry* **1999,** *38* (19), 6082-92.

92. Damoder, R.; Dismukes, G. C., pH-Dependence of the Multiline, Manganese Electron-Paramagnetic-Res Signal for the S_2 State in PSII Particles - Absence of Proton Release during the S_1-to-S_2 Electron-Transfer Step of the Oxygen Evolving System. *Febs. Lett.* **1984,** *174* (1), 157-161.

93. Cole, J.; Boska, M.; Blough, N. V.; Sauer, K., Reversible and Irreversible Effects of Alkaline pH on Photosystem II Electron-Transfer Reactions. *Biochim. Biophys. Acta* **1986,** *848* (1), 41-47.

94. Geijer, P.; Deak, Z.; Styring, S., Proton Equilibria in the Manganese Cluster of PhotosystemII Control the Intensities of the S_0 and S_2 State g Approximately 2 Electron Paramagnetic Resonance Signals. *Biochemistry* **2000,** *39* (23), 6763-72.

95. Bernat, G.; Morvaridi, F.; Feyziyev, Y.; Styring, S., pH Dependence of the Four Individual Transitions in the Catalytic S-cycle during Photosynthetic Oxygen Evolution. *Biochemistry* **2002,** *41* (18), 5830-43.

96. Latimer, M. J.; DeRose, V. J.; Yachandra, V. K.; Sauer, K.; Klein, M. P., Structural Effects of Calcium Depletion on the Manganese Cluster of Photosystem II: Determination by X-Ray Absorption Spectroscopy. *J. Phys. Chem. B* **1998,** *102* (42), 8257-8265.

97. Yachandra, V. K.; Yano, J., Calcium in the Oxygen-Evolving Complex: Structural and Mechanistic Role Determined by X-Ray Spectroscopy. *J. Photochem. Photobiol. B* **2011,** *104* (1-2), 51-59.

98. Lohmiller, T.; Cox, N.; Su, J. H.; Messinger, J.; Lubitz, W., The Basic Properties of the Electronic Structure of the Oxygen-evolving Complex of Photosystem II Are Not Perturbed by Ca^{2+} Removal. *J. Biol. Chem.* **2012,** *287* (29), 24721-24733.

99. Siegbahn, P. E. M., Water Oxidation Energy Diagrams for Photosystem II for Different Protonation States, and the Effect of Removing Calcium. *Phys. Chem. Chem. Phys.* **2014,** *16* (24), 11893-11900.

CHAPTER 3. CALCIUM, AMMONIA, REDOX-ACTIVE TYROSINE YZ, AND PROTON-COUPLED ELECTRON TRANSFER IN THE PHOTOSYNTHETIC OXYGEN-EVOLVING COMPLEX

By

Zhanjun Guo and Bridgette A. Barry*

School of Chemistry and Biochemistry and Petit Institute for Bioengineering and Biosciences, Georgia Institute of Technology, Atlanta, Georgia 30332, United States

Reprinted with permission from *The Journal of Physical Chemistry B*

Guo, Z. and Barry, B. A. Calcium, Ammonia, Redox-Active Tyrosine YZ, and Proton-Coupled Electron Transfer in the Photosynthetic Oxygen-Evolving Complex. *J. Phys. Chem. B*, **2017**, *121* (16), 3987–3996

3.1 Abstract

A redox-active tyrosine, YZ (Y161 in the D1 polypeptide), is essential in photosystem II (PSII), which conducts photosynthetic oxygen evolution. On each step of the light-driven oxygen evolving reaction, YZ radical is formed by a chlorophyll cation radical. YZ radical is then reduced by a Mn_4CaO_5 cluster in a proton coupled electron transfer (PCET) reaction. YZ is hydrogen bonded to His190-D1 and to water molecules in a hydrogen-bonding network, involving calcium. This network is sensitive to disruption with ammonia and to removal and replacement of calcium. Only strontium supports activity. Here, we use electron paramagnetic resonance (EPR) spectroscopy to define the influence of ammonia treatment, calcium removal, and strontium/barium substitution on YZ radical PCET at two pH values. A defined oxidation state of the metal cluster (S2) was trapped by illumination at 190 K. The net reduction and protonation of YZ radical via PCET were monitored by EPR transients collected after a 532 nm laser flash. At 190 K, YZ radical cannot oxidize the Mn_4CaO_5 cluster and decays on the second's time scale by recombination with Q_A^-. The overall decay half-time and biexponential fits were used to analyze the results. At pH 7.5, the YZ radical decay rate decreased in calcium-depleted (CD-PSII) and barium/strontium-reconstituted PSII (Ba-PSII, Sr-PSII), relative to the control, calcium-reconstituted samples (Ca-PSII). At pH 6.0, the YZ radical decay rate was not significantly altered in CD-PSII and Sr-PSII, but decreased in Ba-PSII. A two-pathway model, involving two competing proton donors with different pK_a values, is proposed to explain these results. Ammonia treatment decreased the YZ decay rate in Ca-PSII, Sr-PSII, and CD-PSII, consistent with a reaction that is mediated by the hydrogen-bonding network. However, ammonia treatment did not alter the rate in Ba-PSII. This

result is interpreted in terms of the large ionic radius of barium and the elevated pK_a of barium-bound water, which are expected to disrupt hydrogen bonding. In addition, evidence for an electrostatic interaction between the S_2 protonated water cluster (W_n^+) and the YZ proton donation pathway is presented. This interaction is proposed to increase the rate of the YZ PCET reaction via a change in the acidity of a YZ proton donor.

3.2 Introduction

Photosystem II (PSII) conducts water oxidation during light-driven photosynthetic oxygen evolution. The movement of electrons and protons are coordinated to give proton coupled electron transfer (PCET) reactions. High potential PCET reactions are critical in several important enzymes, including PSII and ribonucleotide reductase.[1] In PSII, light absorption drives the four electron oxidation of water at the oxygen-evolving complex (OEC).[2] The OEC contains a Mn_4CaO_5 cluster, which is the site of water oxidation. On each light-driven step, a tyrosine in the D1 polypeptide (YZ, Y161-D1, Figure 3.1A and B) is transiently oxidized and reduced by a PCET mechanism. YZ is essential for oxygen evolution. In the cryogenic structure, YZ is directly and indirectly hydrogen bonded to calcium through several water molecules, W4, W7 and W3 (Figure 3.1B).[3-4] Hydrogen-bonding interactions are also observed in the room temperature PSII structure.[5] This extensive, calcium-dependent hydrogen-bonding network has been proposed to be important in YZ PCET reactions.[6-8] In this paper, we study the mechanism of YZ PCET, as radical reduction occurs via recombination between YZ• and Q_A^- at low (190 K) temperature.

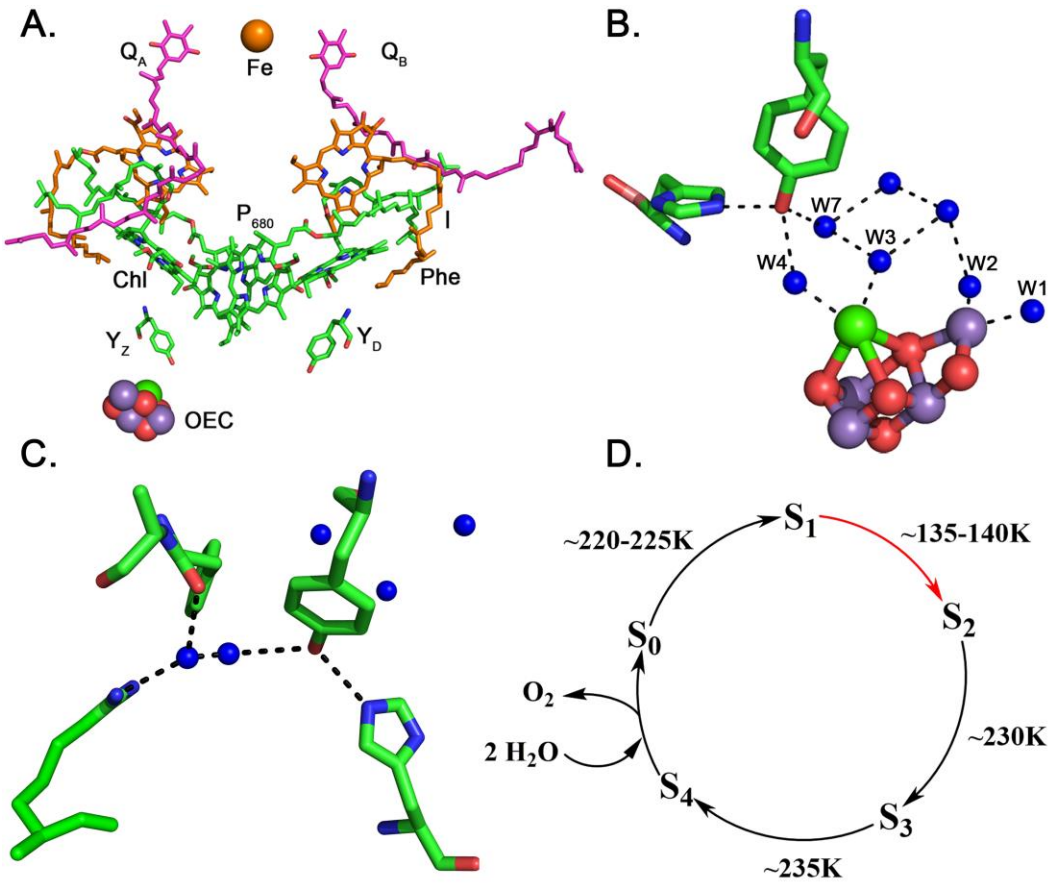

Figure 3.1 (A) Redox-active cofactors involved in oxygen evolution and the S-state cycle. In the OEC, manganese atoms are shown in purple, calcium is shown in green, and oxygens are shown in red. Water is represented by blue spheres. (PDB ID: 4UB6).[4] (B) YZ hydrogen-bonding network showing the calcium-bound water and His190. Selected water ligands are labeled (PDB ID: 4UB6).[4] (C) Environment (within 8 Å) of YD showing a single water molecule with partial occupancy in two positions. (D) S-state cycle of photosynthetic oxygen evolution, showing the half-inhibition temperature of each transition.[9] The red arrow indicates the transition studied here.

Interestingly, PSII contains another redox-active tyrosine, YD (Y160 in the D2 polypeptide, Figure 3.1C), which is not required for oxygen evolution and forms a stable radical.[10] YD• and YZ• radical can be differentiated by their distinct decay rates and by their microwave saturation parameters.[11-12] YD is relatively distant (over 20 Å) from the Mn_4CaO_5 cluster, but within hydrogen-bonding distance of His189 in the D2 polypeptide.

YD does not participate in the OEC hydrogen-bonding network, but interacts with only one assigned water molecule, which has partial occupancy in two sites (Figure 3.1C). EPR and solvent isotope exchange have concluded that these non-covalent, environment interactions give rise to changes in PCET mechanism, when YD and YZ are compared. PCET may occur by three distinct mechanisms: PTET, proton transfer first, followed by electron transfer; ETPT, electron transfer first, followed by proton transfer; and CPET, coupled proton and electron transfer. It was proposed that YZ• decays via a pH independent, CPET mechanism, while YD• decay kinetics exhibit pH dependence, with a PTET mechanism at low pH values and a CPET mechanism at high pH values.[13-16]

Absorption of light by PSII induces a charge separation between the dimeric chl donor, P_{680}, and a bound plastoquinone, Q_A or Q_B (Figure 3.1A). P_{680}^+ subsequently oxidizes YZ, which then removes an electron from the nearby Mn_4CaO_5 cluster.[3-4] The OEC cycles through 5 different oxidation states, named the S_n states, where n = 0-4.[17] The S_1 state is the dark-stable state, and oxygen is produced during the S_3-to-S_0 transition (Figure 3.1D). At room temperature, the kinetics of the S-state transitions have been measured using X-ray absorption spectroscopy (XAS) and other techniques (reviewed in ref[18]). For example, during the S_2-to-S_3 transition, a lag phase in D_2O was recently reported.[19]

Cryogenic temperatures inhibit oxygen evolution. It has been reported that the half-inhibition temperature for the S_1-to-S_2 transition is 130-140 K, while, for other transitions, the temperatures are 220 K~235 K (Figure 3.1D).[9] At 190 K, the S_1-to-S_2 transition can occur, but the other S-state transitions are blocked. At this temperature, YZ can be oxidized by P_{680}^+, but, subsequently, YZ• fails to oxidize the OEC.[12] The Q_A^- to Q_B transition is

also inhibited at 190 K.[20] Therefore, at 190 K, a laser flash generates the YZ• and Q_A^- state, which decays in a recombination reaction.

The role of the hydrogen-bonding, water network in the YZ PCET reactions has not been fully elucidated. It is known that the decay time of YZ• is altered by treatments that remove manganese from PSII (for examples, see refs[21-22]). Treatments to remove manganese also alter the midpoint potential of YZ radical. From the X-ray structures, calcium removal is also expected to change hydrogen-bonding interactions between bound water molecules and YZ (Figure 3.1B). Some effects of calcium removal on YZ have been reported previously.[23-26] Calcium depletion is known to be a more selective treatment compared to manganese removal and can be readily reversed by the re-addition of calcium alone (reviewed in ref[27]). Calcium depletion has been proposed to change protonation and hydrogen bonding around the OEC.[28-29] However, substantial changes in manganese ligation and manganese-manganese distances are not observed.[30-32] Among replacement divalent ions, only strontium is able to support oxygen evolution activity.[33] In particular, barium is an inhibitor of oxygen evolution.[34] The structure of cyanobacterial strontium-reconstituted PSII (Sr-PSII) has been reported and shows a slightly elongated Sr-W3 distance,[35] when compared to calcium reconstituted PSII (Ca-PSII). However, no large changes in the metal cluster structure were reported in Sr-PSII.

Ammonia treatment also changes hydrogen-bonding interactions in the OEC network.[36] Ammonia is a PSII activity inhibitor and coordinates to at least two different binding sites, as assessed by magnetic resonance techniques.[5, 37-41] Ammonia is an inhibitor either at pH 6.0 or pH 7.5.[34, 36, 42-45] At one of the ammonia binding sites, accessed in the absence of PSII extrinsic subunits, chloride competes with ammonia; the other binding site

is regarded to be the substrate binding site.[33] Ammonia is known to be a less effective hydrogen-bonding partner compared with water, and ammonia treatment changes amide I carbonyl frequencies in the OEC. These shifts in frequencies were attributed to alterations in hydrogen bond strength in the OEC network.[36] Ammonia has also been shown to inhibit the formation and/or stabilization of a small internal water cluster, which is protonated during the S_1-to-S_2 transition, either at 190, 263, or 283 K. This protonated water cluster may be on the lumenal proton exit pathway.[34, 42-45] The S_0 state is also associated with formation of a $n(H_2O)H_3O^+$ (W_n^+) cluster.[45] The observation of the infrared signals of the W_n^+ species is not associated with the stable production of YZ radical. Therefore, the W_n^+ clusters are not directly formed via YZ redox reactions but on a separate proton transfer pathway.

Here, we study the $YZ^{\bullet}Q_A^-$ recombination rate and employ treatments designed to disrupt the OEC hydrogen-bonding network, namely, ammonia treatment, calcium depletion, strontium reconstitution, and barium reconstitution. Electron paramagnetic resonance (EPR) spectroscopy and kinetics monitor $YZ^{\bullet}$ in the trapped S_2 state (190 K). The data show that removal of calcium and strontium/barium substitution alter the $YZ^{\bullet}$ PCET reaction rate at pH 7.5, compared to a calcium-reconstituted sample at the same pH. However, at pH 6.0, calcium depletion and strontium reconstitution had no significant effects, while barium substitution did decrease the reaction rate relative to the control. These results are interpreted in terms of a model in which two proton donors, with different pK_a values, compete in the $YZ^{\bullet}$ PCET reaction at 190 K. Barium is proposed to disrupt essential hydrogen-bonding interactions at both pH values. Similarly, ammonia slowed the rate in all samples except barium-reconstituted PSII. The lack of an ammonia effect in

barium-reconstituted PSII is attributed to the large ionic radius of barium and the high, expected pK_a value for barium-bound water.[33-34, 46] These data also provide the first evidence for an interaction between the S_2 $n(H_2O)H_3O^+$ internal water cluster (W_n^+) and YZ• PCET reactions.

3.3 Material and Methods

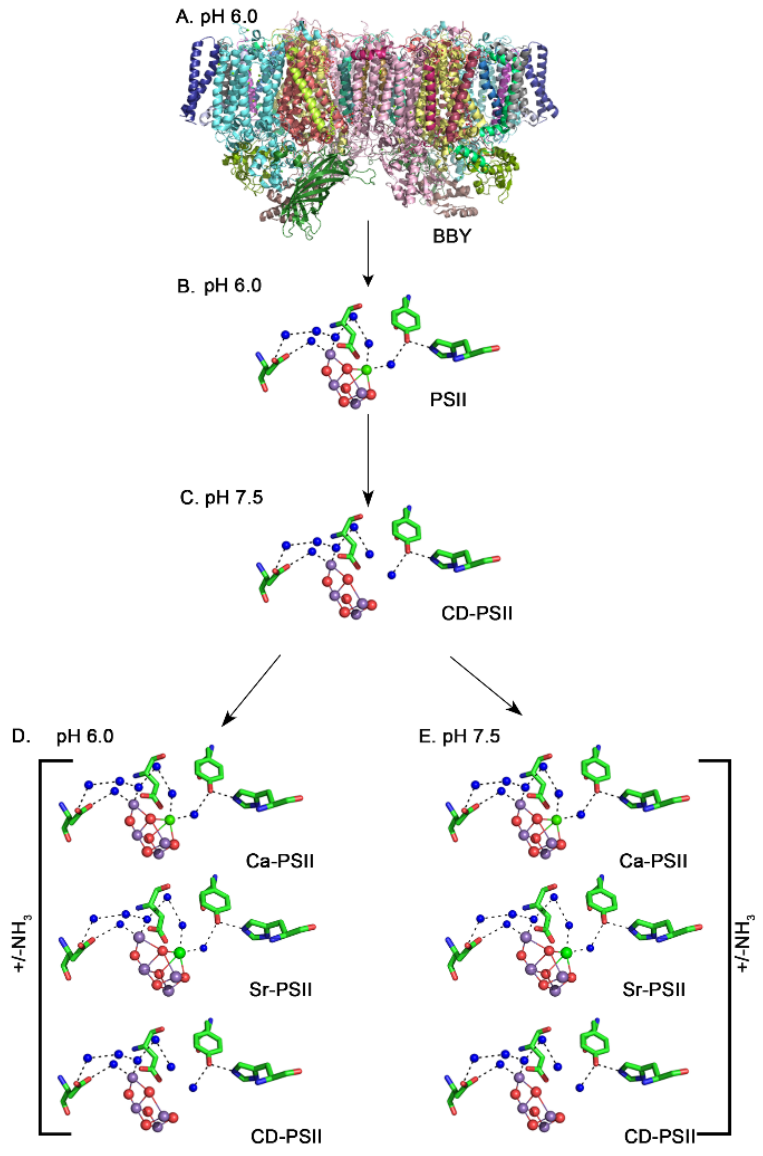

Figure 3.2 Schematic of experimental strategy to purify PSII and reconstitute divalent cations in the OEC. The cyanobacterial PSII structure is shown in A (PDB ID:

4UB6).[4] In each following panel, a portion of the OEC is shown, including YZ (Y161-D1), His190-D1, D170-D1, and D61-D1 (PDB ID: 4IL6 for strontium PSII; PDB ID: 4UB6 for calcium PSII).[4, 35] In the metal cluster, calcium or strontium is shown in green, manganese ions are shown in magenta, and oxygens are shown in red. Water is represented by blue spheres. The depiction of the effect of calcium depletion is speculative. In (A), market spinach was purified using Triton X-100.[47] In (B), PSII was further purified using octylthioglucoside.[48] In (C), PSII was calcium-depleted (CD-PSII) at pH 7.5, SHN buffer. This preparation was either transferred to pH 6.0 (D) or washed and maintained at pH 7.5 (E). At pH 6.0 (D), spectra were recorded from CD-PSII samples and from samples that were reconstituted with calcium (Ca-PSII) and strontium (Sr-PSII). The pH 6.0 CD-PSII, Ca-PSII, and Sr-PSII samples were studied in the presence or absence of ammonia (D). At pH 7.5 (E), spectra were recorded from CD-PSII samples and from samples that were reconstituted with calcium (Ca-PSII) or strontium (Sr-PSII). The pH 7.5 CD-PSII, Ca-PSII, and Sr-PSII samples were studied in the presence and absence of ammonia (E). Barium was reconstituted using the same procedure (Ba-PSII) employed to generate calcium and strontium reconstituted PSII samples.

PSII was isolated from market spinach as described previously.[47-48] An outline of subsequent procedures is presented in Figure 3.2 and has been recently reviewed in ref.[44] All procedures were performed under green safelights. BBY membranes (Figure 3.2A) were treated with octylthioglucoside at pH 6.0 to give OTG-derived core PSII preparations (hereafter referred to as OTG PSII, Figure 3.2B). After purification, these OTG PSII samples were flash frozen in liquid nitrogen, then transferred to a -70 °C freezer, suspended in SMN buffer (400 mM sucrose, 2-(N-morpholino)ethanesulfonic acid (MES)-NaOH pH 6.0, 15 mM NaCl). To remove the extrinsic subunits, OTG PSII was thawed and then resuspended in a pH 7.5 SHN buffer (400 mM sucrose, 50 mM 4-(2-hydroxyethyl)-1-piperazineethanesulfonic acid (HEPES)-NaOH pH 7.5, 15mM NaCl). This procedure was verified by SDS-PAGE to remove PsbP and PsbQ, which are not required for activity in the presence of excess calcium and chloride.[44] Removal of these extrinsic subunits facilitates removal of calcium, which was then depleted by resuspension into an Ethylene glycol-bis(2-aminoethylether)-*N*,*N*,*N′*,*N′*-tetraacetic acid (EGTA)-containing buffer at pH

7.5, as previously described.[44] This preparation is referred to as calcium depleted PSII (CD-PSII) (Figure 3.2C). For use in the experiments, a CD-PSII sample was washed and then resuspended/washed to give either a pH 6.0 CD-PSII sample or a pH 7.5 CD-PSII sample (Figure 3.2D, E). These samples were aliquoted, flash frozen, and stored at -70^{o}C until use. To generate Ca-PSII, the CD-PSII sample, at the correct pH, was thawed and reconstituted by addition of calcium chloride, from a buffered stock at the same pH (Figure 3.2D, E). Barium and strontium reconstitution were performed similarly by addition from a concentrated, buffered stock at the same pH as the Ca-PSII sample. Ammonia treatment was performed on Ca-PSII, Sr-PSII, CD-PSII, and Ba-PSII samples both at pH 6.0 and 7.5 by addition from a buffered stock, as described.[44] The residual EGTA concentration in the CD-PSII sample is estimated to be ~0.75 mM.

Table 3 Steady-state, light-induced oxygen evolution activity in PSII samples

O_2 Evolution Assay Buffer	Sample Description	Oxygen Evolution Rate[1]
SMN, pH 6.0	CD-PSII[2]	200 ± 40
	Ca-PSII[3]	1100 ± 100
	Sr-PSII[4]	800 ± 40
	Ba-PSII[5]	510 ± 60
SHN, pH 7.5	CD-PSII[2]	210 ± 40
	Ca-PSII[3]	1000 ± 110
	Sr-PSII[4]	800 ± 20
	Ba-PSII[5]	390 ± 60

[1]Oxygen evolution rates: μmol O_2 (mg chl·h)$^{-1}$. The average activities of the PSII preparations as isolated were ≥ 1000 μmol O_2 (mg chl·h)$^{-1}$. A negative control, containing 10 μM of the inhibitor, DCMU, gave 140 ± 20 μmol O_2 (mg chl·h)$^{-1}$. The SMN buffer contained 400 mM sucrose, 50 mM MES-NaOH, pH 6.0, 15 mM NaCl. The SHN buffer contained 400 mM sucrose, 50 mM HEPES-NaOH, pH 7.5, 15 mM NaCl.
[2]CD-PSII generated at pH 7.5 by 10 mM EGTA treatment.
[3]Ca-PSII generated by addition of 20 mM $CaCl_2$ from a buffered stock either at pH 6.0 or pH 7.5.
[4]Sr-PSII generated by addition of 20 mM $SrCl_2$ from a buffered stock either at pH 6.0 or pH 7.5.
[5]Ba-PSII generated by addition of 20 mM $BaCl_2$ from a buffered stock either at pH 6.0 or pH 7.5.

Oxygen evolution activities and standard deviations are reported in Table 3(See ref [44]). The OTG PSII sample as isolated had oxygen evolution rates $\geq$ 1000 μmol O_2 (mg chl·h)$^{-1}$. Oxygen evolution measurements are consisten with successful calcium depletion and calcium/strontium/ barium reconstitution. For example, the average oxygen evolution rate of Ca-PSII was 1100 μmol O_2 (mg chl·h)$^{-1}$ at pH 6.0 and was 1000 μmol O_2 (mg chl·h)$^{-1}$ in pH 7.5 buffer. The average oxygen evolution rate of Sr-PSII was 800 μmol O_2 (mg chl·h)$^{-1}$ at pH 6.0 and was 800 μmol O_2 (mg chl·h)$^{-1}$ in pH 7.5 buffer.

When assayed in 20 mM barium chloride, the average oxygen evolution rate of Ba-PSII was 510 ± 60 μmol O_2 (mg chl·h)$^{-1}$ at pH 6.0 and 390 ± 60 μmol O_2 (mg chl·h)$^{-1}$ at pH 7.5 (Table 3). Ba-PSII is inhibited in oxygen evolution rate, when compared to Ca-PSII (Table 3), and there was no statistically significant change in rate when the barium concentration was increased. For example, increasing the barium chloride concentration to 40 mM gave 460 $\pm$ 30 μmol O_2 (mg chl·h)$^{-1}$ at pH 6.0 and 340 $\pm$ 70 μmol O_2 (mg chl·h)$^{-1}$ at pH 7.5. Increasing the barium chloride concentration to 60 mM gave the statistically indistinguishable result, 410 $\pm$ 20 μmol O_2 (mg chl·h)$^{-1}$ at pH 6.0 and 280 $\pm$ 80 μmol O_2 (mg chl·h)$^{-1}$ at pH 7.5.

The CD-PSII sample was judged to be inactive in oxygen evolution (~200 ± 40, pH 6.0; 210 ± 40; pH 7.5) by comparison to Ca-PSII (Table 3) and to a sample treated with the inhibitor, 3-(3,4-dichlorophenyl) 1,1-dimethylurea (DCMU), which gave a residual background signal of 140 ± 20 μmole O_2 (mg chl·h)$^{-1}$. Note that the presence of EGTA during the oxygen evolution measurement did not decrease the steady state oxygen rate in CD-PSII, either at pH 6.0 or 7.5.[44]

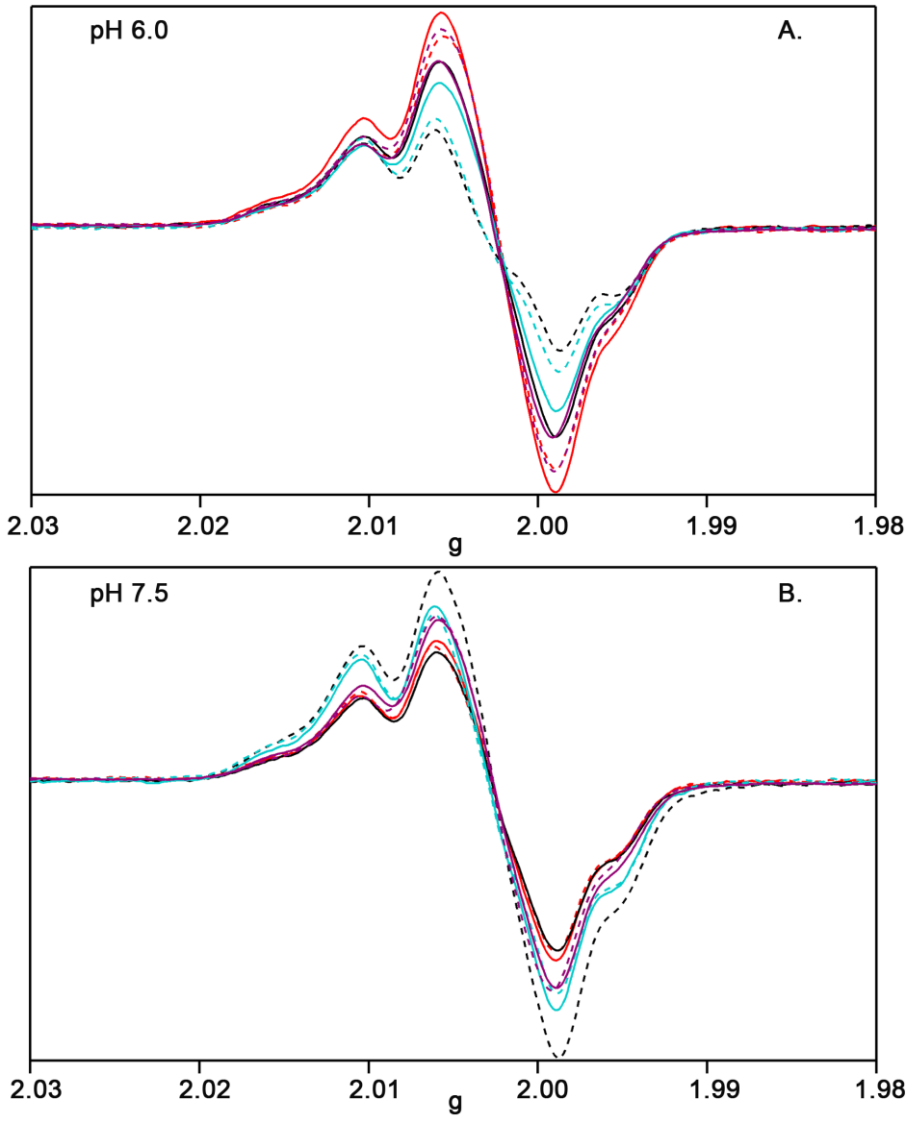

Figure 3.3 Representative EPR spectra of $S_2YZ^\bullet$ recorded under red illumination. Data were acquired from PSII in the presence of 255 mM Cl^-. In (A), pH 6.0; in (B)

pH 7.5. Samples: Ca-PSII (red solid line), Ca-PSII with 200 mM NH_3 (red dash line), Sr-PSII (cyan solid line), Sr-PSII with 200 mM NH_3 (cyan dash line), CD-PSII (black solid line), CD-PSII with 200 mM NH_3 (black dash line), Ba-PSII (violet solid line), Ba-PSII with 200 mM NH_3 (violet dash line). The g-values were ~2.004. Spectra shown in Figure 3A are repeated in this figure for completeness.

To generate the S_2 state, the PSII sample was dark-adapted in the EPR cavity at 190 K for 20 min, then illuminated with red light, which was heat-filtered (600 µmol of photons/m^2·s, Dolan Jenner Industries, Boxborough, MA). The illumination time was 2 minutes. EPR spectra were acquired during this interval (Figure 3.3). The lineshapes of the EPR spectra were similar in all preparations (Figure 3.3). Previous work has shown that 100% of the S_2 state is trapped by this procedure.[12, 15-16] The sample contained 0.5 mM potassium ferricyanide, which was added with homogenization from a freshly made, buffered 100 mM stock solution. Oxidation of manganese occurs during the S_1 to S_2 transition in Ca-PSII and Sr-PSII (reviewed in ref[2]). Previous evidence is also consistent with oxidation of manganese during the S_1 to S_2 transition in CD-PSII and Ba-PSII (reviewed in ref[34]).

After 5 minutes in the dark to equilibrate the sample, transient data were acquired at constant field position using a 532 nm laser flash, produced as the second harmonic of a Nd-YAG Continuum Surelite III laser. The energy density of the laser was 40 mJ/cm^2; the laser spot was expanded using a beam expander to approximately 4 cm x 1 cm. The time between flashes was in total 80 seconds, with a 10 second interval before each flash, which was used to determine the offset, and a 70 second data collection. A second round of offset measurement (10 seconds) and transient data collection (70 seconds) began immediately after the first. In total, 15 rounds of transient data collection were performed for each sample. Data corresponding to the last 14 rounds of collection were averaged.[12] In a control

experiment, the time between the flashes was changed from 80 to 160 seconds.

EPR spectra were recorded on a Bruker (Billerica, MA) EMX spectrometer with a Bruker ER 4102ST cavity and Bruker ER 4131VT temperature controller. The EPR parameters for acquiring field swept spectra were as following: magnetic field, 3375 G; microwave frequency, 9.32 GHz; power, 0.64 mW; modulation amplitude, 2 G; conversion time, 41 ms; time constant, 164 ms; swept time, 21 s. The parameters for transient EPR experiments were: magnetic field, 3337 G; microwave frequency, 9.32 GHz; power, 101 mW; modulation amplitude, 5 G; conversion time, 20 ms; time constant, 164 ms. High microwave power was used to saturate the YD• signal.[12, 15] For the transient data, the offset, recorded 10 seconds before each 532 nm flash, was subtracted. Microwave power saturation studies were conducted on the YZ radicals produced at pH 7.5 in Ca-PSII, CD-PSII, Sr-PSII, and Ba-PSII by the method of ref[12]. Both ammonia-treated and non-treated samples were employed. There was no evidence of power saturation, up to 200 mW, in any of the samples.

Initial intensities and overall $t_{1/2}$ values are presented in Table 4. The data were fit to derive the overall $t_{1/2}$ (Table 4) from biexponential fits (Table 5). The $t_{1/2}$ amplitude, $A_{1/2}$, was calculated from amplitudes in the fit according to a method previously described[15] ($A_{1/2}$ = (A-B)/2+B), where A is the amplitude at t=0 and B is the offset amplitude, estimated from the last data point. Note that the biexponential function was the minimum number of parameters that could be used to give adequate fits to all the data; more complex fits were also possible.

Table 4 Halftimes of $S_2YZ^\bullet$ decay rates and initial $S_2YZ^\bullet$ intensities*

Sample	pH	[NH_3] mM	Initial signal intensity	$t_{\frac{1}{2}}$ s
Ca-PSII[1]	6.0	0	290 ± 40	4.18 ±1.38
		200	290 ± 10	7.86 ± 1.64
	7.5	0	530 ± 50	3.33 ± 1.24
		200	480 ± 90	7.56 ± 1.23
Sr-PSII[2]	6.0	0	460 ± 40	3.36 ± 0.81
		200	430 ± 50	6.11 ± 0.85
	7.5	0	640 ± 90	5.02 ± 0.55
		200	1070 ± 150	8.81 ± 0.28
CD-PSII[3]	6.0	0	450 ± 10	4.04 ± 0.51
		200	490 ± 20	8.71 ± 0.33
	7.5	0	1290 ± 360	5.08 ± 0.55
		200	1740 ± 250	13.01 ± 0.33
Ba-PSII[4]	6.0	0	620 ± 50	8.44 ± 0.52
		200	480 ± 30	7.86 ± 0.91
	7.5	0	640 ± 40	8.36 ± 0.75
		200	600 ± 60	8.74 ± 1.06

***Experiments conducted at 190 K in the presence of 255 mM Cl^-. Signal intensity as assessed after a 532 nm laser flash.**
[1]Ca-PSII generated by addition of 20 mM $CaCl_2$ from a buffered stock either at pH 6.0 or pH 7.5.
[2]Sr-PSII generated by addition of 20 mM $SrCl_2$ from a buffered stock either at pH 6.0 or pH 7.5.
[3]CD-PSII generated at pH 7.5 by 10 mM EGTA treatment.
[4]Ba-PSII generated by addition of 20 mM $BaCl_2$ from a buffered stock either at pH 6.0 or pH 7.5.

Table 5 Kinetic parameters derived from biexponential fits to the transient EPR data*

Sample	pH	[NH_3] mM	A_1	k_1	A_2	k_2	C
Ca-PSII[1]	6.0	0	116 (45)	0.540	131 (51)	0.032	9 (4)
		200	80 (31)	0.857	181 (69)	0.030	0 (0)
	7.5	0	229 (49)	0.558	241 (51)	0.028	0 (0)
		200	140 (33)	0.466	278 (65)	0.028	11 (3)
Sr-PSII[2]	6.0	0	191 (46)	0.738	226 (54)	0.038	0 (0)
		200	125 (32)	0.644	220 (57)	0.031	42 (11)
	7.5	0	246 (42)	0.459	331 (57)	0.028	3 (1)
		200	291 (28)	0.491	735 (72)	0.033	0 (0)
CD-PSII[3]	6.0	0	179 (46)	0.550	213 (54)	0.032	0 (0)
		200	132 (31)	0.388	293 (69)	0.024	0 (0)
	7.5	0	513 (43)	0.456	685 (57)	0.029	1 (0)
		200	344 (20)	0.616	1392 (80)	0.029	0 (0)
Ba-PSII[4]	6.0	0	164 (28)	0.462	412 (72)	0.029	0 (0)
		200	126 (28)	0.851	332 (72)	0.036	0 (0)
	7.5	0	188 (31)	0.524	419 (69)	0.030	0 (0)
		200	165 (31)	0.481	375 (69)	0.029	0 (0)

***Data were fit using the equation $f(t) = A_1 \times e^{(-t \times k_1)} + A_2 \times e^{(-t \times k_2)} + C$. The percentage contribution from each phase (A_1 and A_2) is shown in parenthesis. Units of k_1 and k_2, the derived rate constants, are s^{-1}.**
[1]Ca-PSII generated by addition of 20 mM $CaCl_2$ from a buffered stock either at pH 6.0 or pH 7.5.
[2]Sr-PSII generated by addition of 20 mM $SrCl_2$ from a buffered stock either at pH 6.0 or pH 7.5.
[3]CD-PSII generated at pH 7.5 by 10 mM EGTA treatment.
[4]Ba-PSII PSII generated by addition of 20 mM $BaCl_2$ from a buffered stock either at pH 6.0 or pH 7.5.

3.4 Results

3.4.1 Ca-PSII.

A typical EPR spectrum of $S_2YZ\bullet$, as generated under continuous red illumination, is shown in Figure 3.4. The spectrum was derived from Ca-PSII at pH 7.5. The decrease of intensity at a fixed field was used to monitor the decay of $S_2YZ\bullet$ after the 532 nm flash

(Figure 3.4A, arrow, pH 7.5). Oxidation of YZ is accompanied with a proton transfer reaction and occurs in the nanosecond time scale.[49] This phase of the reaction is not resolved in the transient EPR experiment. Instead, the experiment in Figure 3.4B, red, monitors the reduction of YZ•, which occurs by a PCET reaction, involving both a proton and an electron on the seconds time scale (Figure 3.4B, inset). YZ• decays via recombination with Q_A^-, because electron transfer from Q_A^- to Q_B is blocked at this temperature (190 K). The Q_A^- signal, which is coupled with Fe^{2+} (Figure 3.1A), is not observed at 190 K and does not contribute to the transient data.[50] The YD• signal was saturated by high microwave power during the measurement and also does not contribute to the kinetic data.[12, 15-16] At this field setting, secondary electron donors, such as the narrow chlorophyll and carotenoid radicals, make no significant contribution to the signal.[15-16] Thus, a saturating laser flash given to a PSII sample, which has been pre-illuminated at 190 K, produces the $S_2YZ•Q_A^-$ state. This state decays on the seconds time scale via a one or two step $YZ•Q_A^-$ recombination reaction.[16]

As shown in Figure 3.4B, red, the $S_2YZ•$ signal exhibits biexponential decay on the second's time scale in Ca-PSII at pH 7.5 (data repeated in Figure 3.5B). The data can be fit to give two rate constants of approximately equal amplitude, 0.56 (49%) s^{-1} and 0.028 (51%) s^{-1}, and an overall $t_{1/2}$ of 3.33 ± 1.24 s^{-1}. This value is in agreement with a previous report of the $t_{1/2}$ (2.69 ± 0.35 s) reported at this pH in BBY membranes.[15-16]

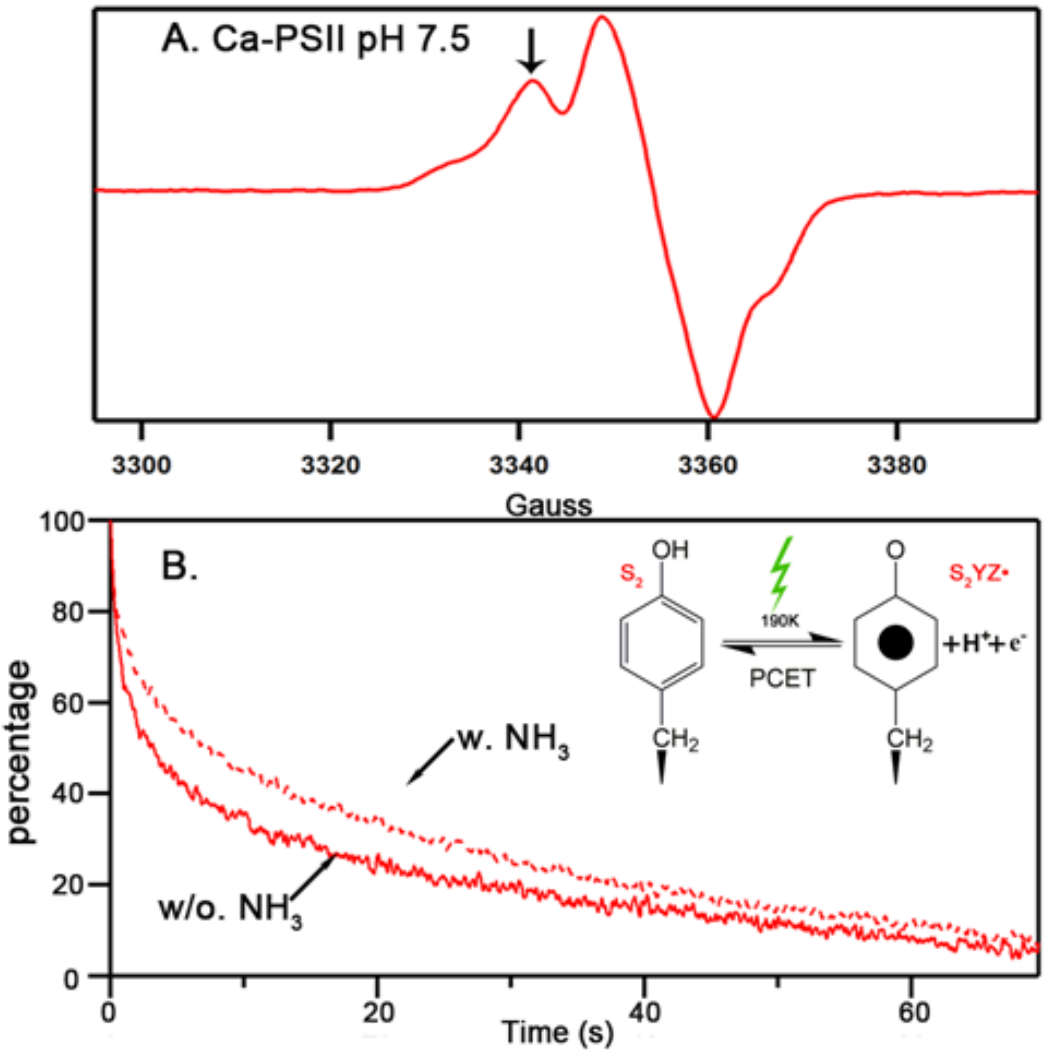

Figure 3.4 (A) EPR spectra of $S_2YZ\bullet$. Data were derived from Ca-PSII at pH 7.5 and 255 mM total chloride under continuous red illumination. The g value is 2.004. The black arrow indicates the field position used to monitor $S_2YZ\bullet$ radical decay kinetics in B. (B) Comparison of transient $S_2YZ\bullet$ kinetic data, in the presence (red dotted line) and absence (red solid line) of 200 mM ammonia. The transients were normalized to 100% at t=0. Inset: schematic of tyrosine PCET reaction. In A, the spectra were recorded with a microwave power of 0.639 mW. In B, the microwave power was increased to 101.3 mW in order to saturate the $YD\bullet$ signal.

Transient kinetic data acquired from Ca-PSII at pH 6.0 and 7.5 are presented in Figure 3.5A and B (red traces). Figure 3.6 compares the $t_{1/2}$ as derived from biexponential fits Table 5) in Ca-PSII (red) at pH 7.5 and 6.0. At pH 6.0 (Figure 3.5A and Figure 3.6),

the $t_{1/2}$ derived here (4.18 $\pm$1.38 s) is indistinguishable from the $t_{1/2}$ at pH 7.5. In addition, the kinetic constants derived from biexponential fits are also similar at the two pH values (Table 5). This is in agreement with the previous conclusion that the $S_2YZ\bullet$ radical decay rate is pH-independent in BBY membranes.[15-16]

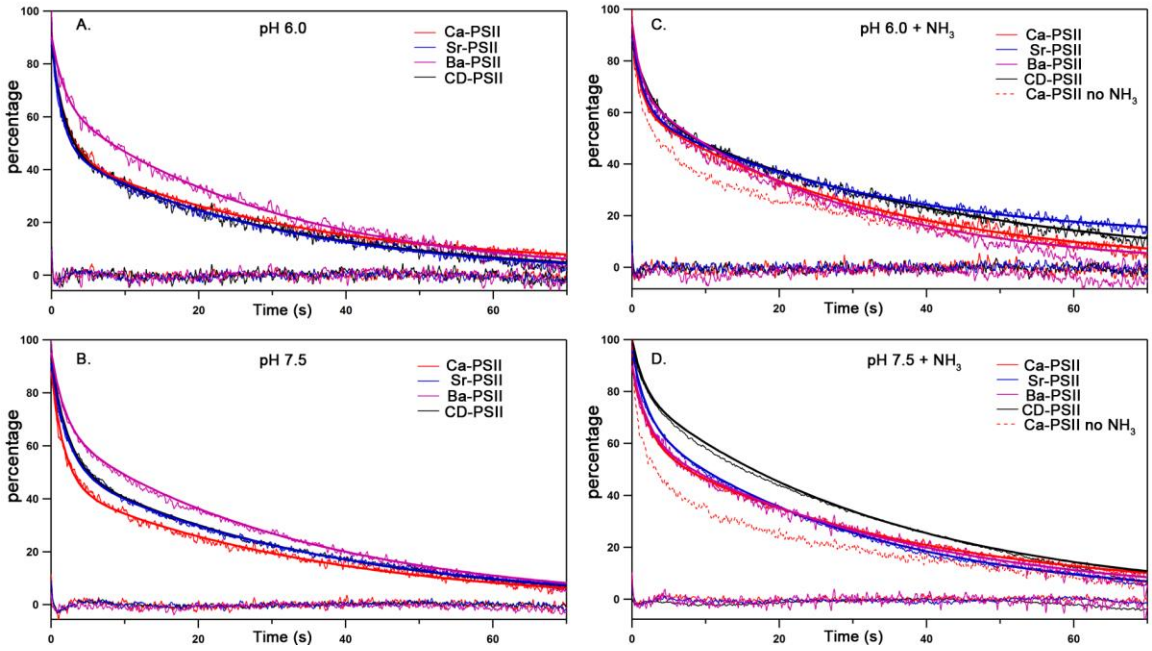

Figure 3.5 Transient EPR data associated with $S_2YZ\bullet$ decay in PSII preparations either in the presence (C and D) or absence (A and B) of ammonia. Data were acquired at pH 6.0 (A and C) or pH 7.5 (B and D). In (A, pH 6.0) and (B, pH 7.5), Ca-PSII (red); Sr-PSII (blue); CD-PSII (black); Ba-PSII (violet). In (C, pH 6.0) and (D, pH 7.5), Ca-PSII with 200 mM NH_3 (red); Sr-PSII with 200 mM NH_3 (blue); CD-PSII with 200 mM NH_3 (black); Ba-PSII with 200 mM NH_3 (violet). In C and D, Ca-PSII transients obtained in the absence of ammonia are reproduced as the dotted line comparison. In each case, the thin line is the data, the thick line, superimposed on the data in the same color, is the result of a biexponential fit, and the residuals are shown at the bottom of the each figure in the corresponding color. Transient data were averages from 4 to 8 samples, with 14 transients recorded per sample.

3.4.2 Sr-PSII.

At pH 6.0, Figure 3.5A and Figure 3.6A shows that indistinguishable kinetic traces (Figure 3.5A) and $t_{1/2}$ values (Figure 3.6A) are obtained when Sr-PSII and Ca-PSII are

compared. However, at pH 7.5, the averaged kinetic traces (Figure 3.5B and Figure 3.6B**),** show that strontium substitution slows the rate relative to the control. The $t_{1/2}$ value (5.02 ± 0.55 s) in Sr-PSII was only modestly increased relative to Ca-PSII at pH 7.5 (3.33 ± 1.24 s) (Figure 3.5 and Figure 3.6). Biexponential fits suggest an underlying change in the rate constant for the fast phase (Sr-PSII, 0.459 s^{-1} (42%); Ca-PSII, 0.558 s^{-1} (49%)) at high pH (Table 5). These data provide evidence that the Ca^{2+} site facilitates YZ PCET at pH 7.5.

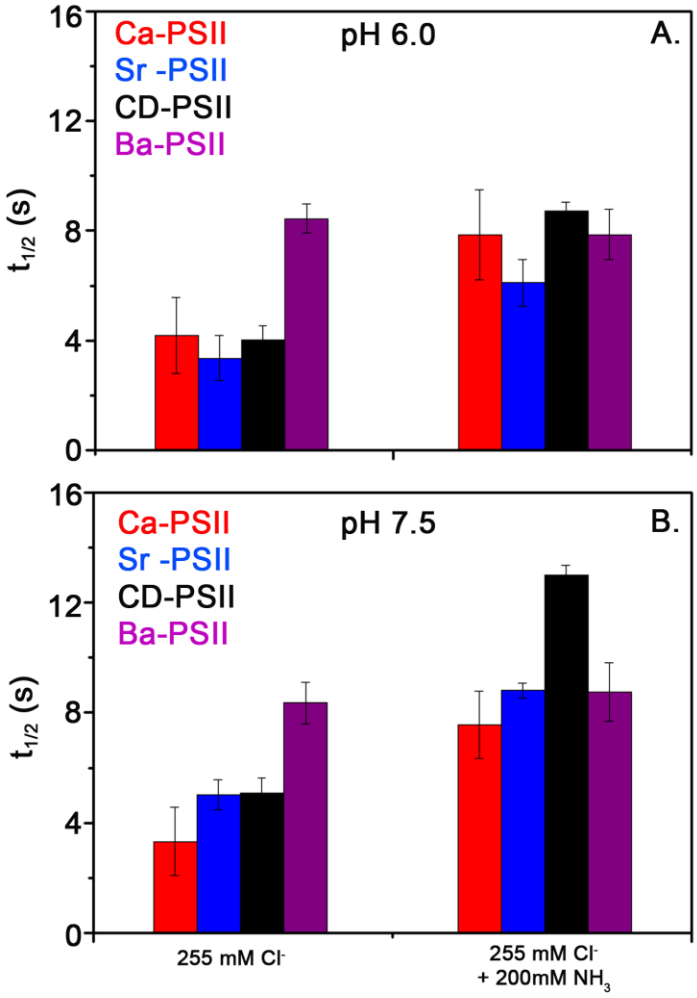

Figure 3.6 Kinetic parameters associated with the S2YZ• PCET reaction. The t1/2 (A, B) was derived from biexponential fits to the kinetic traces (Figure 3.5). In (A, pH 6.0) and (B, pH 7.5), left, without ammonia; right, with 200 mM ammonia. Samples were: Ca-PSII, red, Sr-PSII, blue, CD-PSII, black and Ba-PSII, violet; total chloride, 255 mM. The points are the mean of 56-112 measurements; the error bars correspond to one standard deviation.

3.4.3 Ba-PSII.

At pH 6.0 and 7.5, reconstitution of the inhibitory ion, barium, into the calcium site was associated with a significant slowing of the YZ radical decay rate. The $t_{1/2}$ values of 8.44 $\pm$ 0.52 s (pH 6.0) and 8.36 $\pm$ 0.75 (pH 7.5) are the same within experimental error and significantly larger than the values observed in any of the other samples (Ca-PSII, CD-PSII, Sr-PSII, Table S2, Figure 3.5A and B, and Figure 3.6A and B).

3.4.4 CD-PSII.

The effects of calcium depletion on YZ• PCET were also tested. As shown in Figures 4B and 5B, CD-PSII slows the decay rate at pH 7.5, in a manner corresponding to results obtained from Sr-PSII. Comparing biexponential fits (Table 5 and Figure 3.5), Ca-PSII gave 0.56 s^{-1} (49%), 0.028 s^{-1} (51%) and CD-PSII gave 0.46 s^{-1} (43%), 0.029 s^{-1} (57%) at pH 7.5. This result supports the conclusion that calcium facilitates YZ PCET at this pH value. Interestingly, at pH 6.0, calcium depletion had no significant effect on the velocity of the reaction (Figure 3.5A and Figure 3.6A).

3.4.5 Ammonia Inhibition.

In order to test for the involvement of the OEC hydrogen-bonding network, CD-PSII, Ca-PSII, Sr-PSII, and Ba-PSII were treated with 200 mM NH_4Cl (pH 6.0, 1.15 x 10^{-4} M free base NH_3; pH 7.5, 3.6 x 10^{-3} M free base NH_3, ~40 μM PSII reaction center). Ammonia inhibits oxygen activity of PSII, and X-ray crystallography and magnetic resonance spectroscopies have defined ammonia binding sites. One ammonia binding site competes with chloride (Figure 3.6).[5, 37-41] At the high chloride concentration used here

(255 mM), only the non-chloride competing site would be expected to be occupied.[5, 40, 51] Ammonia binding to PSII has also been shown to alter C=O carbonyl frequencies in the oxygen-evolving complex.[36]

When ammonia was added to Ca-PSII, the decay rate of $S_2YZ\bullet$ decreased (red dotted line) at pH 7.5 (Figure 3.4B). A decrease of YZ radical decay rate in ammonia at pH 7.5 has been reported previously in BBY membranes. Here, the reported change $t_{1/2}$ is smaller (2 fold), compared to change previously reported in BBY membranes (17 fold)[15-16]. This could be due to the decrease in time between data acquisition cycles, which was employed here. To investigate this, experiments were conducted on ammonia-treated, Ca-PSII at pH 7.5 with two different repetition rates, either a flash every 80 s or a flash every 160 s. With a flash every 80 s, the half-life was 7.56 ± 1.23 sec, and the initial intensity was 480 ± 92. With a flash every 160 s, the half-life was 9.98 ± 2.21 sec, and the initial intensity was 310 ± 120. Therefore, increasing the time between flashes does have an effect, albeit modest, when the decay of the radical is relatively long in ammonia-treated PSII. The remaining difference between the ammonia-treated OTG PSII preparations and BBY membranes appears to be preparation-dependent.

Ammonia is known to be an inhibitor of steady-state oxygen evolution activity at pH 6.0 and 7.5.[36] Figures 4C and D shows that ammonia treatment decreases the rate of YZ decay at pH 6.0, as well as pH 7.5. Biexponential fits (Table 5 and Figure 3.6) reveal that the ammonia effect is on the relative amplitudes of the fast and slow phases, as well as the rate constants.

Addition of ammonia to Sr-PSII and CD-PSII also decreased the decay rate of $S_2YZ\bullet$ at pH 6.0 and 7.5 (Figure 3.5C and D, Figure 3.6A and B, and Table 4). The largest

change in decay time was observed in CD-PSII at pH 7.5, suggesting that calcium depletion may result in a new interaction between ammonia and the hydrogen-bonding network. These observations support the conclusion that YZ PCET involves PCET through the hydrogen-bonding network at both pH values. Interestingly, however, ammonia treatment did not alter the lifetime in Ba-PSII (Table 4 and Figure 3.6), regardless of the pH value. This is attributed to the expected increase in the pK_a of barium-bound water (13.4 versus 12.8 for Ca^{2+}), its large ionic radius (1.34 Å versus 0.99 Å for Ca^{2+}),[34, 46] and subsequent disruption of hydrogen-bonding interactions.

3.5 Discussion

3.5.1 Summary.

We have studied the PCET reaction that accompanies recombination of YZ• and Q_A^- in PSII. We confirm that the 190 K YZ• PCET reaction rate is independent of pH in the control, Ca-PSII. These data were acquired at pH 6.0 and 7.5 and are in agreement with a previous report using a different (BBY) PSII preparation.[15] At pH 6.0, the YZ• decay rate was similar in Ca-PSII, Sr-PSII, and CD-PSII, but slowed significantly when barium was substituted at the calcium site. At pH 7.5, calcium depletion and strontium/barium substitution all slowed the YZ• decay rate. The magnitude of the effect was similar in Sr-PSII and CD-PSII, but much more significant in Ba-PSII. As discussed below, these data support the interpretation that there are two pathways for YZ• reduction at 190 K; one of these pathways is proposed to involve calcium-bound water and depend on OEC calcium occupancy. The results support the conclusion that both barium substitution and ammonia treatment cause a change in OEC hydrogen-bonding.

3.5.2 $YZ\bullet Q_A^-$ Recombination Mechanism.

Under the 190 K conditions employed here, the decay of YZ• occurs by recombination with an electron, derived from Q_A^-, and a proton. We assume that this temperature monitors an intermediate that is relevant to the oxygen-evolving reactions. Q_A^- may recombine with YZ• in a one-step or two-step mechanism. In the case of a single step, direct reaction, the measured reaction rate is many orders of magnitude greater than predicted by electron transfer theory and cofactor-cofactor distances in the cryogenic X-ray structure.[3,16, 52-53] A two-step mechanism for YZ radical decay is feasible.[16] Equation 1 and 2 summarize the two-step mechanism.

Equation 1

$$YZP_{680}^{+}\ Q_A^{-} \underset{k_2}{\overset{k_1}{\rightleftharpoons}} YZ\bullet P_{680}\ Q_A^{-}$$

Equation 2

$$YZP_{680}^{+}\ Q_A^{-} \xrightarrow{k_{in}} YZP_{680}\ Q_A$$

For this mechanism, the velocity expression is written:

Equation 3:

$$v = k_{in}\,[YZP_{680}^{+}\ Q_A^{-}]$$

, which can be rearranged to give:

Equation 4:

$$v = k_{in} \frac{k_2}{k_1} [YZ\bullet P_{680}Q_A^-]$$

As shown above, in a two-step mechanism, the velocity depends on the rate of $P_{680}^+Q_A^-$ recombination, k_{in}, as well as the equilibrium constant governing the PCET reaction between YZ• and P_{680}. The k_{in} recombination rate has been reported as $\sim 7 \times 10^2$ or 5×10^3 s^{-1} (0.2-1.4 ms) and is pH and solvent isotope independent.[54] We assume that k_{in} is not altered by substitutions at the calcium site.

The value of k_1, the rate constant of YZ oxidation, has been reported on the nanosecond time scale (20-200 ns) with a rate that is S state dependent.[55] Using these k_{in} and k_1 values and our experimentally measured velocity in Ca-PSII, k_{obs} (~0.2-0.3 s^{-1}), this two-step mechanism predicts the value of k_2 to be ~10^4 s^{-1}. In the discussion below, we assume that substitutions at the calcium site alter the velocity through changes in k_2 (reduction of YZ•).

3.5.3 Confirmation and Interpretation of the pH Independent Rate of YZ• Reduction.

Interestingly, in experiments on Ca-PSII, the overall rate of the pH 7.5 reaction is identical to the overall rate of the pH 6.0 reaction. This lack of pH dependence is in agreement with results obtained on BBY membranes[15-16] and is in contrast to previous observations for YD• PCET, which were pH dependent.[13-14] The pH dependent YD results were explained by proposing a change in mechanism. In particular, it was proposed that YD• reduction occurs via a PTET mechanism at low pH values and a CPET mechanism at high pH values. A proton inventory at high pH was concluded to be consistent with two proton donation pathways, one involving a single proton (and possibly His189-D2) and the

other involving water. The PSII structure does reveal a hydrogen bond between YD and His189-D2 (2.8 Å) and a single water molecule with partial occupancy (3.1 Å).

To explain the distinction between the YD and YZ results it was proposed that YZ radical PCET occurs by a pH independent mechanism that is either ETPT with ET rate limiting or CPET.[14,15] The solvent isotope effect measured in the S_2 state was considered to be more suggestive of CPET. Note that the experiments in ref [14, 15] explored the S state dependence of the YZ recombination rate and the solvent isotope effect. The results presented here support those earlier conclusions.

3.5.4 Proton Transfer to YZ• Occurs through the OEC Hydrogen-Bonding Network.

We report that ammonia treatment decreases the rate of YZ radical PCET in all samples, both at pH 6 and 7.5. A decrease in rate was reported previously for ammonia-treated BBY membranes at pH 7.5. Significantly, ammonia had no effect on the decay of the YD radical, which does not participate in the OEC hydrogen-bonding network (Figure 3.1 C).[16] The significant ammonia effect on YZ• PCET, observed in Ca-PSII, Sr-PSII, and CD-PSII, is consistent with PCET through a hydrogen-bonded network. The lack of ammonia effect in Ba-PSII is suggestive of a significant alteration in OEC interactions. Such a change is expected due to the large size of barium and the high, predicted pK_a of barium-bound water.[33-34, 46]

High-resolution X-ray structures, involving S_3-enriched PSII and ammonia-bound S_3-enriched PSII, have provided information concerning ammonia-binding sites in PSII.[5] It was inferred that ammonia can replace one of terminal water ligands of Mn4 (W1 or W2, Figure 3.1B), with displacement of W1 favored based on magnetic resonance data.[40, 51] A shift in W2 position was also noted (Figure 3.1B). This change in position was attributed

either to ammonia substitution or to a different protonation state of W2 at the different pH values employed (hydroxide ligand at pH 7.5 with ammonia-bound S_3-enriched PSII; protonated at pH 6.5 with S_3-enriched PSII).[5] These suggested positions for ammonia binding are all consistent with our results (Figure 3.7).

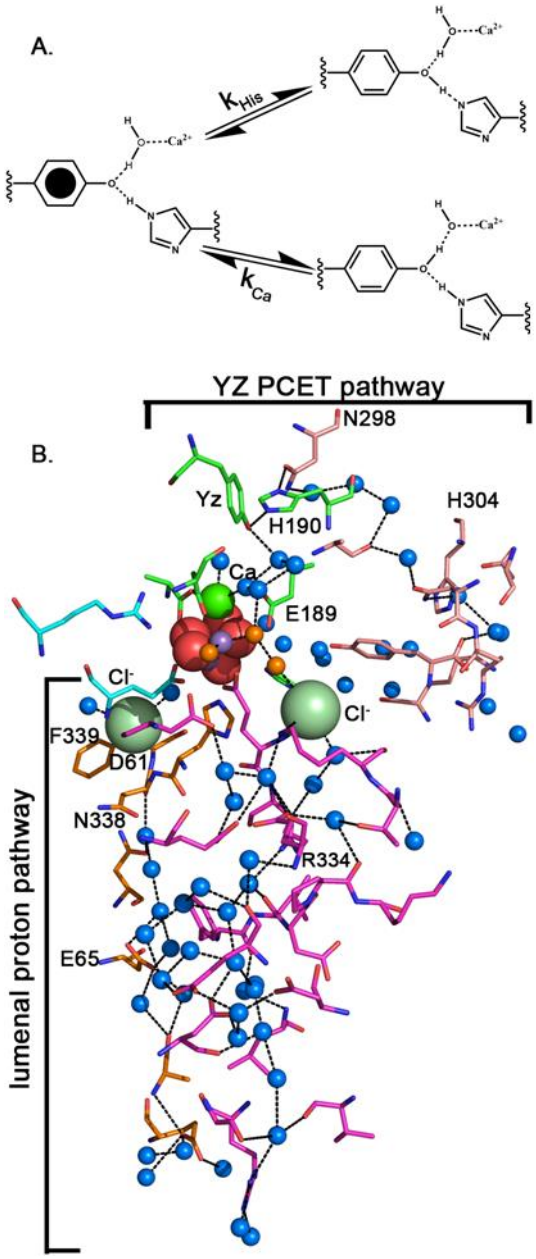

Figure 3.7 (A) Schematic diagram of the proposed proton donation pathway for YZ•, showing two possible donors; (B) Putative YZ• PCET pathway and chloride-dependent proton exit pathways to the lumen (1.9 Å, cyanobacterial PSII, PDB ID:

4UB6).[3-4] The residues shown are in subunits, D1, D2, CP43, CP47, PsbO, and PsbV. In the OEC, calcium is in green, oxygen is in red and manganese is in purple. Blue spheres represent water molecules, as assigned in ref.[3] Orange spheres represent proposed ammonia binding sites.[5, 40-41, 51] Selected amino acid side chains in the D1 subunit are labeled.

3.5.5 Calcium depletion has differential effects on YZ• decay at pH 6.0 and 7.5.

We report that calcium depletion decreases the rate of YZ• decay at pH 7.5, either in the presence or absence of ammonia. Calcium depletion has previously been proposed to change the protonation and hydrogen bonding of Mn_4CaO_5 ligands.[28-29] To explain our results, we suggest that calcium depletion is associated with deprotonation of a water ligand to give a coordinating hydroxide. Note that the effects of barium are similar at the two pH values.

3.5.6 YZ• PCET Involves Two, Competing Proton Donors.

To explain the differential pH effects observed in CD-PSII and Sr-PSII, we propose two competing pathways for PCET to YZ• (Figure 3.7A). There are several reasons to propose two pathways, including (1) the X-ray crystal structures of PSII, (2) previous studies of His190 and Glu 189 mutants, and (3) the differential effects of strontium replacement and calcium depletion at pH 6 and 7.5, as documented here. First, X-ray structures of PSII suggest the possibility of multiple proton donation pathways to YZ radical, one involving His190- D1 and one involving water.[3-4] Cryogenic structures of PSII reveal a short hydrogen bond (2.5 Å) between the YZ singlet state and His190-D1 (Figure 3.1B).[3-4] The hydrogen bond to histidine is also present, but may be somewhat longer (2.8 Å), in a recent room temperature PSII structure.[5] In the cryogenic PSII structures, a diamond-shaped water network also interacts both with YZ and calcium (Figure 3.1B).

The YZ-water hydrogen bond is 2.7 Å; the distance from YZ to calcium-bound water is 2.8 Å. Internal water is also predicted in the room temperature structure. Thus, PSII structures are consistent with His190-D1, metal bound water, and water acting as possible proton donors to YZ•. Unfortunately, the pK_a values of His190 and the metal-bound waters in the S_2 singlet and radical states are not known.[56] However, imidazole groups in proteins, water ligands to calcium, and water ligands to strontium typically have pK_a values of 6.4, 12.6, and 13.2, respectively.[57-58]

Second, while chemical complementation has provided evidence that His190-D1 plays a role in YZ• PCET,[59] the effects of the HQ190-D1 mutation on the EPR signal of YZ were modest, especially at low temperature.[60] It was concluded that His190 and Glu189 in the D1 subunit provide structural stabilization in the oxygen-evolving complex. The fact the EPR spectra and kinetic data were relatively unaltered at low temperature can be interpreted as evidence for another proton donor to YZ•.[60]

Third, we observe differential effects of calcium depletion and strontium replacement at pH 6 and 7.5. At pH 6.0, the rate of YZ PCET is independent of these manipulations. At pH 7.5, calcium depletion and strontium reconstitution slow the rate by a similar amount. In a straightforward interpretation, such data could result from a two competing YZ• PCET pathways (Figure 3.7A), with a putative histidine pathway dominating at low pH and an activated water pathway dominating at high pH.

At pH 7.5, k_{Ca}, the activated water pathway, is proposed to be the dominant pathway. We favor this interpretation because strontium reconstitution and calcium depletion both decreased the overall velocity of the reaction, consistent with $k_{His} << k_{Ca}$.

This is reasonable, because His190-D1 is expected to be in the fully or partially unprotonated state at this pH.

At pH 6.0, k_{His} is proposed to be the dominant pathway. We favor this interpretation because strontium reconstitution and calcium depletion had no significant effect on the overall velocity of the reaction at this pH, consistent with $k_{His} >> k_{Ca}$. Note that the same CD-PSII preparations were used at both pH values and that oxygen evolution rates were consistent with effective removal and reconstitution of calcium/strontium at both pH values. The conclusion that k_{His} dominates at pH 6.0 is reasonable, because His190-D1 is expected to be in the imidazolium cationic state at this pH value. Interpretations, in which occupancy at the calcium site exerts an electrostatic effect on the rate, are not favored, because Sr-PSII and CD-PSII gave similar rates at pH 7.5. Results obtained in Ba-PSII are attributed to distortion of the calcium site.

Note that an interpretation in which a substantial conformational change leads to a pK_a shift is not favored. Such a change seems unlikely at 190 K, and a large conformational change is not currently proposed to accompany the S state transitions.[61]

3.5.7 Relationship to Previous Work Using Calcium Depletion.

The effects of calcium depletion on PSII have been reviewed.[26-27] It was suggested previously that occupancy at the calcium site influences YZ PCET. It was also proposed that there are separate proton donors and acceptors for YZ.

To give one example, previous EPR work has studied the effects of calcium depletion on YZ• reduction at room temperature.[23] In those EPR studies of calcium-depleted BBY membranes, the reaction rate was reported to slow at pH 6.5, leading to photoaccumulation of a putative YZ radical signal under illumination, relative to a control.

This is in contrast to our results at pH 6.0, in which no significant effect on YZ radical reduction was observed in CD-PSII. However, the calcium depletion method used in ref 23 employed a different procedure (high salt washing) to deplete calcium, and the measurements were conducted at 273 K. In OTG PSII, we have reported that high salt washing is associated with less effective reconstitution of calcium,[34, 43] and, therefore, we employ this distinct method. The calcium depletion method or the higher temperature employed in the measurements of ref 23 may have been associated with destabilization of the proton transfer pathway.

In another example, it was concluded that calcium depletion changes the oxidation rate of YZ. In those optical spectroscopic studies of YZ oxidation in plant PSII, the effect of calcium depletion was found to be pH dependent.[24] The rate of electron transfer from YZ to P_{680}^{+} was slowed by three orders of magnitude when calcium was removed and when assays were conducted either at pH 6 or 7.5. The effects were judged to be similar to the effects associated with manganese depletion.[24] Note that slowing of the YZ oxidation rate by several orders of magnitude would not change the results of our experiments, which have a significant lag time before the beginning of data acquisition. In that previous work on calcium depleted PSII, proton release was observed along with the development of a solvent isotope effect (from 1.1 to 2.5). It was concluded that one role of calcium is to tune the pK_a of the base which acts as a proton acceptor for YZ. Conversely, the unprotonated state of this base would be required for the high affinity of the calcium binding site. In the absence of calcium, it was proposed that the pK_a of the base, for example His 190, is increased (from 4.5 to 7). The CD-induced pK_a shift was proposed to disrupt a facilitating hydrogen bond interaction between YZ-OH and $H^{+}B$ and therefore decrease the

contribution of fast components. Calcium depletion had a greater impact at pH 6.0, as assessed from the kinetic halftimes.

3.5.8 Relationship to Previous Work Using Strontium Substitution.

The effect of strontium reconstitution on YZ decay was assessed by EPR spectroscopy.[62] Strontium-substituted BBY membranes at room temperature were used. Sr-PSII displayed slower reduction kinetics during the $S_2YZ^{\bullet}$ reduction reaction (half-time 900 μs), compared to the kinetics observed (half time 200 μs) in Ca-PSII. There was no significant pH effect. Again, this paper reports results distinct from the data presented here. This difference may be due to the method used to remove calcium or to some destabilization of the PCET pathway under the multiple flash, room temperature conditions of ref[62].

3.5.9 Influence of $n(H_2O)H_3O^+$ Cluster on $YZ^{\bullet}$ PCET in the S_2 State.

Previously, an internal protonated water cluster has been identified in the S_2 state of PSII.[42-45] The protonated water cluster, $n(H_2O)H_3O^+$ or W_n^+ was associated with the S_1-to-S_2 transition and promoted at 190 K using red illumination in Ca-PSII. The W_n^+ infrared signal was also detected using with saturating laser flashes to advance the S states at higher temperatures.[42-43, 45] The formation of the protonated cluster was attributed to a proton transfer event in one of the lumenal proton exit pathways (Figure 3.7B). Notably, under conditions in which the W_n^+ infrared band from the water cluster was observed, YZ radical had already decayed and was not present in significant concentration. Therefore, the PCET pathway associated with the S_2 cationic cluster is distinct from $YZ^{\bullet}$ PCET pathway.

Previous proposals for the lumenal proton exit pathways and YZ proton transfer pathway are summarized in Figure 3.7B.

Interestingly, the changes in the YZ• decay rate, reported here, correlate with alterations observed in previous studies of the W_n^+ signal. For example, the W_n^+ infrared band was not observed in CD-PSII and Sr-PSII at pH 7.5. However, the band was observed in CD-PSII and Sr-PSII at pH 6.0. This pH-induced change was attributed to a different localization of W_n^+ in the pathway or to instability of W_n^+ in CD-PSII and Sr-PSII at pH 7.5.[44] It was suggested that this change may be caused by protonation of an amino acid residue, possibly His337, in the lumenal proton exit pathway (Figure 3.7B). To explain the correlation between W_n^+ and YZ• PCET reaction rate, described here, we propose that the charge on the protonated water cluster, W_n^+, increases the pK_a of the YZ• donor, by stabilizing its conjugate base.

3.6 Conclusions

The data presented here provide new information concerning the hydrogen-bonding network and S_2YZ• PCET at cryogenic temperature. At this temperature, the oxygen evolving reactions are blocked, and we characterize an intermediate in the YZ• pathway. Correlations with previous infrared studies of W_n^+ suggest that calcium and pH modulate both proton exit pathways and the S_2YZ• PCET reaction. We conclude that both proton exit and S_2YZ• PCET pathways are calcium dependent at high pH. Finally, we present evidence that barium and ammonia both disrupt the OEC hydrogen-bonding network.

3.7 References

1. Dempsey, J. L.; Winkler, J. R.; Gray, H. B., Proton-Coupled Electron Flow in Protein Redox Machines. *Chem. Rev.* **2010,** *110* (12), 7024-39.

2. Cox, N.; Pantazis, D. A.; Neese, F.; Lubitz, W., Biological Water Oxidation. *Acc. Chem. Res.* **2013,** *46* (7), 1588-96.

3. Umena, Y.; Kawakami, K.; Shen, J. R.; Kamiya, N., Crystal Structure of Oxygen-Evolving Photosystem II at a Resolution of 1.9 A. *Nature* **2011,** *473* (7345), 55-60.

4. Suga, M.; Akita, F.; Hirata, K.; Ueno, G.; Murakami, H.; Nakajima, Y.; Shimizu, T.; Yamashita, K.; Yamamoto, M.; Ago, H.; Shen, J. R., Native Structure of Photosystem II at 1.95 A Resolution Viewed by Femtosecond X-Ray Pulses. *Nature* **2015,** *517* (7532), 99-103.

5. Young, I. D.; Ibrahim, M.; Chatterjee, R.; Gul, S.; Fuller, F. D.; Koroidov, S.; Brewster, A. S.; Tran, R.; Alonso-Mori, R.; Kroll, T.; Michels-Clark, T.; Laksmono, H.; Sierra, R. G.; Stan, C. A.; Hussein, R.; Zhang, M.; Douthit, L.; Kubin, M.; de Lichtenberg, C.; Vo Pham, L.; Nilsson, H.; Cheah, M. H.; Shevela, D.; Saracini, C.; Bean, M. A.; Seuffert, I.; Sokaras, D.; Weng, T. C.; Pastor, E.; Weninger, C.; Fransson, T.; Lassalle, L.; Brauer, P.; Aller, P.; Docker, P. T.; Andi, B.; Orville, A. M.; Glownia, J. M.; Nelson, S.; Sikorski, M.; Zhu, D.; Hunter, M. S.; Lane, T. J.; Aquila, A.; Koglin, J. E.; Robinson, J.; Liang, M.; Boutet, S.; Lyubimov, A. Y.; Uervirojnangkoorn, M.; Moriarty, N. W.; Liebschner, D.; Afonine, P. V.; Waterman, D. G.; Evans, G.; Wernet, P.; Dobbek, H.; Weis, W. I.; Brunger, A. T.; Zwart, P. H.; Adams, P. D.; Zouni, A.; Messinger, J.; Bergmann, U.; Sauter, N. K.; Kern, J.; Yachandra, V. K.; Yano, J., Structure of Photosystem II and Substrate Binding at Room Temperature. *Nature* **2016,** *540* (7633), 453-457.

6. Saito, K.; Shen, J. R.; Ishida, T.; Ishikita, H., Short Hydrogen Bond between Redox-Active Tyrosine Yz and D1-His190 in the Photosystem II Crystal Structure. *Biochemistry* **2011,** *50* (45), 9836-9844.

7. Retegan, M.; Cox, N.; Lubitz, W.; Neese, F.; Pantazis, D. A., The First Tyrosyl Radical Intermediate Formed in the S_2-S_3 Transition of Photosystem II. *Phys. Chem. Chem. Phys.* **2014,** *16* (24), 11901-10.

8. Ugur, I.; Rutherford, A. W.; Kaila, V. R., Redox-Coupled Substrate Water Reorganization in the Active Site of Photosystem II: The Role of Calcium in Substrate Water Delivery. *Biochim. Biophys. Acta* **2016,** *1857* (6), 740-8.

9. Styring, S.; Rutherford, A. W., Deactivation Kinetics and Temperature Dependence of the S-State Transitions in the Oxygen-Evolving System of Photosystem II Measured by EPR Spectroscopy. *Biochim. Biophys. Acta* **1988,** *933* (2), 378-387.

10. Barry, B. A., Proton Coupled Electron Transfer and Redox Active Tyrosines in Photosystem II. *J. Photochem. Photobiol. B* **2011,** *104* (1-2), 60-71.

11. Pujols-Ayala, I.; Barry, B. A., Tyrosyl Radicals in Photosystem II. *Biochim. Biophys. Acta* **2004,** *1655* (1-3), 205-16.

12. Ioannidis, N.; Zahariou, G.; Petrouleas, V., The EPR Spectrum of Tyrosine Z(Center Dot) and Its Decay Kinetics in O_2-Evolving Photosystem II Preparations. *Biochemistry* **2008,** *47* (24), 6292-6300.

13. Jenson, D. L.; Evans, A.; Barry, B. A., Proton-Coupled Electron Transfer and Tyrosine D of Photosystem II. *J. Phys. Chem. B* **2007,** *111* (43), 12599-12604.

14. Jenson, D. L.; Barry, B. A., Proton-Coupled Electron Transfer in Photosystem II: Proton Inventory of a Redox Active Tyrosine. *J. Am. Chem. Soc.* **2009,** *131* (30), 10567-10573.

15. Keough, J. M.; Jenson, D. L.; Zuniga, A. N.; Barry, B. A., Proton Coupled Electron Transfer and Redox-Active Tyrosine Z in the Photosynthetic Oxygen-Evolving Complex. *J. Am. Chem. Soc.* **2011,** *133* (29), 11084-11087.

16. Keough, J. M.; Zuniga, A. N.; Jenson, D. L.; Barry, B. A., Redox Control and Hydrogen Bonding Networks: Proton-Coupled Electron Transfer Reactions and Tyrosine Z in the Photosynthetic Oxygen-Evolving Complex. *J. Phys. Chem. B* **2013,** *117* (5), 1296-1307.

17. Kok, B.; Forbush, B.; Mcgloin, M., Cooperation of Charges in Photosynthetic O_2 Evolution: 1. A Linear 4-step Mechanism. *Photochem. Photobiol.* **1970,** *11* (6), 457-475.

18. Yano, J.; Kern, J.; Yachandra, V. K.; Nilsson, H.; Koroidov, S.; Messinger, J., Light-Dependent Production of Dioxygen in Photosynthesis. *Met. Ions Life Sci.* **2015,** *15*, 13-43.

19. Zaharieva, I.; Dau, H.; Haumann, M. Sequential and Coupled Proton and Electron Transfer Events in the S2→ S3 Transition of Photosynthetic Water Oxidation Revealed by Time-Resolved X-Ray Absorption Spectroscopy. http://pubs.acs.org/doi/pdfplus/10.1021/acs.biochem.6b01078.

20. de Paula, J. C.; Innes, J. B.; Brudvig, G. W., Electron Transfer in Photosystem II at Cryogenic Temperatures. *Biochemistry* **1985,** *24* (27), 8114-20.

21. Babcock, G. T.; Sauer, K., The Rapid Component of Electron Paramagnetic Resonance Signal II: A Candidate for the Physiological Donor to Photosystem II in Spinach Chloroplasts. *Biochim. Biophys. Acta* **1975,** *376*, 329-344.

22. Dekker, J. P.; Van Gorkom, H. J.; Brok, M.; Ouwehand, L., Optical Characterization of Photosystem II Electron Donors. *Biochim. Biophys. Acta* **1984,** *764*, 301-309.

23. Lydakis-Simantiris, N.; Dorlet, P.; Ghanotakis, D. F.; Babcock, G. T., Kinetic and Spectroscopic Properties of the Y-z Center Dot Radical in Ca^{2+} and Cl^--Depleted Photosystem II Preparations. *Biochemistry* **1998,** *37* (18), 6427-6435.

24. Haumann, M.; Junge, W., Evidence for Impaired Hydrogen-Bonding of Tyrosine YZ in Calcium-Depleted Photosystem II. *Biochim. Biophys. Acta* **1999,** *1411* (1), 121-33.

25. Haumann, M.; Mulkidjanian, A.; Junge, W., Tyrosine-Z in Oxygen-Evolving Photosystem II: A Hydrogen-Bonded Tyrosinate. *Biochemistry* **1999,** *38* (4), 1258-67.

26. Miqyass, M.; Marosvolgyi, M. A.; Nagel, Z.; Yocum, C. F.; van Gorkom, H. J., S-state Dependence of the Calcium Requirement and Binding Characteristics in the Oxygen-Evolving Complex of Photosystem II. *Biochemistry* **2008,** *47* (30), 7915-24.

27. Miqyass, M.; van Gorkom, H. J.; Yocum, C. F., The PSII Calcium Site Revisited. *Photosyn. Res.* **2007,** *92* (3), 275-287.

28. Siegbahn, P. E. M., Water Oxidation Energy Diagrams for Photosystem II for Different Protonation States, and the Effect of Removing Calcium. *Phys. Chem. Chem. Phys.* **2014,** *16* (24), 11893-11900.

29. Saito, K.; Ishikita, H., Influence of the Ca^{2+} Ion on the Mn_4Ca Conformation and the H-Bond Network Arrangement in Photosystem II. *Biochim. Biophys. Acta* **2014,** *1837* (1), 159-166.

30. Latimer, M. J.; DeRose, V. J.; Yachandra, V. K.; Sauer, K.; Klein, M. P., Structural Effects of Calcium Depletion on the Manganese Cluster of Photosystem II: Determination by X-Ray Absorption Spectroscopy. *J. Phys. Chem. B* **1998,** *102* (42), 8257-8265.

31. Yachandra, V. K.; Yano, J., Calcium in the Oxygen-Evolving Complex: Structural and Mechanistic Role Determined by X-Ray Spectroscopy. *J. Photochem. Photobiol. B* **2011,** *104* (1-2), 51-59.

32. Lohmiller, T.; Cox, N.; Su, J. H.; Messinger, J.; Lubitz, W., The Basic Properties of the Electronic Structure of the Oxygen-evolving Complex of Photosystem II Are Not Perturbed by Ca^{2+} Removal. *J. Biol. Chem.* **2012,** *287* (29), 24721-24733.

33. Yocum, C. F., The Calcium and Chloride Requirements of the O_2 Evolving Complex. *Coordin. Chem. Rev.* **2008,** *252* (3-4), 296-305.

34. Polander, B. C.; Barry, B. A., Calcium and the Hydrogen-Bonded Water Network in the Photosynthetic Oxygen-Evolving Complex. *J Phys. Chem. Lett.* **2013,** *4* (5), 786-91.

35. Koua, F. H. M.; Umena, Y.; Kawakami, K.; Shen, J. R., Structure of Sr-substituted Photosystem II at 2.1 Angstrom Resolution and Its Implications in the Mechanism of Water Oxidation. *Proc. Natl. Acad. Sci. USA* **2013,** *110* (10), 3889-3894.

36. Polander, B. C.; Barry, B. A., A Hydrogen-Bonding Network Plays a Catalytic Role in Photosynthetic Oxygen Evolution. *Proc. Nat. Acad. Sci. USA* **2012,** *109*, 6112-6117.

37. Britt, R. D.; Zimmermann, J. L.; Sauer, K.; Klein, M. P., Ammonia Binds to the Catalytic Mn of the Oxygen-Evolving Complex of Photosystem II: Evidence by Electron-Spin Echo Envelope Modulation Spectroscopy. *J. Am. Chem. Soc.* **1989,** *111* (10), 3522-3532.

38. Boussac, A.; Rutherford, A. W.; Styring, S., Interaction of Ammonia with the Water Splitting Enzyme of Photosystem II. *Biochemistry* **1990,** *29* (1), 24-32.

39. Kim, D. H.; Britt, R. D.; Klein, M. P.; Sauer, K., The Manganese Site of the Photosynthetic Oxygen-Evolving Complex Probed by EPR Spectroscopy of Oriented Photosystem II Membranes: the g = 4 and g = 2 Multiline Signals. *Biochemistry* **1992,** *31* (2), 541-547.

40. Navarro, M. P.; Ames, W. M.; Nilsson, H.; Lohmiller, T.; Pantazis, D. A.; Rapatskiy, L.; Nowaczyk, M. M.; Neese, F.; Boussac, A.; Messinger, J.; Lubitz, W.; Cox, N., Ammonia Binding to the Oxygen-Evolving Complex of Photosystem II Identifies the Solvent-Exchangeable Oxygen Bridge (μ-oxo) of the Manganese Tetramer. *Proc. Natl. Acad. Sci. USA* **2013,** *110* (39), 15561-15566.

41. Vinyard, D. J.; Askerka, M.; Debus, R. J.; Batista, V. S.; Brudvig, G. W., Ammonia Binding in the Second Coordination Sphere of the Oxygen-Evolving Complex of Photosystem II. *Biochemistry* **2016,** *55* (31), 4432-6.

42. Polander, B. C.; Barry, B. A., Detection of an Intermediary, Protonated Water Cluster in Photosynthetic Oxygen Evolution. *Proc. Natl. Acad. Sci. USA* **2013,** *110* (26), 10634-9.

43. Polander, B. C.; Barry, B. A., Calcium, Strontium, and Protein Dynamics during the S2 to S3 Transition in the Photosynthetic Oxygen-Evolving Cycle. *J. Phys. Chem. Lett.* **2013,** *4*, 3356-3362.

44. Guo, Z.; Barry, B. A., Cryogenic Trapping and Isotope Editing Identify a Protonated Water Cluster as an Intermediate in the Photosynthetic Oxygen-Evolving Reaction. *J. Phys. Chem. B* **2016,** *120* (34), 8794-8808.

45. Brahmachari, U.; Barry, B. A., Dynamics of Proton Transfer to Internal Water during the Photosynthetic Oxygen-Evolving Cycle. *J. Phys. Chem. B* **2016,** *120* (44), 11464-11473.

46. Vrettos, J. S.; Stone, D. A.; Brudvig, G. W., Quantifying the Ion Selectivity of the Calcium Site in Photosystem II: Evidence for Direct Involvement of Ca^{2+} in O_2 Formation. *Biochemistry* **2001,** *40*, 7937-7945.

47. Berthold, D. A.; Babcock, G. T.; Yocum, C. F., A Highly Resolved, Oxygen-Evolving Photosystem-Ii Preparation from Spinach Thylakoid Membranes: Electron-Paramagnetic-Res and Electron-Transport Properties. *FEBS Lett.* **1981,** *134* (2), 231-234.

48. Mishra, R. K.; Ghanotakis, D. F., Selective Extraction of CP 26 and CP 29 Proteins without Affecting the Binding of the Extrinsic Proteins (33, 23 and 17 kDa) and the DCMU Sensitivity of a Photosystem-II Core Complex. *Photosynth. Res.* **1994,** *42* (1), 37-42.

49. Renger, G.; Renger, T., Photosystem II: The Machinery of Photosynthetic Water Splitting. *Photosyn. Res.* **2008,** *98* (1-3), 53-80.

50. Steenhuis, J. J.; Barry, B. A., The Protein and Ligand Environment of the S_2 State in Photosynthetic Oxygen Evolution: a Difference FT-IR Study. *J. Phys. Chem. B* **1997,** *101*, 6652-6660.

51. Oyala, P. H.; Stich, T. A.; Debus, R. J.; Britt, R. D., Ammonia Binds to the Dangler Manganese of the Photosystem II Oxygen-Evolving Complex. *J. Am. Chem. Soc.* **2015,** *137* (27), 8829-8837.

52. Marcus, R. A.; Sutin, N., Electron Transfers in Chemistry and Biology. *Biochim. Biophys. Acta* **1985,** *811* (3), 265-322.

53. Page, C. C.; Moser, C. C.; Chen, X. X.; Dutton, P. L., Natural Engineering Principles of Electron Tunnelling in Biological Oxidation-Reduction. *Nature* **1999,** *402* (6757), 47-52.

54. Ahlbrink, R.; Haumann, M.; Cherepanov, D.; Bogershausen, O.; Mulkidjanian, A.; Junge, W., Function of Tyrosine Z in Water Oxidation by Photosystem II: Electrostatical Promotor Instead of Hydrogen Abstractor. *Biochemistry* **1998,** *37* (4), 1131-1142.

55. Brettel, K.; Schlodder, E.; Witt, H. T., Nanosecond Reduction Kinetics of Photooxidized Chlorophyll-Alpha-II (P_{680}) in Single Flashes as a Probe for the Electron Pathway, H^+ Release and Charge Accumulation in the O_2 Evolving Complex. *Biochim. Biophys. Acta* **1984,** *766* (2), 403-415.

56. Shen, J. R., The Structure of Photosystem II and the Mechanism of Water Oxidation in Photosynthesis. *Annu. Rev. Plant. Biol.* **2015,** *66*, 23-48.

57. Thomas, K. H.; George, J. T., Structural Basis of Perturbed pKa Values of Catalytic Groups in Enzyme Active Sites. *Life* **2002,** *53*, 85-98.

58. Speight, J. G., *Lange's Handbook of Chemistry*. McGraw-Hill New York: New York, U.S.A., 2005.

59. Hays, A. M. A.; Vassiliev, I. R.; Golbeck, J. H.; Debus, R. J., Role of D1-His190 in Proton-Coupled Electron Transfer Reactions in Photosystem II: A Chemical Complementation Study. *Biochemistry* **1998,** *37* (32), 11352-11365.

60. Pujols-Ayala, I.; Barry, B. A., Histidine 190-D1 and Glutamate 189-D1 Provide Structural Stabilization in Photosystem II. *Biochemistry* **2002,** *41* (38), 11456-11465.

61. Sauter, N. K.; Echols, N.; Adams, P. D.; Zwart, P. H.; Kern, J.; Brewster, A. S.; Koroidov, S.; Alonso-Mori, R.; Zouni, A.; Messinger, J.; Bergmann, U.; Yano, J.; Yachandra, V. K., No Observable Conformational Changes in PSII. *Nature* **2016,** *533* (7603), E1-2.

62. Westphal, K. L.; Lydakis-Simantris, N.; Cukier, R. I.; Babcock, G. T., Effects of Sr^{2+} Substitution on the Reduction Rates of Yz in PSII Membranes: Evidence for Concerted Hydrogen-Atom Transfer in Oxygen Evolution. *Biochemistry* **2000,** *39*, 16220-16229.

CHAPTER 4. CALCIUM, CONFORMATIONAL SELECTION, AND REDOX-ACTIVE TYROSINE YZ IN THE PHOTOSYNTHETIC OXYGEN EVOLVING CLUSTER

By

Zhanjun Guo, Jiayuan He and Bridgette A. Barry*

School of Chemistry and Biochemistry and Petit Institute for Bioengineering and Biosciences, Georgia Institute of Technology, Atlanta, Georgia 30332, United States

4.1 Abstract

In Photosystem II (PSII), YZ (Tyr161 of the D1 polypeptide) participates in radical transfer between the primary chlorophyll donor and the Mn_4CaO_5 cluster. With flashing illumination, the metal cluster cycles among 5 states, termed $S_{0\text{-}4}$, and the essential YZ is transiently oxidized and reduced on each flash. Electron transfer to the neutral YZ radical is coupled with a proton transfer (PCET) reaction. Calcium is required for activity; of all reconstituted divalent ions, only strontium reconstitutes activity. YZ is predicted to hydrogen bond to calcium-bound water and to His190D1 in X-ray structures of PSII. Here, we report the first vibrational spectroscopic study of the YZ radical and YZ singlet states in the presence of an intact metal cluster. The S_2 state is trapped by illumination at 190 K; flash illumination generates the S_2YZ radical state, which decays by recombination with Q_A^-, as monitored by EPR spectroscopy. Using reaction-induced FT-IR spectroscopy, calcium depletion, and strontium and barium reconstitution, we identify calcium, strontium, and barium-sensitive tyrosyl radical and singlet bands in the S_2 state. The frequencies of these bands are correlated with the expected pK_a's of metal-bound water and are indicative either of hydrogen bond or electrostatic interactions between calcium/strontium, and YZ radical. The data also provide evidence that YZ singlet is hydrogen bonded as a proton acceptor to calcium-bound water. Analysis of the amide I region indicates that calcium selects for a PCET reaction in a subset of the YZ conformers, which are trapped in the S_2 state. These results support the interpretation that YZ undergoes a redox-coupled conformational change under illumination, which is calcium dependent.

4.2 Introduction

Photosystem II (PSII) carries out the process of light-driven photosynthetic oxygen evolution (Figure 4.1A). This reaction is essential for the maintenance of aerobic life on earth and is a model for the development of sustainable alternative energy. Absorption of light by PSII induces a charge separation between the dimeric chl donor, P_{680}, and a bound plastoquinone, Q_A or Q_B (Figure 4.1A). P_{680}^+ subsequently oxidizes YZ, which then removes an electron from the nearby Mn_4CaO_5 cluster.[1-2] The Mn_4CaO_5 cluster is the site of water binding and oxidation. The YZ radical/ YZ redox couple acts as the interface between the one electron chemistry of the reaction center and the four electrons-four protons reaction, which is required to release oxygen from water. On each light-driven step, YZ, which is tyrosine in the D1 polypeptide (Y161-D1, Figure 4.1B) is transiently oxidized and reduced by a PCET mechanism (Figure 4.1C). YZ is essential for oxygen evolution. In X-ray structures from cyanobacteria and higher plants, YZ is hydrogen bonded to His190 in the D1 polypeptide. YZ is also hydrogen bonded to a calcium-bound water molecule (Figure 4.1B).[1-5] The extensive, calcium-dependent hydrogen-bonding network, which is evident in the PSII X-ray structures, has been proposed to be important in YZ PCET reactions. [6-9]

With flash illumination, the oxygen evolving complex cycles through 5 different oxidation states, named the S_n states, where n = 0-4.[10] The S_1 state is the dark-stable state, and oxygen is produced during the S_3-to-S_0 transition (Figure 4.1C). Cryogenic temperatures inhibit oxygen evolution by blocking some of these transitions. At 190 K, the S_1-to-S_2 transition can occur, but the other S-state transitions do not. When a flash is given to the S_2 state at this temperature, YZ is oxidized by P_{680}^+, but, subsequently, YZ radical

fails to oxidize the OEC.[11] The Q_A^- to Q_B transition is also inhibited at 190 K.[12] Therefore, in the 190 K trapped S_2 state, a laser flash generates the YZ radical and Q_A^- state, which recombines via PCET reaction.[9, 13-14]

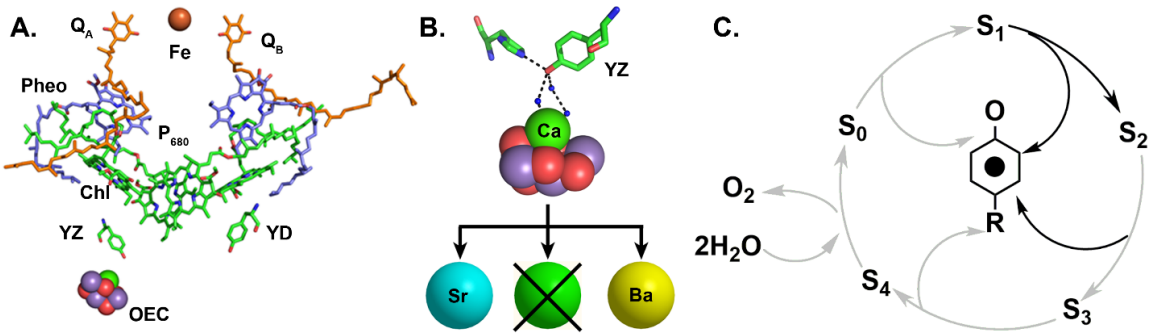

Figure 4.1 (A) Redox cofactors involved in oxygen evolution reaction in PSII. In the OEC, manganese atoms are shown in purple, calcium is shown in green, and oxygens are shown in red. (PDB ID:4UB6).[2] (B) YZ and its hydrogen-bonding partners. Water is represented by blue spheres, (PDB ID: 4UB6).[2] Illustration of cation substitution and calcium depletion, starting with Ca-PSII, (Sr^{2+} is depicted in cyan sphere, and Ba^{2+} in yellow). (C) S-state cycle of OEC, the black arrow indicates the only S-state transition allowed at 190 K. Inset, during each of the flash induced S-state transition, YZ is oxidized and reduced by a PCET reaction.

The role of calcium in the YZ PCET reactions has not been fully elucidated. It is known that the decay time and midpoint potential of YZ• are altered by manganese removal (for examples, see refs 15-16). Calcium depletion is also expected to change hydrogen-bonding interactions between bound water molecules and YZ (Figure 4.1B), and effects have been reported previously at some pH values.[9, 17-19] Calcium depletion is known to be a more selective treatment compared to manganese removal and can be readily reversed by the re-addition of calcium alone (reviewed in ref 20). Although calcium depletion is expected to change hydrogen bonding to water,[21-22] substantial changes in manganese ligation and manganese-manganese distances have not been observed.[3, 23-25] Among the

divalent ions, only strontium is able to support oxygen evolution activity.[26] In particular, barium, with its larger ionic radius, is an inhibitor of oxygen evolution.[9, 27] The structure of cyanobacterial strontium-reconstituted PSII (Sr-PSII) has been reported and while it shows no large changes, this structure does exhibit a slightly elongated Sr-water distance,[28] when compared to calcium containing PSII.

Here, we study the interactions of YZ radical and YZ singlet with their environments using reaction induced Fourier transform infrared (RIFT-IR) spectroscopy. This technique gives high resolution spectroscopic information concerning the structure of YZ singlet and YZ radical.[29] The bands of radical and singlet are distinguishable, due to the expected dramatic changes in force constant caused by oxidation of the aromatic ring.[30] To our knowledge this is the first report of the vibrational spectrum, containing YZ radical minus YZ singlet, in an oxygen-evolving PSII preparation.

4.3 Materials and Methods

Highly active PSII was purified from marketable spinach using Triton X-100, to generate thylakoid-enriched membranes called BBY, followed by octylthioglucoside (OTG) treatment, to get OTG-PSII samples.[31-32] OTG-PSIIs were flash frozen in SMN buffer (400 mM Sucrose, 50 mM 2-(N-morphplino)-ethanesulfonic acid (MES)-NaOH pH 6.0, 15 mM NaCl) with liquid nitrogen, and transferred to a -70 °C freezer for further use. The oxygen evolution for OTG-PSII samples was measured using the same method described before[33] and the average is higher than 1000 μmol O_2 (mg chl·h)$^{-1}$ at pH 6.0. Calcium depletion and calcium /strontium /barium reconstitution were performed as described previously.[9, 34] Briefly, OTG-PSII samples were thawed, resuspended in SHN buffer (400 mM sucrose, 50 mM 4-(2-hydroxyethyl)-1-piperazineethanesulfonic acid

(HEPES)-NaOH, pH 7.5, 15 mM NaCl) with 10 mM EGTA (ethylene glycol-bis(2-aminoethyl ether)-N,N,N',N'-tetraacetic acid) twice. The samples, referred as calcium depleted PSII (CD-PSII), were resuspended in either SMN or SHN buffer and flash frozen in liquid nitrogen for further use. To generate the cation reconstituted samples, CD-PSII were thawed and reconstituted with a buffered, concentrated salt stock at the same pH. Oxygen evolution activities were similar as before.[9] OEC was removed by alkaline Tris (tris(hydroxymethyl)-aminomethane)) treatment for control purpose.[35] OTG-PSII was shaking and incubated under room light at 1.5 mg chl/mL in Tris-HCl buffer (800 mM Tris, pH 8.0, 2 mM EDTA) for 30 min. The sample was pelleted and then resuspended in SH buffer (50 mM HEPES, pH 8.0, 400 mM sucrose) three times. After that, the sample was resuspended in SMN buffer.

Reaction-induced FT-IR (RIFT-IR) spectroscopy measurements were performed at pH 6.0 or pH 7.5 and 190 K using a cryostat.[34, 36-37] The chloride concentration was maintained at 255 mM, the divalent cation concentration was at 20 mM, and potassium ferricyanide was 7 mM. Ferricyanide was added from a freshly prepared 100 mM stock solution. For additional control, NH_2OH was used as an inhibitor to prevent YZ radical to oxidize OEC. The final concentration of NH_2OH is 10 mM, Ca^{2+} concentration was 20 mM, [Cl^-] was 255 mM and no potassium ferricyanide was added to the sample.

For all preparations, the RIFT-IR sample was centrifuged at 50,000 g for 10 min to form a pellet. The pellet, which was never completely dried, was spread on a CaF_2 window, and sandwiched with a second CaF_2 window with a spacer in-between. The sample was wrapped with parafilm to prevent dehydration during the measurements. Parameters for FT-IR spectroscopy were: 8 cm^{-1} resolution, four levels of zero filling; Happ-Genzel

apodization function; 60 kHz mirror speed; and Mertz phase correction. A germanium window was used to block the internal He-Ne laser of the spectrometer from turning the samples over. For most experiments, at room temperature, the sample was preflashed by one single 532 nm laser flash (40 mJ/cm^2) and dark-adapted for 20 min to synchronize the sample to 100% S_1 state. After the dark-adaption, the sample was cooled to 190 K. The sample was maintained for 10 min at 190 K to stabilize the temperature. Then after six 15 sec RIFT-IR scans (S_1 state), external illumination was given by a He-Ne laser (633 nm, 0.1 mJ) for 90 s to accumulate S_2 state. After illumination, six 15 sec scans were taken (S_2 state). These data are used to construct the S2 difference spectra. To construct YZ difference spectra, the S_2 trapped sample was given by a train of single 532 nm laser flashes followed by 90 sec of rapid scan data collection. In total, 15 flashes were given and 15 rounds of rapid scan data collection were performed after each flash for each sample. Data corresponding to the last 14 loops were averaged.[9, 11] The difference spectra were constructed by ratio of the single-channel data as described in Figure 4.2. For Mn-depleted and Ca-PSII containing NH_2OH, no pre-flash or red-light illumination were introduced to the samples to avoid closing PSII centers. The difference spectra were normalized to an amide II intensity of 0.5 to correct for difference in path length and sample thickness.

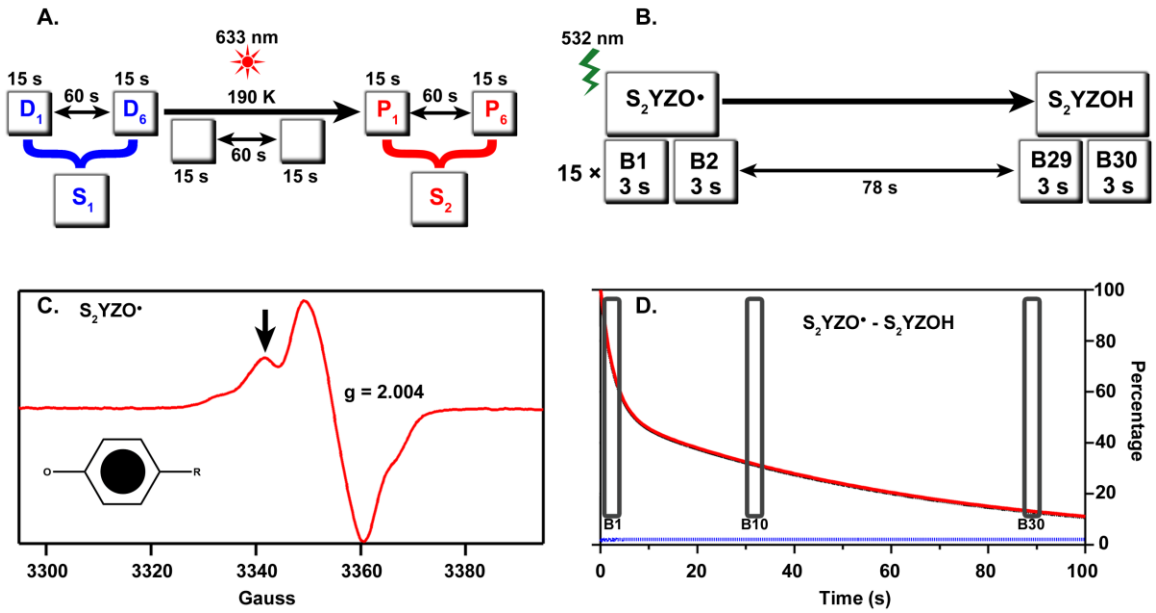

Figure 4.2 Schematic of method used to monitor $S_2YZ•$. (A) The S_2 state is generated by red illumination at 190 K. RIFT-IR data collection for the S_1-to-S_2 state transition is illustrated. Each data block is 15 s, and the $S_2Q_A^-$-minus-S_1Q_A spectrum is generated, P6-minus-D6. (B) A laser flash generates YZ radical. RIFT-IR data collection for the $S_2YZ•Q_A^-$ recombination reaction is illustrated. Each data block is 3 s, and the $S_2YZ•$-minus-S_2YZ spectrum is generated, B1 minus B30. To probe the reaction at later times, B10-B30 is used in Figure 4.11. (C) Representative EPR spectrum of $S_2YZ•$ in Ca-PSII. Black arrow indicates the field position used to monitor $S_2YZ•Q_A^-$ recombination. Inset: structure of tyrosine radical. (D) Representative EPR transient data monitoring $S_2YZ•$ in Ca-PSII. The boxes show the data blocks and time scales used to construct YZ radical difference spectra (B1-minus-B30; B10-minus-B30).

4.4 Results

4.4.1 Spectroscopic Method

In the presence of an intact and functional metal cluster, YZ radical is generated by a flash on the nanosecond time scale (via oxidation by P_{680}^+) and reduced on the microsecond to millisecond time scale by the Mn_4CaO_5 cluster. To obtain the YZ radical minus YZ singlet spectrum in the presence of the Mn_4CaO_5 cluster, we first trapped the S_2 state by continuous illumination at 190 K (Figure 4.2A). This approach has been used in

our published EPR studies to generate the S_2 state and then to monitor the decay kinetics of YZ radical after a laser flash (Figure 4.3).[9, 14]

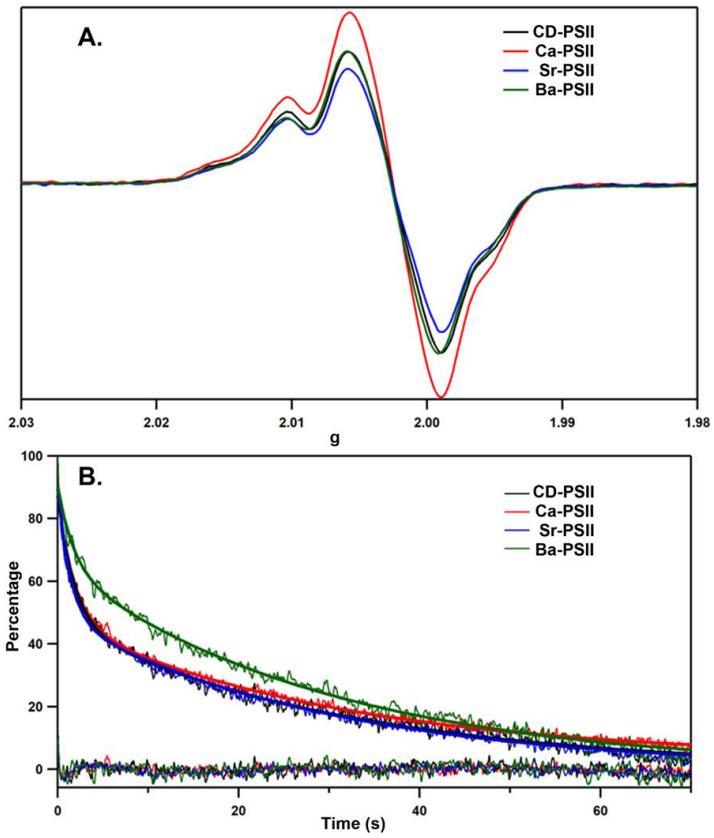

Figure 4.3 Representative EPR spectra of $S_2YZ\bullet$ recorded under red light illumination(A) and average transient EPR spectra of $S_2YZ\bullet Q_A^-$ recombination reaction (B) at pH 6.0. Samples: Ca-PSII (red), CD-PSII (black), Sr-PSII (blue) and Ba-PSII (green).

In the experiment described here, which monitors the RIFT-IR signal of YZ radical, the experiment was performed similarly to those published EPR experiments. A 532 nm flash is given to the S_2 trapped sample (Figure 4.2B) after a dark adaptation. This flash generates $S_2YZ\bullet Q_A^-$ (Figure 4.2C), as detected by the EPR control experiments shown in Figure 4.2C and D and in Figure 4.3, decays on the seconds time scale. For RIFT-IR studies, the decay of the signal was monitored for a total of 90 s (Figure 4.2D). To emphasize vibrational contributions from YZ radical, data recorded in two time blocks

were used to make the RIFT-IR spectrum, 3 s at time point B1 (t=0 s) and 3 s at time point B30 (t=87 s) (Figure 4.2B). These data are known to contain a YZ radical contribution because EPR transients recorded under the same conditions provide evidence for YZ radical decay on this time scale (Figure 4.2D).[9] The S_2 state is stable at this temperature, so the decay of the S_2 state is minimal on the seconds time scale. Q_A^- to Q_B transfer is blocked at this temperature.[12] These methods have been reported previously.[9, 34] As an additional time point, data obtained in B10 (30 s) and B30 (87 s) were also used to construct a RIFT-IR spectrum, which is expected to correspond to additional radical decay after the flash, when compared to B1-B30.

4.4.2 Samples

Four preparations were compared in these experiments (see Experimental Methods). PSII was calcium depleted, and then reconstituted either with calcium (Ca-PSII, 1100 μmol O_2 (mg chl·h)$^{-1}$), strontium (Sr-PSII, 800 μmol O_2 (mg chl·h)$^{-1}$), barium (Ba-PSII, 510 μmol O_2 (mg chl·h)$^{-1}$) or was used in the calcium-depleted form (CD-PSII, 200 μmol O_2 (mg chl·h)$^{-1}$). As discussed, although CD-PSII and Ba-PSII are inhibited, a S_2 like state can be trapped at 190 K in each case.[9] Notably, all preparations have similar yields of S_2YZ radical at pH 6 (Figure 4.3) and similar decay times except for Ba-PSII (half-life for Ca-PSII, 4.18 ± 1.38 s; Sr-PSII, 3.36 ± 0.81 s; CD-PSII, 4.04 ± 0.51 s and Ba-PSII, 8.44 ± 0.52 s). But due to the data collection time scale employed here (90 s), the contribution fo radical will be similar in all preparations. Thus, B1-B30 spectra, recorded from all four preparations, will reflect YZ•Q_A^--minus-YZQ_A as trapped in the S_2 state.

Figure 4.4A presents first the $S_2Q_A^-$-minus-S_1Q_A spectrum obtained from Ca-PSII (Figure 4.4A, according to method Figure 4.2A). The $S_2Q_A^-$-minus-S_1Q_A spectra are characteristic of this transition and have been reported previously.[34] Any YZ radical contribution to these $S_2Q_A^-$-minus-S_1Q_A spectra will be minimal because there is a ~2 minute dark adaptation time after the red illumination is discontinued. This allows time for YZ radical to decay. The YD radical contribution is minimal due to a preflash, which is at room temperature before the sample is cooled to 190 K.

Figure 4.4B present spectra obtained of $S_2YZ\bullet Q_A^-$-minus-S_2YZQ_A according to method Figure 4.2B, B1-B30, as described above. The spectrum in Figure 4.4B has been expanded by a factor of 5 relative to Figure 4.4A for comparison purposes. As shown, in some regions of the mid-IR, the S_2 and YZ associated spectra are easily distinguishable by the relative intensities of vibrational bands. For example, bands at 1606, 1324 and 1301 cm^{-1} are characteristic of $S_2YZ\bullet Q_A^-$-minus-S_2YZQ_A and are not observed in the $S_2Q_A^-$-minus-S_1Q_A spectrum. The noticeable relative intensity differences at 1718, 1579, 1554 and 1534 cm^{-1} also help to distinguish $S_2YZ\bullet Q_A^-$-minus-S_2YZQ_A from $S_2Q_A^-$-minus-S_1Q_A.

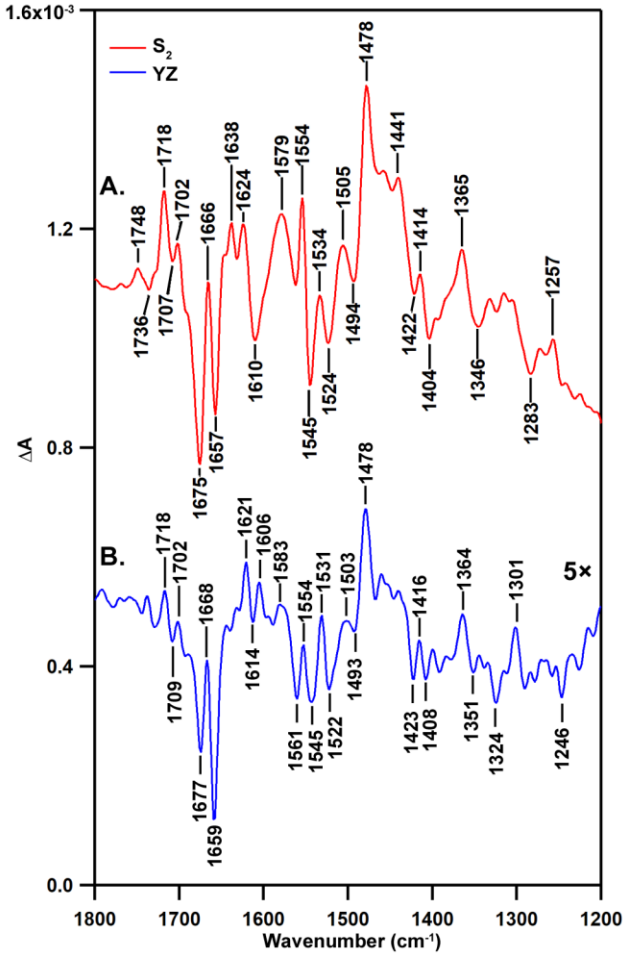

Figure 4.4 RIFT-IR spectra (1800-1200 cm^{-1}) at 190K, comparing the S_1-to-S_2 transition (A, red) with the $S_2YZ•Q_A^-$ (B, blue) recombination spectrum in Ca-PSII at pH 6.0. Spectra are averages of 13 (A) and 15 (B) samples. Spectra are offset along the y axis for presentation purpose. Spectra B has been scaled for comparison purpose (multiplied by $\sqrt{5}$ to correct for the time scale difference and another $\sqrt{5}$ for presentation purpose). Spectra were constructed as B1-B30, Figure 4.2D.

4.4.3 1600-1400 cm^{-1} during $S_2YZ•Q_A^-$ Recombination Reaction

The spectrum in Figure 4.4B is repeated in Figure 4.5F and compared to a spectrum acquired from CD-PSII (Figure 4.5E). Importantly, YZ radical yield and decay are similar in these two preparations (Figure 4.3), so the amplitude of the RIFT-IR spectral contributions should be the same. Figure 4.5 expands the 1600 to 1400 cm^{-1} region, which

reflects expected ring and CO stretching modes of YZ radical as positive bands. In model studies, these bands are observed at 1577 (ring stretch), 1516 (CO stretch), and 1448 (ring stretch) cm^{-1} respectively.[30, 38] These bands are shifted in position from the frequency in the singlet state and thus will appear in these difference spectra as unique positive signals.

In CD-PSII at pH 6.0, spectra resemble data previously reported from manganese depleted, PSII (Mn-depleted), which cannot oxidize water, at higher temperature. In that work, selective isotopic labeling either of Q_A^- or YZ radical showed that both species contribute to the 1480 cm^{-1} band.[39-40] However, the contributions of the Q_A^- species appear to be difficult to detect under these conditions, as shown by a comparison to controls containing hydroxylamine (where Q_A^- is expected to accumulate but YZ radical is not formed[41]). A control obtained from Mn-depleted (Tris washed) PSII, which is also distinct from the S_2YZ radical spectrum, is also shown (Figure 4.6). Below, we will discuss the assignment of the S_2YZ radical spectrum.

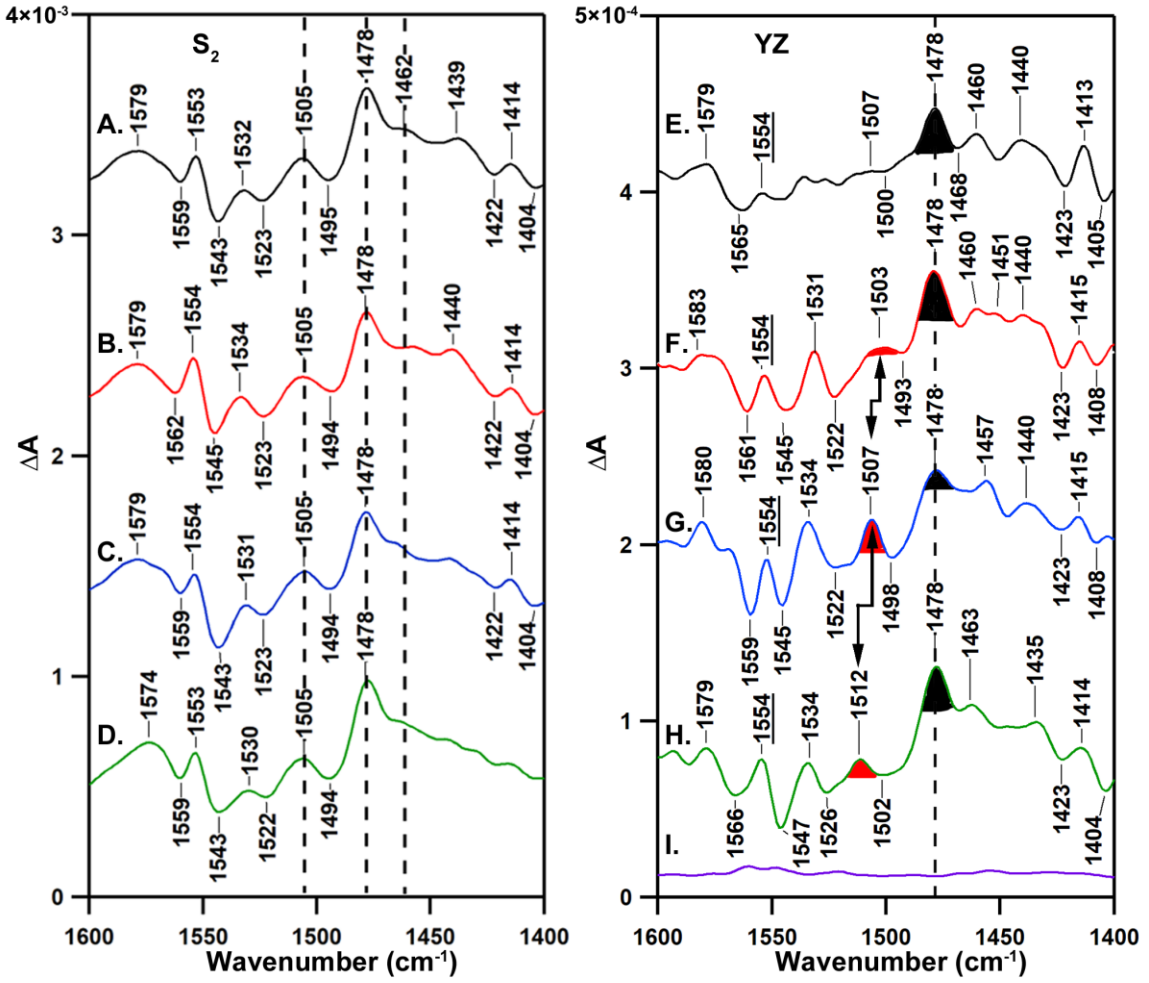

Figure 4.5 RIFT-IR spectra (1600-1400 cm^{-1}) at 190K, showing the impact of divalent cation substitution on the S_1-to-S_2 transition (left panel) and the $S_2YZ•Q_A^-$ recombination spectrum (right panel) at pH 6.0. In the left panel, representing the S_1-to-S_2 transition, CD-PSII is black (A); Ca-PSII is red (B); Sr-PSII is blue (C) and Ba-PSII is green (D). Spectra are averages of 12 (A), 13 (B), 11 (C), 14 (D). In the right panel, representing $S_2YZ•Q_A^-$ recombination, CD-PSII is black (E); Ca-PSII is red (F); Sr-PSII is blue (G); Ba-PSII is green (H) and baseline, which is purple (I), is generated by S_2-minus-S_2. Spectra are averages of 17 (E), 15 (F), 15 (G) and 18 (H) samples. Spectra are offset along the y axis for presentation purpose. Spectra were constructed as B1-B30, Figure 4.2D.

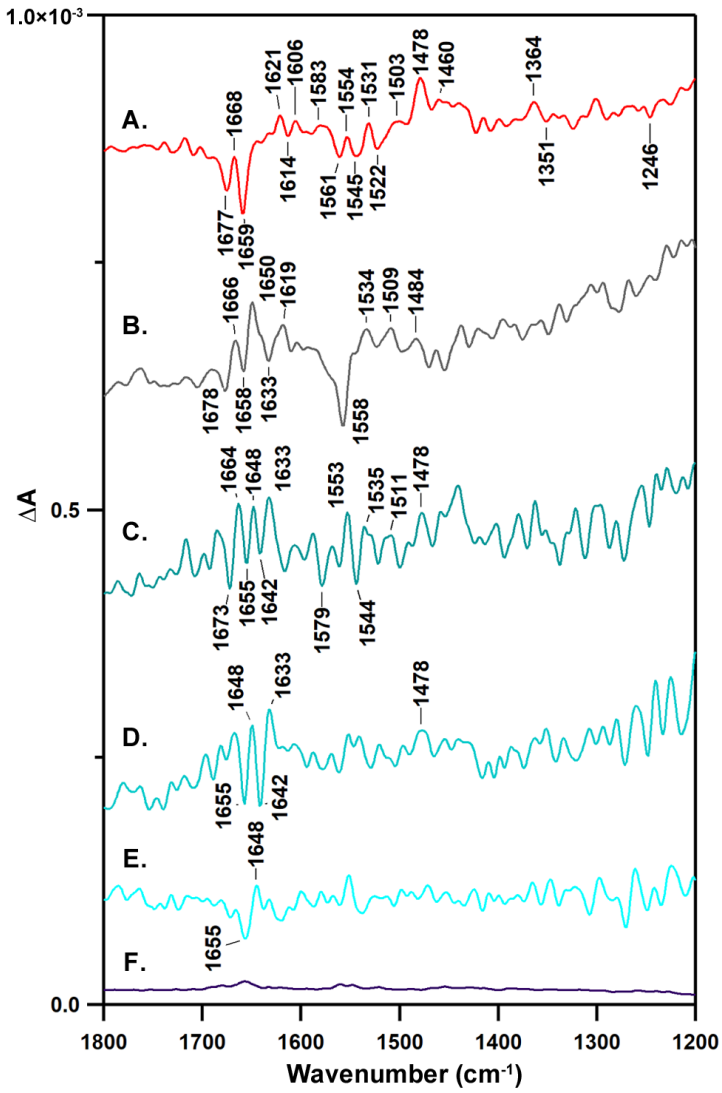

Figure 4.6 RIFT-IR spectra (1800-1200 cm^{-1}) at 190K, showing $S_2YZ•Q_A^-$ recombination reaction of the Ca-PSII (A, red), Ca-PSII with 10 mM NH_2OH (B, grey) and Mn-depleted PSII (C, D, E, cyan) at pH 6.0. Spectra A, B and C were generated by B1 minus B30 (B1 and B30 were referred to spectra presented in Figure 4.2B); spectra D was generated by B2 minus B30 (B2 and B30 were referred to spectra presented in Figure 4.2B) and spectra E was generated by B28 minus B30 (B28 and B30 were referred to spectra presented in Figure 4.2B). Spectra are averages of 15 (A), 8 (B) samples and 6 (C, D, E) samples. Spectra are offset along the y axis for presentation purpose. See Figure 4.2D for schematic.

4.4.4 CO Stretching Bands of the YZ Radical

As shown in Figure 4.5A-D, removal of calcium and replacement with other cations does not have a significant effect on the $S_2Q_A^-$-minus-S_1Q_A spectra. However, in the $YZ•Q_A^-$-minus-YZQ_A spectrum of Ca-PSII (Figure 4.5F), a band is observed at 1503 cm^{-1}, which has an intensity sensitive to calcium depletion. Further, strontium replacement shifts this band to 1507 cm^{-1}, and barium replacement shifts the band to 1512 cm^{-1}. The frequency of this band in Ba-PSII is similar to tyrosyl radicals produced by UV photolysis in aqueous buffer. Based on its frequency and the EPR control experiments (Figure 4.2 and Figure 4.3), we assign this band to υ7a stretching mode of YZ radical, in the presence of the manganese cluster and in one trapped conformational state. Note that the corresponding band is broad and of low intensity in the absence of calcium at pH 6.0 (Figure 4.5E). Based on isotopic labeling at higher temperatures, the 1478 cm^{-1} band in Figure E-H is assigned to the CO of the YZ radical, in a different trapped conformational state. This band does not appear to be calcium-sensitive and also appears in the calcium-depleted spectrum, where it most likely overlaps a Q_A^- contribution. This interpretation suggests that there are at least two conformational states of YZ radical, which differ in the interaction with the calcium ion. Broadening of one of the CO bands at pH 6 may be due to protonation of His190, which is predicted to hydrogen bond to YZ.[1]

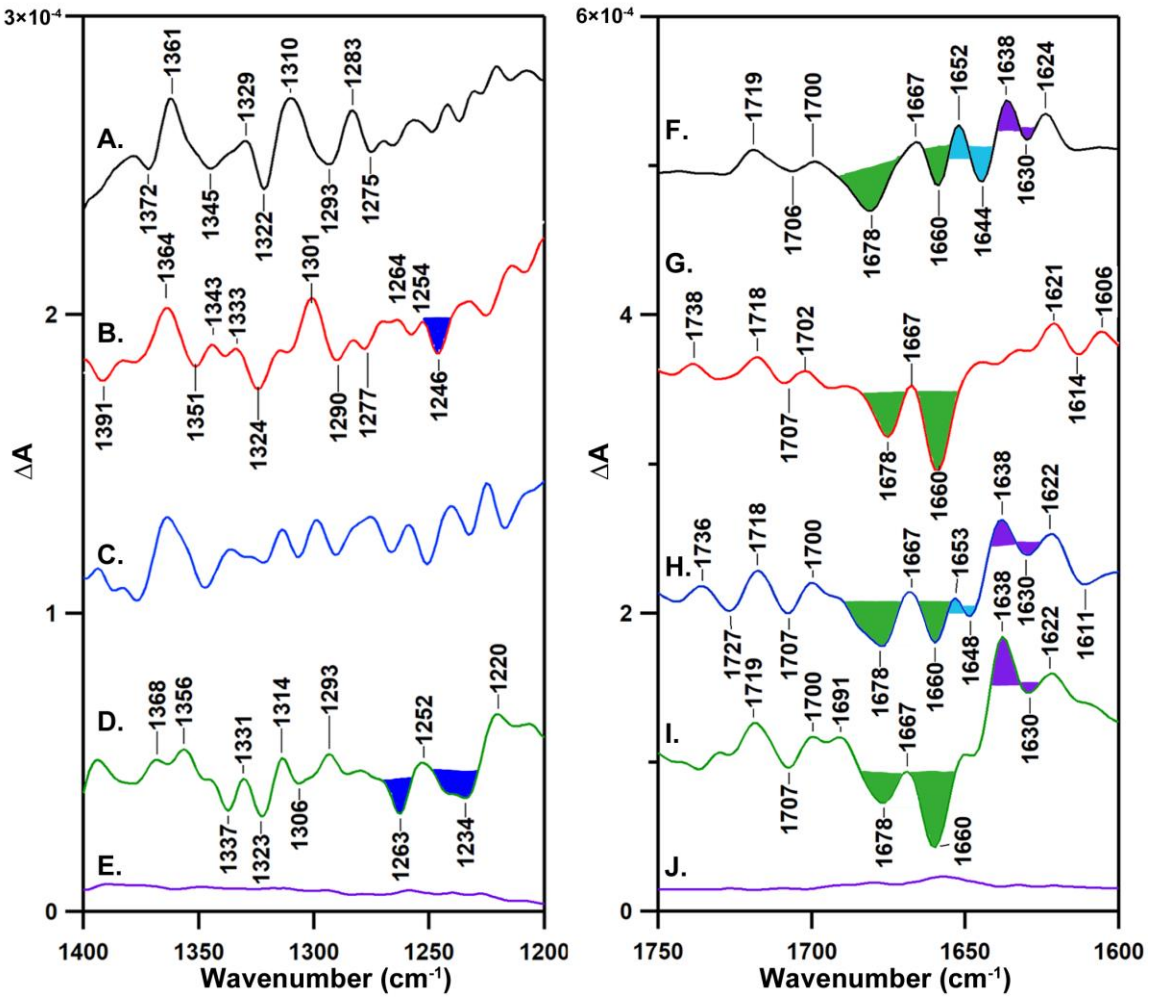

Figure 4.7 RIFT-IR spectra (1400-1200 cm^{-1}, left panel and 1750-1600 cm^{-1}, right panel) at 190K, showing the impact of divalent cation substitution on the $S_2YZ^{\bullet}Q_A^-$ recombination reaction at pH 6.0. CD-PSIIs are shown in black (A, F); Ca-PSIIs are shown in red (B, G); Sr- PSIIs are shown in blue (C, H); Ba-PSIIs are shown in green (D, I) and baselines, which are purple (E, J), are generated by S_2-minus-S_2. Spectra are averages of 17 (A, F), 15 (B, G), 15 (C, H) and 18 (D, I) samples. Spectra are offset along the y axis for presentation purpose. Spectra were constructed as B1-B30, Figure 4.2D.

4.4.5 CO Stretching Bands of YZ Singlet

Figure 4.7, left panel shows the expanded region from 1400 to 1200 cm^{-1}, predicted by model compound studies to contain the CO mode of the YZ singlet state. The CO stretch of tyrosine is expected as a negative band at 1260-1240 cm^{-1}, depending on the strength

and type of hydrogen bonding to the phenolic oxygen.[42] A band is observed at 1245 cm^{-1} in Ca-PSII (Figure 4.7B), but is absent in CD-PSII. In Sr-PSII (Figure 4.7C), the spectra are complex in this region; but in Ba-PSII (Figure 4.7D), two bands are observed. These data support assignment of a calcium-dependent 1245 cm^{-1} band to the YZ singlet state. The frequency is suggestive of a protonated YZ hydrogen bonding as a proton acceptor.[42] Again, bands are observed in this region in the S_2-minus-S_1 spectra (Figure 4.8, left panel), but those bands are not as identical in frequency and not calcium dependent.

4.4.6 pH Dependence of the CO Stretching Bands

RIFT-IR spectra were also acquired at pH 7.5 and compared to the pH 6.0 spectra. As seen in Figure 4.9F and Figure 4.10F, at pH 7.5, the CD-PSII sample exhibits a positive band at 1507 cm^{-1} and a negative band at 1256 cm^{-1}. This is distinct from the pH 6.0 spectrum obtained from this sample (Figure 4.5F and Figure 4.7A). Changes are also observed in CO stretching bands in Ca-PSII, Sr-PSII and Ba-PSII samples when the pH is changed. For example, in this Ca-PSII sample, a shift of 1503 cm^{-1} to 1498 cm^{-1} is observed when pH 6.0 to pH 7.5 acquired spectra are compared. This result provides evidence for a pH-induced alteration in hydrogen bonding to the YZ radical. This is expected, because histidine is likely to change protonation state in this pH range, and His190D1 is hydrogen bonded to YZ in crystal structures.[1] Interestingly, however, a 1246 cm^{-1} band is observed at both pH values (trace B in Figure 4.7 and trace G in Figure 4.10) indicating that the hydrogen-bonding interactions of the YZ singlet are relatively insensitive to pH change.

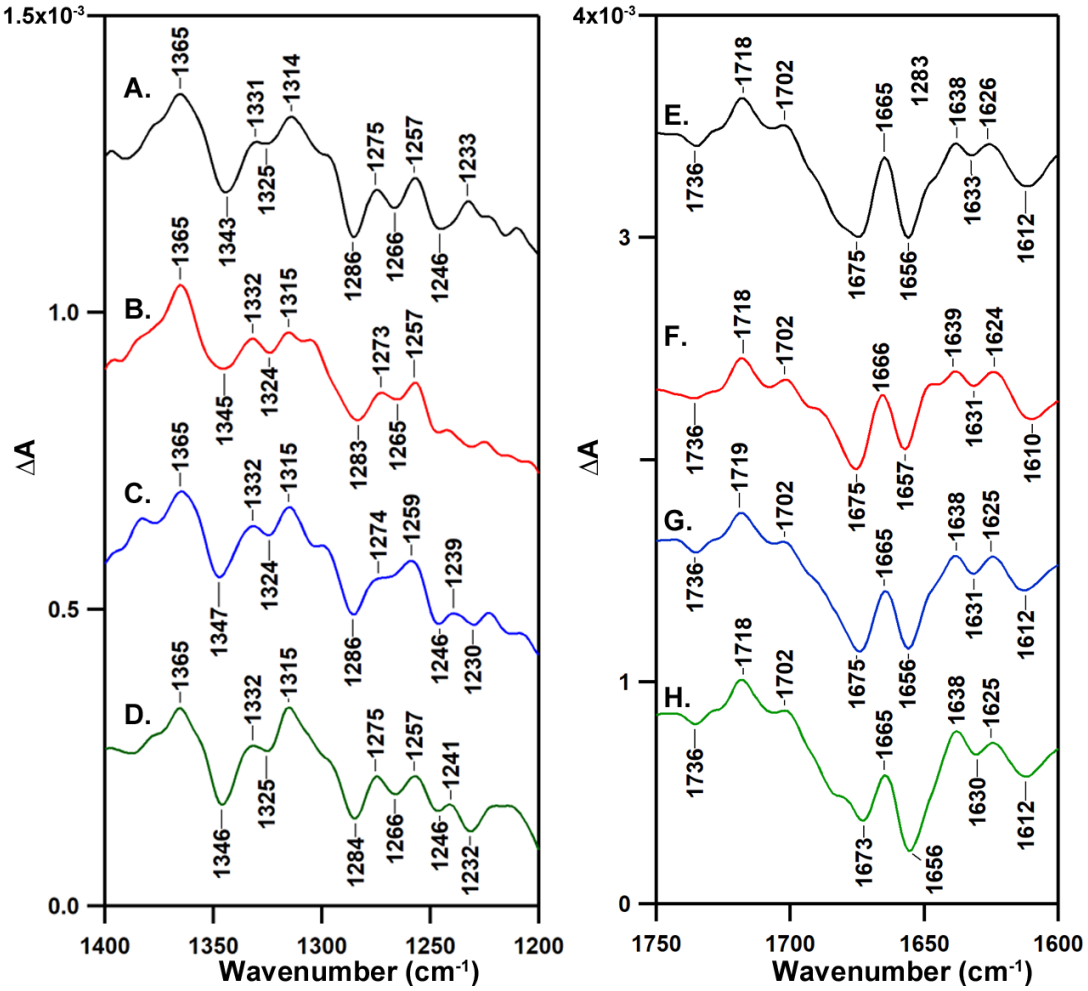

Figure 4.8 RIFT-IR spectra (1400-1200 cm^{-1}, left panel and 1750-1600 cm^{-1}, right panel) at 190K, showing the impact of divalent cation substitution on the S_1-to-S_2 transition at pH 6.0. CD-PSII is black (A, E); Ca-PSII is red (B, F); Sr-PSII is blue (C, G) and Ba-PSII is green (D, H). Spectra are averages of 12 (A, E), 13 (B, F), 11 (C, G), 14 (D, H). Spectra are offset along the y axis for presentation purpose. Spectra were constructed as B1-B30, Figure 4.2D.

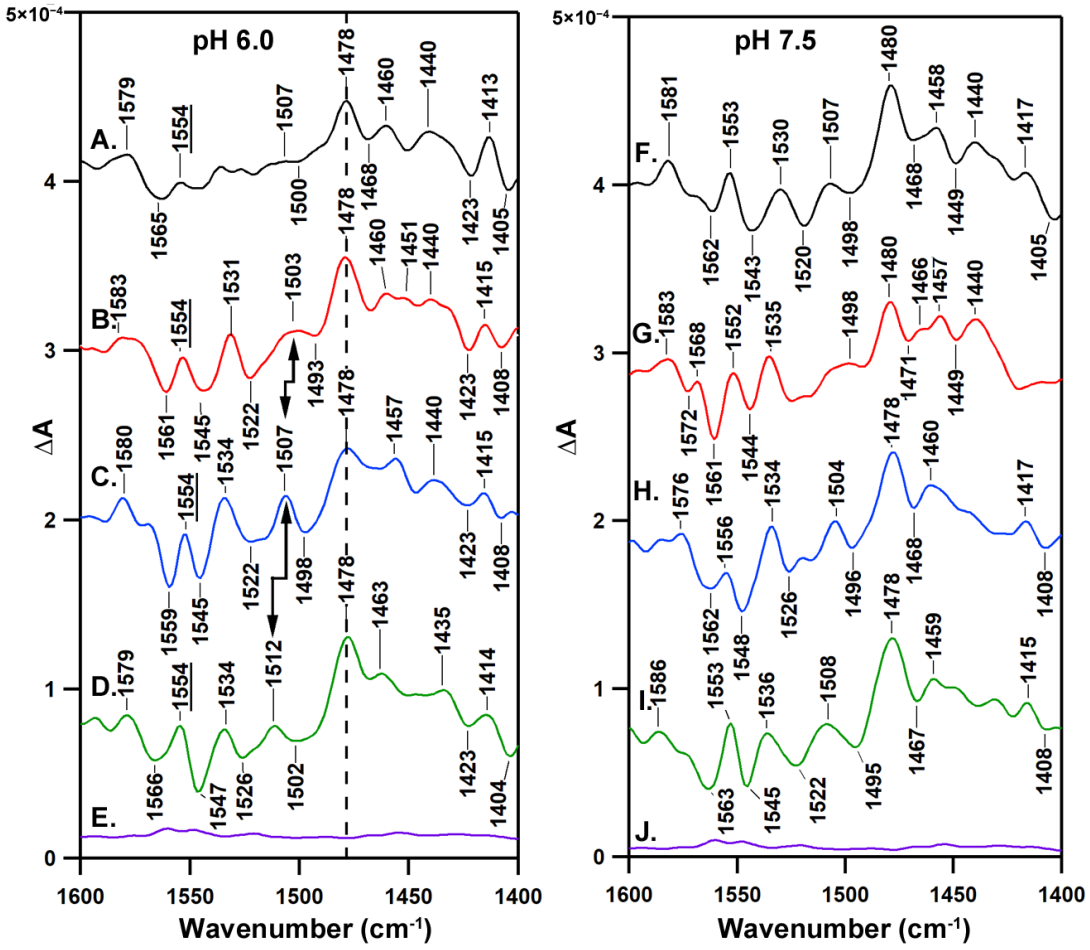

Figure 4.9 RIFT-IR spectra (1600-1400 cm^{-1}) at 190K, showing divalent cation substitution on the $S_2YZ•Q_A^-$ recombination reaction at pH 6.0 (left panel) and pH 7.5 (right panel). CD-PSII is black (A, F); Ca-PSII is red (B, G); Sr-PSII is blue (C, H); Ba-PSII is green (D, I), and baseline, which is purple (E, J), is generated by S_2-minus-S_2. Spectra are averages of 17 (A), 15 (B), 15 (C), 18 (D), 17 (F), 14 (G), 17 (H), and 18 (I). samples. Spectra are offset along the y axis for presentation purpose. Spectra were constructed as B1-B30, Figure 4.2D.

4.4.7 Amide I Region

Figure 4.7, right panel shows the 1750 to 1600 cm^{-1} region of the $YZ•Q_A^-$ recombination spectrum; in this region, amide I bands are expected at 1650 cm^{-1}. In model peptides and ribonucleotide reductase (RNR), oxidation/reduction of tyrosine is associated with amide I and II contributions to the spectrum.[43-44] These contributions are characteristic

of sequence and also reflect the detailed backbone and dihedral angle associated with the trapped conformer. The observation of two different CO vibrational bands, as discussed above, is consistent with the presence of at least two YZ radical conformers. All the spectra in Figure 4.7F-I exhibit negative, positive, negative bands at 1678, 1667, and 1660 cm^{-1}, which can be attributed to backbone and dihedral angle (green fill). In Ba-PSII (Figure 4.7I), the amide region exhibits additional bands at positive 1638 and negative 1630 cm^{-1} (dark blue fill), considered here as markers for an additional conformer, which is trapped under 190 K illumination. Comparison of spectra acquired in Ba-PSII with data acquired in Sr-PSII (Figure 4.7H) shows that the strontium-selected conformer is similar to Ba-PSII in this region. In addition, Sr-PSII exhibits additional amide bands at positive 1653 and negative 1648 cm^{-1} (light blue fill). In CD-PSII, the amide region of the spectrum contains amide bands characteristic of all putative conformers (Figure 4.7).

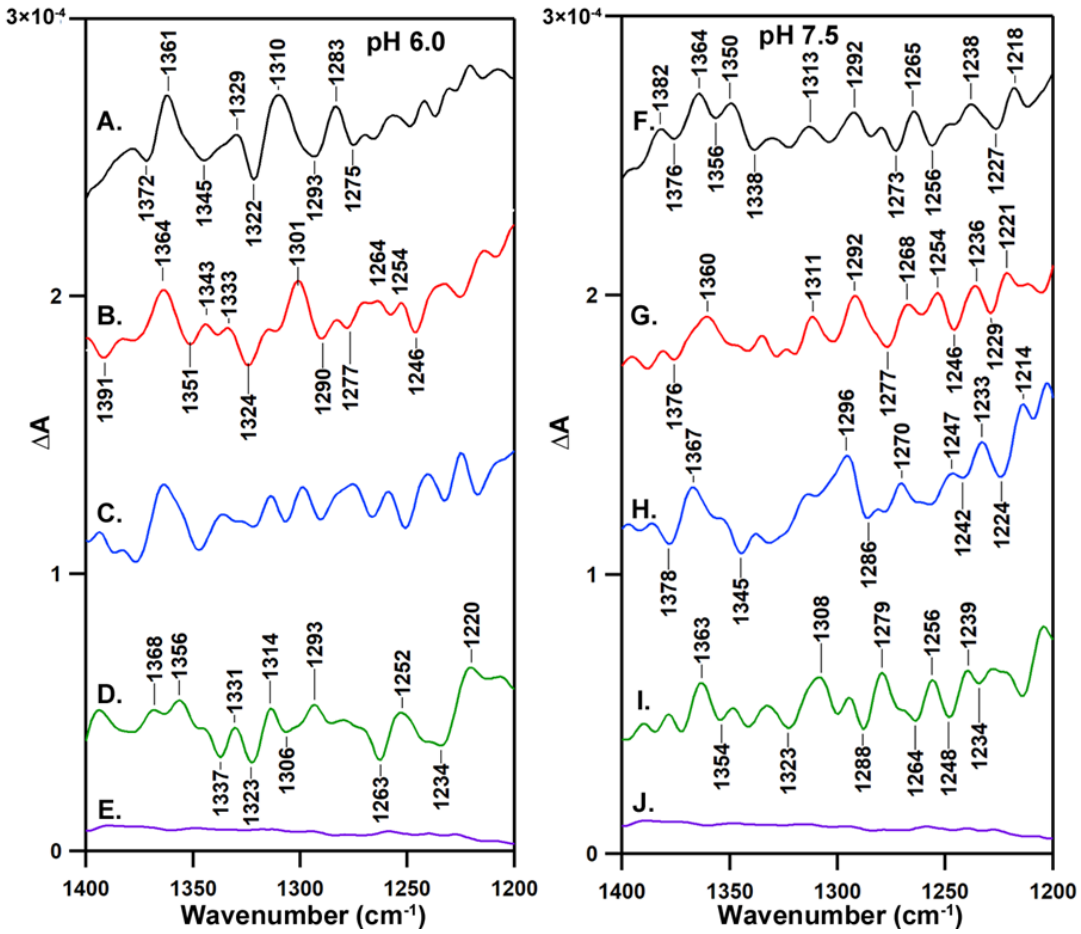

Figure 4.10 RIFT-IR spectra (1400-1200 cm^{-1}) at 190K, showing divalent cation substitution on the $S_2YZ•Q_A^-$ recombination reaction at pH 6.0 (left panel) and pH 7.5 (right panel). CD-PSII is black (A, F); Ca-PSII is red (B, G); Sr-PSII is blue (C, H); Ba-PSII is green (D, I), and baseline, which is purple (E, J), is generated by S_2-minus-S_2. Spectra are averages of 17 (A), 15 (B), 15 (C), 18 (D), 17 (F), 14 (G), 17 (H), and 18 (I). samples. Spectra are offset along the y axis for presentation purpose. Spectra were constructed as B1-B30, Figure 4.2D.

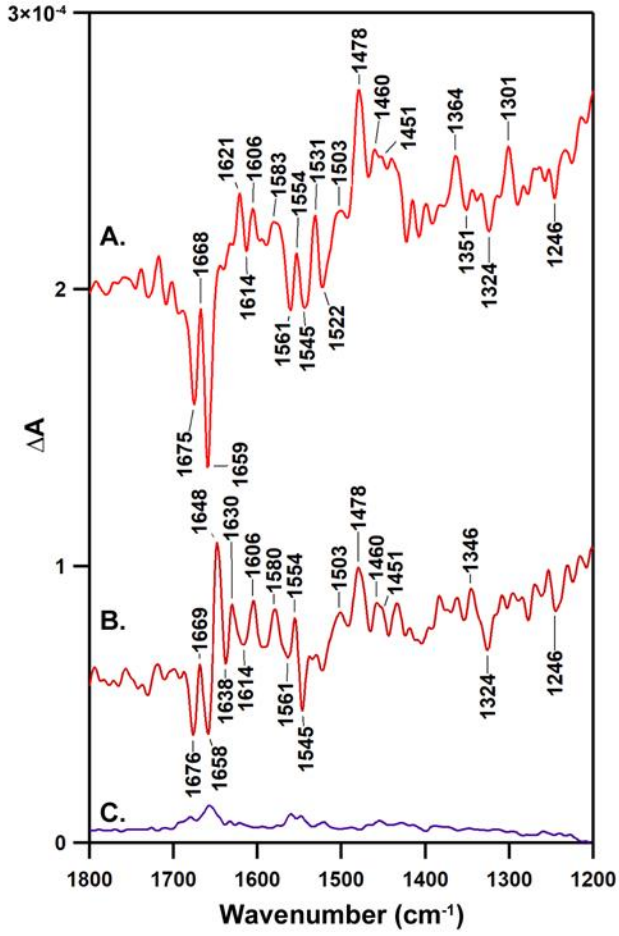

Figure 4.11 RIFT-IR spectra (1800-1200 cm^{-1}) at 190K, showing $S_2YZ•QA^{-}$ recombination reaction of the Ca-PSII at different time scale (A, red, B1 minus B30, corresponding to 0 s minus 90 s and B, brown, B10 minus B30, corresponding to 30 s minus 90 s, at pH 6.0. Spectra are average of 15 samples. Spectra are offset along the y axis for presentation purpose. See Figure 4.2D for schematic.

As discussed above, the amide I region of Ca-PSII is distinct from that of Sr-PSII and Ba-PSII when $YZ•Q_A^-$ data are compared immediately following the laser flash (B1-B30, Figure 4.2). However, in Ca-PSII, additional amide I conformational marker bands appear at later times (B10-B30 spectrum) (Figure 4.11). These data show that calcium occupancy selects for a PCET reaction in a subset of YZ conformation states. When the pH 6.0 experiments are compared to those recorded at pH 7.5 (Figure 4.12), the amide band frequencies are shifted, but the same pattern applies. In Sr-PSII, Ba-PSII, CD-PSII, similar

amide I regions are observed in the B1-minus-B30 spectra, and the amide I regions of these three samples more complex, when compared to the amide I region of Ca-PSII. The amide I region of the CD-PSII spectrum appears to be the most complex at pH 7.5, as also noted at pH 6.0.

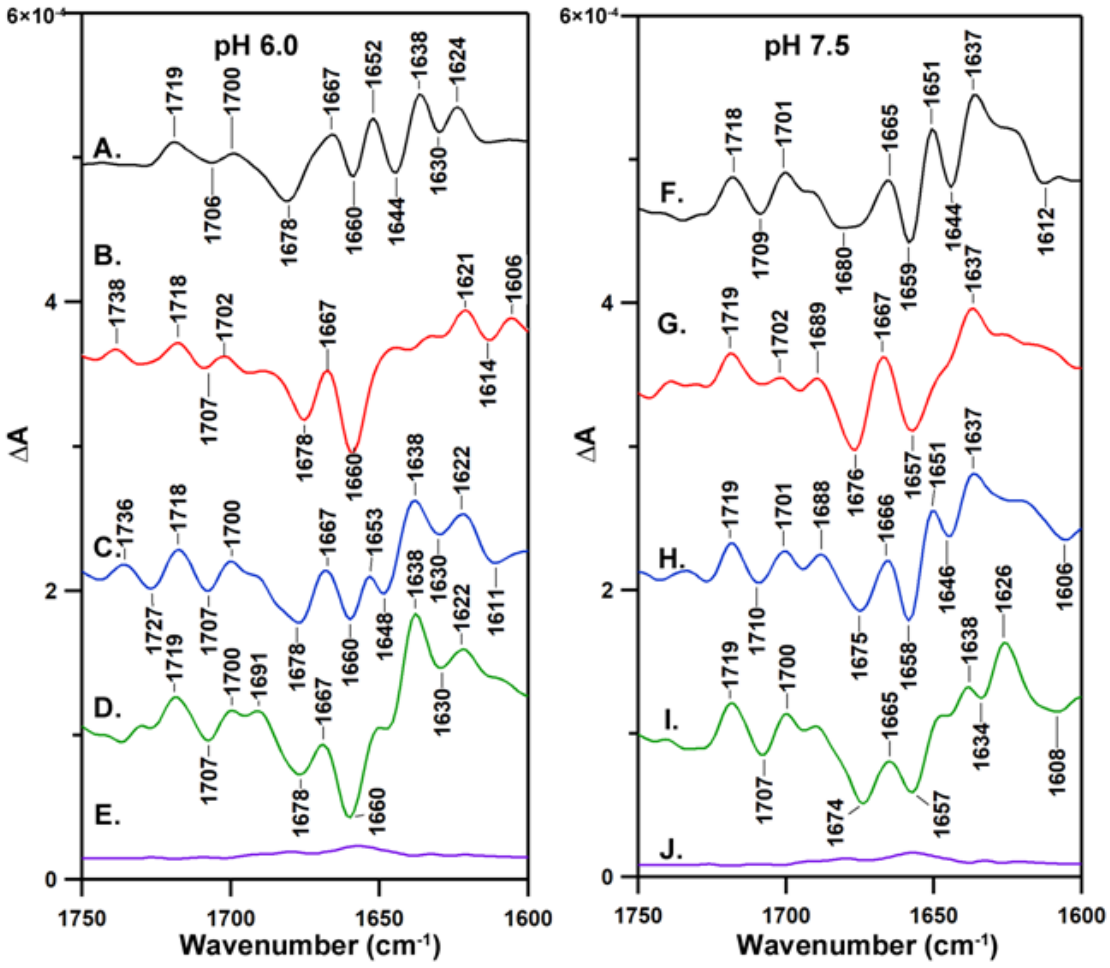

Figure 4.12 RIFT-IR spectra (1750-1600 cm^{-1}) at 190K, showing divalent cation substitution on the $S_2YZ•Q_A^-$ recombination reaction at pH 6.0 (left panel) and pH 7.5 (right panel). CD-PSII is black (A, F); Ca-PSII is red (B, G); Sr-PSII is blue (C, H); Ba-PSII is green (D, I), and baseline, which is purple (E, J), is generated by S_2-minus-S_2. Spectra are averages of 17 (A), 15 (B), 15 (C), 18 (D), 17 (F), 14 (G), 17 (H), and 18 (I) samples. Spectra are offset along the y axis for presentation purpose. Spectra were constructed as B1-B30, Figure 4.2D.

4.4.8 1550 and 1750 cm^{-1} Region

In the YZ difference spectra, bands are observed at 1740-1710 cm^{-1} (Figure 4.7). We attribute these bands to the transfer of Bohr protons to aspartate and glutamate residues in response to the YZ PCET reactions.

In model compounds, the ν8a ring stretching vibrational band of the radical is expected as a positive band at 1556 cm^{-1}.[30] The singlet is expected to have ring stretching modes at ~1600 and 1500 cm^{-1},[30] which will be negative contributions in the PSII spectrum. In the $YZ•Q_A^-$ recombination spectrum, the change in intensity in the 1507 cm^{-1} band, when CD-PSII and Ca-PSII are compared, is associated with an increase in intensity at 1531 cm^{-1}. All the spectra have a contribution at 1554 cm^{-1}. The frequencies of these bands are consistent with an assignment to ring stretching bands.

4.4.9 3160-1800 cm^{-1} during $S_2YZ•Q_A^-$ recombination reaction

In Figure 4.13, the comparison was made between S_1-to-S_2 transition and $S_2YZ•Q_A^-$ recombination reaction over in 3160-1800 cm^{-1}. During S_1-to-S_2 transition, shown in Figure 4.13 the left panel, there is a broad IR band centered at 2740 cm^{-1} at 190K which was previously assigned to pronated water cluster. The broad IR band is calcium-independent at pH 6.0.[34] In addition to previous publish results, here we showed that Ba-PSII also has a broad IR band at the same position, further proves the independence of this peak to calcium occupancy at pH 6.0. In $S_2YZ•Q_A^-$ recombination reaction, there is not a significant signal in all the spectra comparing to baseline. A comparison between different pH has also been made during $S_2YZ•Q_A^-$ recombination reaction in the same region (Figure

4.14). Again, due to the baseline issue, we couldn't conclude whether there is a defined IR signal over this region.

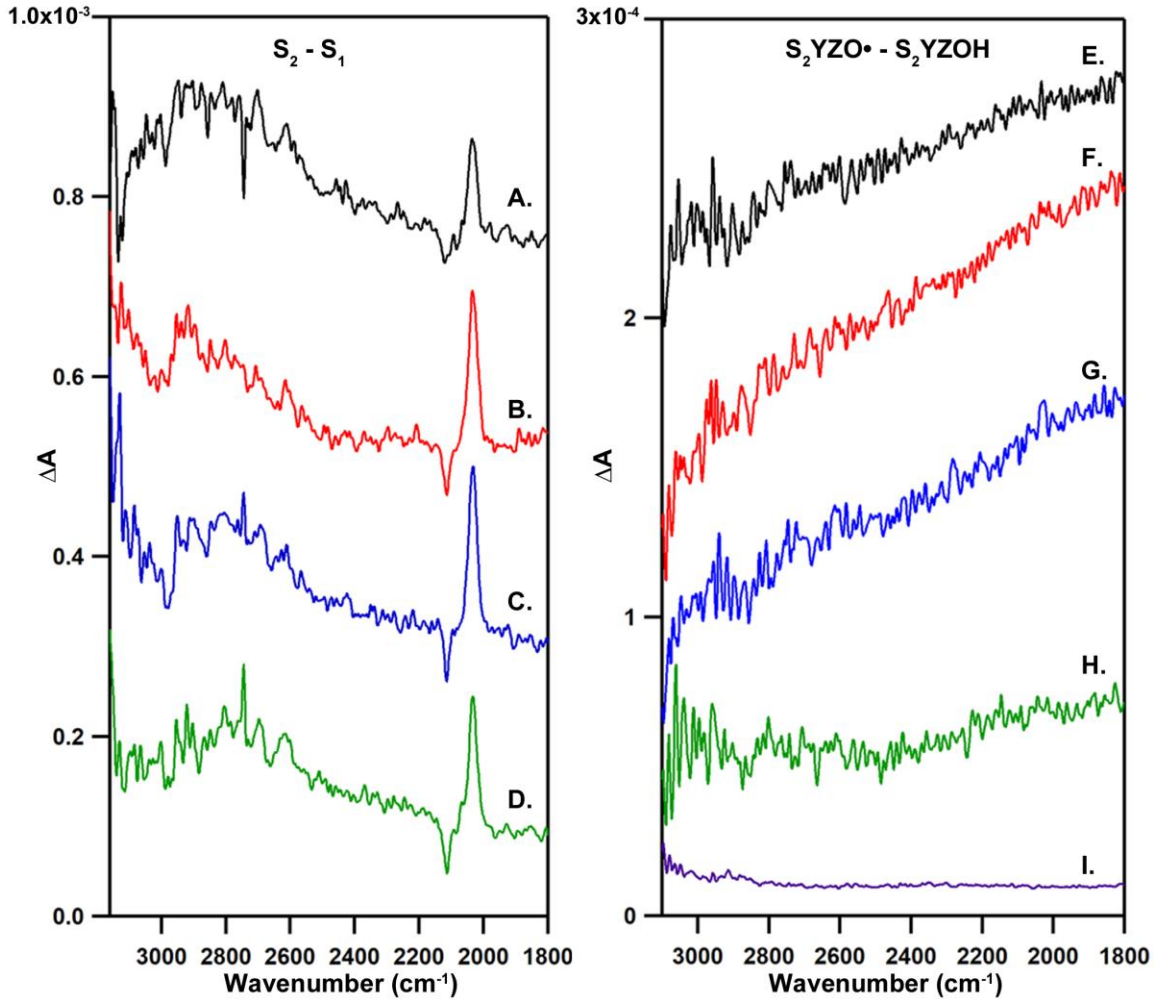

Figure 4.13 RIFT-IR spectra (3160-1800 cm^{-1}) at 190K, showing divalent cation impacts on the S_1-to-S_2 transition (left panel) and $S_2YZ•Q_A^-$ recombination reaction (right panel) at pH 6.0. In the left panel which depicts the divalent cation effects on the S_1-to-S_2 transition, CD-PSII is shown in black (A), Ca-PSII is shown in red (B), Sr-PSII is shown in blue (C) and Ba-PSII is shown in green (D). Spectra are averages of 12 (A), 13 (B), 11 (C), 14 (D). In the right panel which shows the effect of divalent cation on $S_2YZ•Q_A^-$ recombination reaction, in (E), CD-PSII (black): in F, Ca-PSII (red); in G, Sr-PSII (blue); in H, Ba-PSII (green), in I, baseline generated by S_2-minus-S_2 (purple). Spectra are averages of 17 (E), 15 (F), 15 (G) and 18 (H) samples. Spectra are offset along the y axis for presentation purpose. Spectra were constructed as B1-B30, Figure 4.2D.

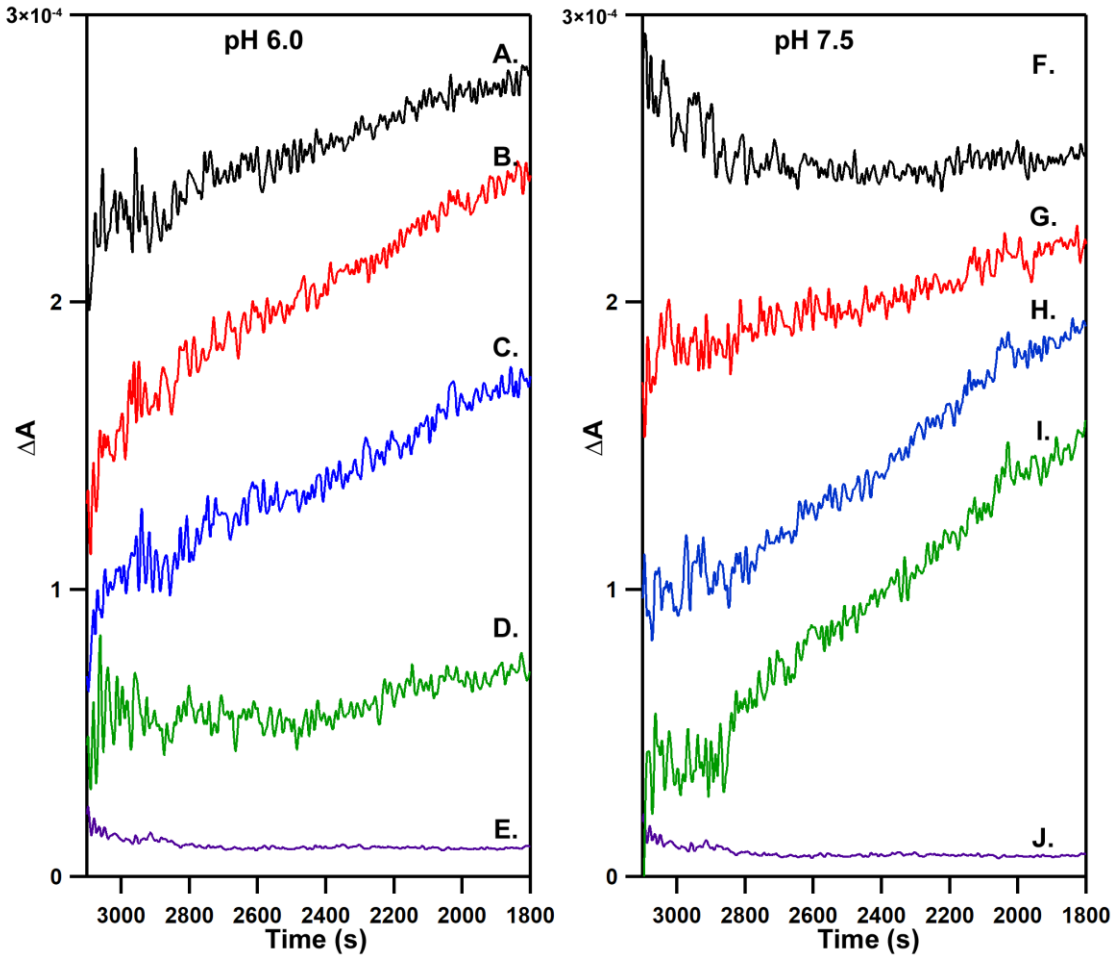

Figure 4.14 RIFT-IR spectra (3160-1800 cm^{-1}) at 190K, showing divalent cation substitution on the $S_2YZ•Q_A^-$ recombination reaction at pH 6.0 (left panel) and pH 7.5 (right panel). CD-PSII is black (A, F); Ca-PSII is red (B, G); Sr-PSII is blue (C, H); Ba-PSII is green (D, I), and baseline, which is purple (E, J), is generated by S_2-minus-S_2. Spectra are averages of 17 (A), 15 (B), 15 (C), 18 (D), 17 (F), 14 (G), 17 (H), and 18 (I). samples. Spectra are offset along the y axis for presentation purpose. Spectra were constructed as B1-B30, Figure 4.2D.

4.4.10 3750-3550 cm^{-1} during $S_2YZ•Q_A^-$ recombination reaction

In Figure 4.13, the comparison was made between the S_1-to-S_2 transition and $S_2YZ•Q_A^-$ recombination reaction over in 3750-3550 cm^{-1}. During the S_1-to-S_2 transition, shown in the left panel, the analog peak of 3668/3656 cm^{-1} was observed at 3685/3676 cm^{-1} in Ca-PSII at pH 6.0 here. The band was assigned to OH stretching modes of a W_n^+ cluster.[34] The peak is sensitive to calcium depletion and strontium/barium substitution. Additional peak at 3623/3587 cm^{-1} was observed only at CD-PSII here. The coupled bands were assigned to an "active" water in PSII.[34] The band was also sensitive to calcium depletion and strontium/barium substitution. During the $S_2YZ•Q_A^-$ recombination reaction, shown in right panel, 3658/3649 cm^{-1} was observed in CD-PSII. And the bands were shifted to 3649/3640 cm^{-1} in Sr-PSII. The bands were not observed in Ca-PSII and Ba-PSII. Additional isotope exchange experiments will be utilized to decide the assignments of the bands.

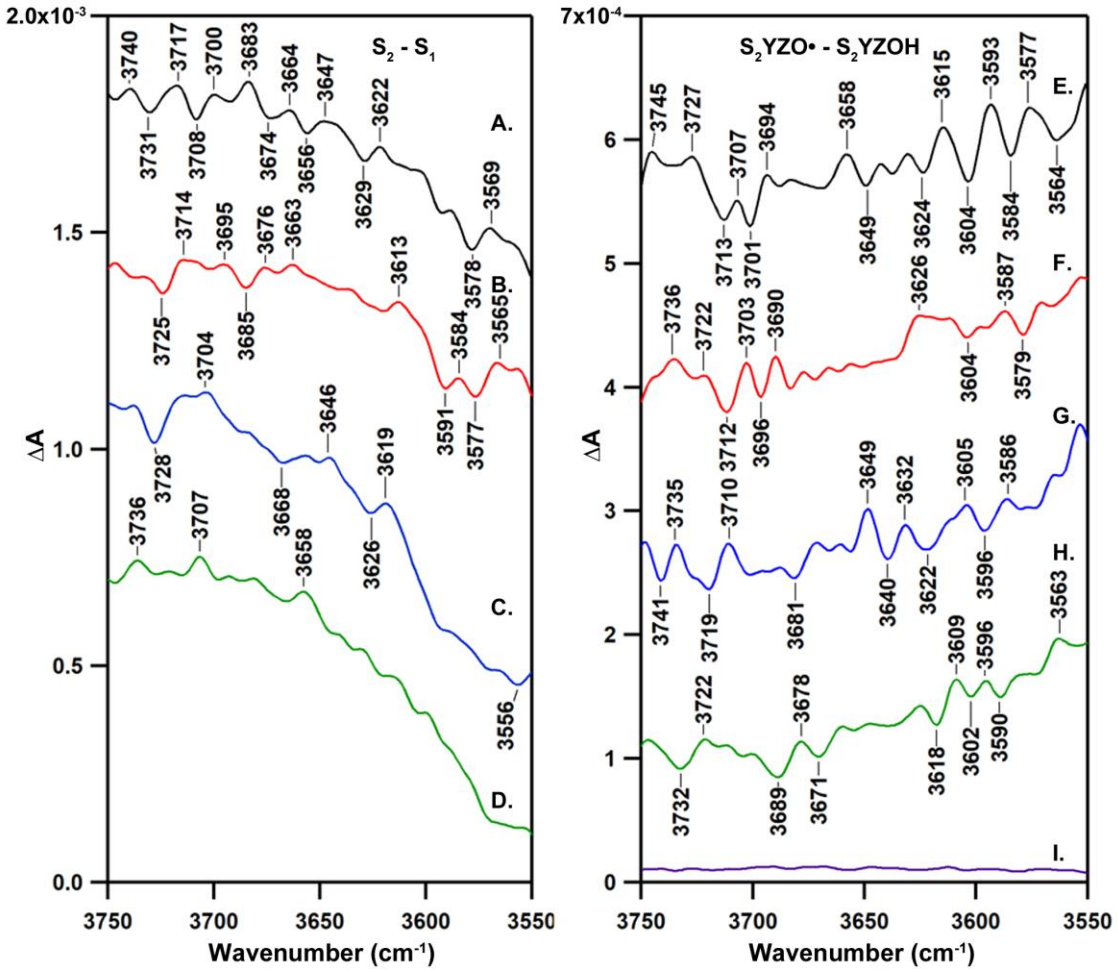

Figure 4.15 RIFT-IR spectra (3750-3550 cm^{-1}) at 190K, showing divalent cation impacts on the S_1-to-S_2 transition (left panel) and $S_2YZ•Q_A^-$ recombination reaction (right panel) at pH 6.0. In the left panel which depicts the divalent cation effects on the S_1-to-S_2 transition, CD-PSII is shown in black (A), Ca-PSII is shown in red (B), Sr-PSII is shown in blue (C) and Ba-PSII is shown in green (D). Spectra are averages of 12 (A), 13 (B), 11 (C), 14 (D). In the right panel which shows the effect of divalent cation on $S_2YZ•Q_A^-$ recombination reaction, in (E), CD-PSII (black): in F, Ca-PSII (red); in G, Sr-PSII (blue); in H, Ba-PSII (green), in I, baseline generated by S_2-minus-S_2 (purple). Spectra are averages of 17 (E), 15 (F), 15 (G) and 18 (H) samples. Spectra are offset along the y axis for presentation purpose. Spectra were constructed as B1-B30, Figure 4.2D.

4.5 Discussion

Biological radical transfer reactions are important in many enzymatic processes and are facilitated by redox active tyrosines. In proteins such as photosystem II and ribonucleotide reductase, conserved tyrosine side chains act as an electron transfer intermediates and reaction initiators, respectively. In photosystem II, YZ radical accepts an electron from the Mn_4CaO_5 cluster and drives transitions in the S state cycle. The midpoint potential of tyrosine depends on pH.[45] The driving force for each S state transition is small.[46] Therefore, the tyrosyl radical must be reprotonated on each electron transfer in order to preserve the high midpoint potential of YZ.

To control the high reactivity of the radical state, a conformational control mechanism could be adopted. For example, a translation of the aromatic ring, when the radical and singlet states are compared, can make/break hydrogen bonds or change water accessibility. These changes can then be crucial in mechanism, since the making and breaking of a hydrogen bond (~3 kcal/mol) is significant in the energetics of PSII reactions. Redox coupled structural changes have been proposed to occur at two points in the RNR PCET pathway, Y122 and Y73.[47-49] A redox-coupled change in secondary structure has been observed and simulated in beta hairpin peptides.[50] Thus, conformational gating could be a general method of targeting and controlling PCET pathways in enzymes.

This report provides the first vibrational spectroscopic study of the YZ radical and YZ singlet states in the presence of the Mn_4CaO_5 cluster and the first report of conformational selection in PSII. To obtain this information, PSII sample was trapped in the S_2 state, and the recombination of YZ radical and Q_A^- was monitored at 190 K. These are conditions in which YZ radical cannot oxidize the S_2 state, and so the cycle is blocked.

However, the metal cluster is intact, and relevant hydrogen-bonding interactions to the YZ radical and singlet state should be preserved. Using this approach, we present evidence for calcium-induced changes in the vibrational frequencies of YZ radical and YZ singlet bands. In presence of calcium, a positive band at 1503 cm^{-1} is observed, assigned here to a conformer of YZ radical which interacts electrostatically with the calcium ion. The band at 1503 cm^{-1} shifts to 1507 cm^{-1} with strontium replacement and to 1512 cm^{-1} with barium replacement in the calcium site. The expected pK_a's of metal bound water for calcium, strontium, and barium are 12.7, 13.2 and 13.4 (see ref (27) and references therein). Therefore, the observed upshift in the series from barium, strontium, to calcium is consistent with a hydrogen bond via a metal bound water, which becomes more acidic as the ionic radius of the metal decreases. An electrostatic interaction, due to the change in ionic radius of the divalent ion, is also possible.

Similarly, for YZ singlet, divalent ion replacement or removal alters the frequency of a negative band at 1245 cm^{-1}. In Sr-PSII at pH 6, this band is shifted and reduced in intensity, perhaps to the presence of multiple interactions. In barium PSII, two bands are observed at 1263 and 1234 cm^{-1}. This result is consistent a hydrogen bonding or electrostatic interaction between calcium and the YZ singlet state.

Interestingly, when calcium is removed, the 1503, 1451, and 1246 cm^{-1} bands are reduced significantly in intensity at pH 6.0. The calcium-depleted spectrum at pH 6.0 resembles that previously attributed to YZ in Mn-depleted PSII at higher temperatures.[29, 51-54] In that work, isotopic labeling and kinetic analysis was used to assign the 1478 cm^{-1} band to overlapping contributions of YZ radical and Q_A^-. Note that an alternant spectrum, assigned to YZ in manganese-depleted PSII, is not observed here (see ref 29 for a

discussion). The data presented from these experiments may account for transient infrared measurements on the microsecond time scale in oxygen evolving PSII. It was proposed that the CO vibrational band of YZ radical may be shifted away from 1483 cm^{-1} on that time scale in oxygen-evolving PSII.[55] These spectra rationalize that result, if the microsecond experiment reflects mainly PCET reactions in the calcium-sensitive YZ radical conformer, which has a CO band at 1503 cm^{-1}.

The calcium sensitive YZ radical bands are downshifted from those of tyrosyl radical in solution, where the bands are observed at 1516 cm^{-1}.[30] In a matrix experiment, phenoxyl radical has been reported to have a CO vibrational band at 1481 cm^{-1}.[56] When compared to E. coli RNR, the bands are upshifted from those of the Y122 radical, which has a CO stretching mode at 1499 cm^{-1}.[57-58] In that case, the radical is not hydrogen bonded, but is located in a hydrophobic environment.[47] Therefore, the unique CO frequency of YZ radical reflects hydrogen bonding in a high dielectric environment and its interactions with H190 and calcium. The YZ singlet band at 1245 cm^{-1} is characteristic of a strongly hydrogen bonded, protonated tyrosine, which accepts a hydrogen bond. Failure to observe the band in CD-PSII and Sr-PSII is attributed to broadening and distribution of hydrogen bond interactions.

One focus of our study is on the coupling of the YZ PCET reactions with backbone and dihedral angle changes. This can be assessed from the amide I regions. These data are consistent with a calcium-dependent selection mechanism. It has been shown previously that oxidation of tyrosine in dipeptides[43], pentapeptides[59], and 18-mer beta hairpins[38] leads to appearance of amide I vibrational bands in the RIFT-IR spectrum, associated with UV photolysis and radical generation. For RNR, $^{13}C_1$ isotopic labeling of the tyrosine backbone

and DFT simulations led to the conclusion that the spectral pattern in the amide I and II regions is diagnostic of the backbone and dihedral angle change. This so-called B radical to A singlet conformational change, detected for Y122 radical in RNR, corresponding to an approximately 100° change of backbone dihedral angle, was modeled to translate the phenolic oxygen and make/break a hydrogen bond to D84.[44]

To explain our results, the cryogenic illumination used here is proposed to trap multiple conformers of the YZ-Mn_4CaO_5 cluster. In Ca-PSII, the pattern of bands in the amide I region is characterized by two negative bands at 1678 and 1660 cm^{-1}. These marker bands are observed in Ba-PSII and Sr-PSII, but the Ba-PSII and Sr-PSII exhibit additional amide bands. We hypothesize that these bands are characteristic of another YZ radical conformation. Distinctive amide I marker bands appear in Ca-PSII spectra on a longer time scale. Calcium depletion alters the amide region suggesting that interactions with calcium are important in conformer selection.

Previous isotopic labeling experiments indicate that the 1480 cm^{-1} band is likely to exhibit small contributions both from Q_A^- and the YZ radical. A control experiment to establish the magnitude of the Q_A^- contribution under these conditions is presented here. This control uses hydroxylamine to trap Q_A^- contributions at the expense of redox reactions in the hydroxylamine reagent. It has been reported that YZ radical is not produced in the presence of hydroxylamine.[41] The spectral result indicates that the contribution of Q_A^- to the 1480 cm^{-1} band may be present but small. An additional control used "Tris-washed" or manganese-depleted PSII, which lacks the active metal cluster. A laser flash given to this preparation generates YZ radical and Q_A^-. The spectrum obtained from this preparation is

distinct from those obtained from Ca-PSII, Sr-PSII, Ba-PSII, and CD-PSII at this temperature.

In structures of PSII, YZ is hydrogen bonded to histidine 190 in the D1 polypeptide and calcium bound water. Our previous EPR results led us to propose a two-pathway model for proton transfer to YZ radical.[9] One, dominant at low pH, most likely involves histidine 190 in the D1 polypeptide. A second pathway might involve water bound to calcium. These current results are consistent with this picture and with hydrogen bonding between calcium bound-water and YZ conformers both in the radical and singlet states. Such an outcome is consistent with a role for this water in proton transfer. Our results also provide evidence for a distinct local conformational change in the YZ side chain, which is restricted in Ca-PSII. This strategy of a controlled, conformational rearrangement may be important in targeting PCET pathways in other enzymes.

4.6 References

1. Umena, Y.; Kawakami, K.; Shen, J. R.; Kamiya, N., Crystal Structure of Oxygen-Evolving Photosystem II at a Resolution of 1.9 A. *Nature* **2011,** *473* (7345), 55-60.

2. Suga, M.; Akita, F.; Hirata, K.; Ueno, G.; Murakami, H.; Nakajima, Y.; Shimizu, T.; Yamashita, K.; Yamamoto, M.; Ago, H.; Shen, J. R., Native Structure of Photosystem II at 1.95 A Resolution Viewed by Femtosecond X-Ray Pulses. *Nature* **2015,** *517* (7532), 99-103.

3. Young, I. D.; Ibrahim, M.; Chatterjee, R.; Gul, S.; Fuller, F. D.; Koroidov, S.; Brewster, A. S.; Tran, R.; Alonso-Mori, R.; Kroll, T.; Michels-Clark, T.; Laksmono, H.; Sierra, R. G.; Stan, C. A.; Hussein, R.; Zhang, M.; Douthit, L.; Kubin, M.; de Lichtenberg, C.; Vo Pham, L.; Nilsson, H.; Cheah, M. H.; Shevela, D.; Saracini, C.; Bean, M. A.; Seuffert, I.; Sokaras, D.; Weng, T. C.; Pastor, E.; Weninger, C.; Fransson, T.; Lassalle, L.; Brauer, P.; Aller, P.; Docker, P. T.; Andi, B.; Orville, A. M.; Glownia, J. M.; Nelson, S.; Sikorski, M.; Zhu, D.; Hunter, M. S.; Lane, T. J.; Aquila, A.; Koglin, J. E.; Robinson, J.; Liang, M.; Boutet, S.; Lyubimov, A. Y.; Uervirojnangkoorn, M.; Moriarty, N. W.; Liebschner, D.; Afonine, P. V.; Waterman, D. G.; Evans, G.; Wernet, P.; Dobbek, H.; Weis, W. I.; Brunger, A. T.; Zwart, P. H.; Adams, P. D.; Zouni, A.; Messinger, J.; Bergmann, U.; Sauter, N. K.; Kern, J.; Yachandra, V. K.; Yano, J., Structure of Photosystem II and Substrate Binding at Room Temperature. *Nature* **2016,** *540* (7633), 453-457.

4. Wei, X. P.; Su, X. D.; Cao, P.; Liu, X. Y.; Chang, W. R.; Li, M.; Zhang, X. Z.; Liu, Z. F., Structure of Spinach Photosystem II-LHCII Supercomplex at 3.2 Angstrom Resolution. *Nature* **2016,** *534* (7605), 69-74.

5. Su, X.; Ma, J.; Wei, X.; Cao, P.; Zhu, D.; Chang, W.; Liu, Z.; Zhang, X.; Li, M., Structure and Assembly Mechanism of Plant C2S2M2-Type PSII-LHCII Supercomplex. *Science* **2017,** *357* (6353), 815-820.

6. Saito, K.; Shen, J. R.; Ishida, T.; Ishikita, H., Short Hydrogen Bond between Redox-Active Tyrosine Yz and D1-His190 in the Photosystem II Crystal Structure. *Biochemistry* **2011,** *50* (45), 9836-9844.

7. Lohmiller, T.; Krewald, V.; Navarro, M. P.; Retegan, M.; Rapatskiy, L.; Nowaczyk, M. M.; Boussac, A.; Neese, F.; Lubitz, W.; Pantazis, D. A.; Cox, N., Structure, ligands and substrate coordination of the oxygen-evolving complex of photosystem II in the S-2 state: a combined EPR and DFT study. *Phys. Chem. Chem. Phys.* **2014,** *16* (24), 11877-11892.

8. Ugur, I.; Rutherford, A. W.; Kaila, V. R., Redox-Coupled Substrate Water Reorganization in the Active Site of Photosystem II: The Role of Calcium in Substrate Water Delivery. *Biochim. Biophys. Acta* **2016,** *1857* (6), 740-8.

9. Guo, Z.; Barry, B. A., Calcium, Ammonia, Redox-Active Tyrosine YZ, and Proton-Coupled Electron Transfer in the Photosynthetic Oxygen-Evolving Complex. *J. Phys. Chem. B* **2017,** *121* (16), 3987-3996.

10. Kok, B.; Forbush, B.; Mcgloin, M., Cooperation of Charges in Photosynthetic O_2 Evolution: 1. A Linear 4-step Mechanism. *Photochem. Photobiol.* **1970,** *11* (6), 457-475.

11. Ioannidis, N.; Zahariou, G.; Petrouleas, V., The EPR Spectrum of Tyrosine Z* and Its Decay Kinetics in O_2-Evolving Photosystem II Preparations. *Biochemistry* **2008,** *47* (24), 6292-6300.

12. de Paula, J. C.; Innes, J. B.; Brudvig, G. W., Electron Transfer in Photosystem II at Cryogenic Temperatures. *Biochemistry* **1985,** *24* (27), 8114-20.

13. Keough, J. M.; Jenson, D. L.; Zuniga, A. N.; Barry, B. A., Proton Coupled Electron Transfer and Redox-Active Tyrosine Z in the Photosynthetic Oxygen-Evolving Complex. *J. Am. Chem. Soc.* **2011,** *133* (29), 11084-11087.

14. Keough, J. M.; Zuniga, A. N.; Jenson, D. L.; Barry, B. A., Redox Control and Hydrogen Bonding Networks: Proton-Coupled Electron Transfer Reactions and Tyrosine Z in the Photosynthetic Oxygen-Evolving Complex. *J. Phys. Chem. B* **2013,** *117* (5), 1296-1307.

15. Babcock, G. T.; Sauer, K., The Rapid Component of Electron Paramagnetic Resonance Signal II: A Candidate for the Physiological Donor to Photosystem II in Spinach Chloroplasts. *Biochim. Biophys. Acta* **1975,** *376*, 329-344.

16. Dekker, J. P.; Van Gorkom, H. J.; Brok, M.; Ouwehand, L., Optical Characterization of Photosystem II Electron Donors. *Biochim. Biophys. Acta* **1984,** *764*, 301-309.

17. Lydakis-Simantiris, N.; Betts, S. D.; Yocum, C. F., Leucine 245 is a Critical Residue for Folding and Function of the Manganese Stabilizing Protein of Photosystem II. *Biochemistry* **1999,** *38* (47), 15528-15535.

18. Haumann, M.; Mulkidjanian, A.; Junge, W., Tyrosine-Z in Oxygen-Evolving Photosystem II: A Hydrogen-Bonded Tyrosinate. *Biochemistry* **1999,** *38* (4), 1258-67.

19. Miqyass, M.; Marosvolgyi, M. A.; Nagel, Z.; Yocum, C. F.; van Gorkom, H. J., S-state Dependence of the Calcium Requirement and Binding Characteristics in the Oxygen-Evolving Complex of Photosystem II. *Biochemistry* **2008,** *47* (30), 7915-24.

20. Miqyass, M.; van Gorkom, H., Calcium Requirement for S-State Transitions. *Photosynth. Res.* **2007,** *91* (2-3), 175-175.

21. Siegbahn, P. E. M., Water Oxidation Energy Diagrams for Photosystem II for Different Protonation States, and the Effect of Removing Calcium. *Phys. Chem. Chem. Phys.* **2014,** *16* (24), 11893-11900.

22. Saito, K.; Ishikita, H., Influence of the Ca^{2+} Ion on the Mn_4Ca Conformation and the H-Bond Network Arrangement in Photosystem II. *Biochim. Biophys. Acta* **2014,** *1837* (1), 159-166.

23. Latimer, M. J.; DeRose, V. J.; Yachandra, V. K.; Sauer, K.; Klein, M. P., Structural Effects of Calcium Depletion on the Manganese Cluster of Photosystem II: Determination by X-Ray Absorption Spectroscopy. *J. Phys. Chem. B* **1998,** *102* (42), 8257-8265.

24. Lohmiller, T.; Cox, N.; Su, J. H.; Messinger, J.; Lubitz, W., The Basic Properties of the Electronic Structure of the Oxygen-evolving Complex of Photosystem II Are Not Perturbed by Ca^{2+} Removal. *J. Biol. Chem.* **2012,** *287* (29), 24721-24733.

25. Lohmiller, T.; Krewald, V.; Sedoud, A.; Rutherford, A. W.; Neese, F.; Lubitz, W.; Pantazis, D. A.; Cox, N., The First State in the Catalytic Cycle of the Water-Oxidizing Enzyme: Identification of a Water-Derived μ-Hydroxo Bridge. *J. Am. Chem. Soc.* **2017,** *139* (41), 14412-14424.

26. Yocum, C. F., The Calcium and Chloride Requirements of the O_2 Evolving Complex. *Coordin. Chem. Rev.* **2008,** *252* (3-4), 296-305.

27. Polander, B. C.; Barry, B. A., Calcium and the Hydrogen-Bonded Water Network in the Photosynthetic Oxygen-Evolving Complex. *J. Phys. Chem. Lett.* **2013,** *4* (5), 786-791.

28. Koua, F. H. M.; Umena, Y.; Kawakami, K.; Shen, J. R., Structure of Sr-substituted Photosystem II at 2.1 Angstrom Resolution and Its Implications in the Mechanism of Water Oxidation. *Proc. Natl. Acad. Sci. USA* **2013,** *110* (10), 3889-3894.

29. Pujols-Ayala, I.; Barry, B. A., Tyrosyl Radicals in Photosystem II. *Biochim. Biophys. Acta* **2004,** *1655* (1-3), 205-16.

30. Range, K.; Ayala, I.; York, D.; Barry, B. A., Normal Modes of Redox-Active Tyrosine: Conformation Dependence and Comparison to Experiment. *J. Phys. Chem. B* **2006,** *110* (22), 10970-81.

31. Berthold, D. A.; Babcock, G. T.; Yocum, C. F., A Highly Resolved, Oxygen-Evolving Photosystem-II Preparation from Spinach Thylakoid Membranes: EPR and Electron-Transport Properties. *Febs. Lett.* **1981,** *134* (2), 231-234.

32. Mishra, R. K.; Ghanotakis, D. F., Selective Extraction of CP 26 and CP 29 Proteins without Affecting the Binding of the Extrinsic Proteins (33, 23 and 17 kDa) and the DCMU Sensitivity of a Photosystem-II Core Complex. *Photosyn. Res.* **1994,** *42* (1), 37-42.

33. Barry, B. A., Tyrosyl Radicals in Photosystem II. *Methods Enzymol.* **1995,** *258*, 303-19.

34. Guo, Z.; Barry, B. A., Cryogenic Trapping and Isotope Editing Identify a Protonated Water Cluster as an Intermediate in the Photosynthetic Oxygen-Evolving Reaction. *J. Phys. Chem. B* **2016,** *120* (34), 8794-8808.

35. Yamamoto, Y.; Tamura, N.; Nishimura, M., Release of Polypeptides from Highly Active O_2 - Evolving Photosystem II Preparation by this Treatment. *Febs. Lett.* **1981,** *133* (2), 265-268.

36. Steenhuis, J. J.; Barry, B. A., A Difference Infrared Study of Protein Structural Changes in the Photosynthetic Water-Oxidizing Complex. *J. Am. Chem. Soc.* **1996,** *118* (47), 11927-11932.

37. Steenhuis, J. J.; Barry, B. A., Protein and Ligand Environments of the S_2 State in Photosynthetic Oxygen Evolution: a Difference FT-IR Study. *J. Phys. Chem. B* **1997,** *101* (33), 6652-6660.

38. Pagba, C. V.; Barry, B. A., Redox-Induced Conformational Switching in Photosystem-II-Inspired Biomimetic Peptides: A UV Resonance Raman Study. *J. Phys. Chem. B* **2012,** *116* (35), 10590-10599.

39. Razeghifard, M. R.; Kim, S.; Patzlaff, J. S.; Hutchison, R. S.; Krick, T.; Ayala, I.; Steenhuis, J. J.; Boesch, S. E.; Wheeler, R. A.; Barry, B. A., In Vivo, in Vitro, and Calculated Vibrational Spectra of Plastoquinone and the Plastosemiquinone Anion Radical. *J. Phys. Chem. B* **1999,** *103* (44), 9790-9800.

40. Kim, S.; Patzlaff, J. S.; Krick, T.; Ayala, I.; Sachs, R. K.; Barry, B. A., Isotope-Based Discrimination between the Infrared Modes of Plastosemiquinone Anion Radicals and Neutral Tyrosyl Radicals in Photosystem II. *J. Phys. Chem. B* **2000,** *104* (41), 9720-9727.

41. Ghanotakis, D. F.; Babcock, G. T., Hydroxylamine as an Inhibitor between Z and P680 in Photosystem-II. *Febs Lett.* **1983,** *153* (1), 231-234.

42. Takeuchi, H.; Watanabe, N.; Satoh, Y.; Harada, I., Effects of Hydrogen-Bonding on the Tyrosine Raman Bands in the 1300-1150 cm-1 Region. *J. Raman Spectrosc.* **1989,** *20* (4), 233-237.

43. Ayala, I.; Range, K.; York, D.; Barry, B. A., Spectroscopic Properties of Tyrosyl Radicals in Dipeptides. *J. Am. Chem. Soc.* **2002,** *124* (19), 5496-5505.

44. Offenbacher, A. R.; Burns, L. A.; Sherrill, C. D.; Barry, B. A., Redox-Linked Conformational Control of Proton-Coupled Electron Transfer: Y122 in the Ribonucleotide Reductase beta 2 Subunit. *J. Phys. Chem. B* **2013,** *117* (28), 8457-8468.

45. Harriman, A., Further Comments on the Redox Potentials of Tryptophan and Tyrosine. *J. Phys. Chem. B* **1987,** *91* (24), 6102-6104.

46. Krishtalik, L. I., Energetics of Multielectron Reactions - Photosynthetic Oxygen Evolution. *Biochim. Biophys. Acta* **1986,** *849* (1), 162-171.

47. Hogbom, M.; Galander, M.; Andersson, M.; Kolberg, M.; Hofbauer, W.; Lassmann, G.; Nordlund, P.; Lendzian, F., Displacement of the Tyrosyl Radical Cofactor in Ribonucleotide Reductase Obtained by Single-Crystal High-Field EPR and 1.4-Angstrom X-Ray Data. *Proc. Natl. Acad. Sci. USA* **2003,** *100* (6), 3209-3214.

48. Offenbacher, A. R.; Minnihan, E. C.; Stubbe, J.; Barry, B. A., Redox-Linked Changes to the Hydrogen-Bonding Network of Ribonucleotide Reductase beta 2. *J. Am. Chem. Soc.* **2013,** *135* (17), 6380-6383.

49. Kasanmascheff, M.; Lee, W.; Nick, T. U.; Stubbe, J.; Bennati, M., Radical Transfer in E. Coli Ribonucleotide Reductase: A Nh2y731/R(411)A-Alpha Mutant Unmasks a New Conformation of the Pathway Residue 731. *Chem. Sci.* **2016,** *7* (3), 2170-2178.

50. Hwang, H.; McCaslin, T. G.; Hazel, A.; Pagba, C. V.; Nevin, C. M.; Paylova, A.; Barry, B. A.; Gumbart, J. C., Redox-Driven Conformational Dynamics in a Photosystem-II-Inspired beta-Hairpin Maquette Determined through Spectroscopy and Simulation. *J Phys. Chem. B* **2017,** *121* (15), 3536-3545.

51. Macdonald, G. M.; Bixby, K. A.; Barry, B. A., A Difference Fourier-Transform Infrared Study of 2 Redox-Active Tyrosine Residues in Photosystem-II. *P. Nat.l Acad. Sci. U.S.A.* **1993,** *90* (23), 11024-11028.

52. Kim, S. Y.; Ayala, I.; Steenhuis, J. J.; Gonzalez, E. T.; Barry, B. A., Infrared Spectroscopic Identification of the C-O Stretching Vibration Associated with the Tyrosyl Z Center Dot and D Center Dot Radicals in Photosystem II. *Biochim. Biophys. Acta* **1998,** *1364* (3), 337-360.

53. Ayala, I.; Kim, S.; Steenhuis, J. J.; Razeghifard, M. R.; Barry, B. A., A Kinetic Study of the Vibrational Spectrum Associated with the Reduction of Tyrosyl Radical Z Center Dot in Photosystem II. *Biophys. J.* **1999,** *76* (1), A248-A248.

54. Pujols-Ayala, I.; Sacksteder, C. A.; Barry, B. A., Redox-active tyrosine residues: Role for the peptide bond in electron transfer. *Journal of the American Chemical Society* **2003,** *125* (25), 7536-7538.

55. Barry, B. A.; Cooper, I. B.; De Riso, A.; Brewer, S. H.; Vu, D. M.; Dyer, R. B., Time-Resolved Vibrational Spectroscopy Detects Protein-Based Intermediates in the Photosynthetic Oxygen-Evolving Cycle. *Proc. Natl. Acad. Sci. U.S.A.* **2006,** *103* (19), 7288-91.

56. Spanget-Larsen, J.; Gil, M.; Gorski, A.; Blake, D. M.; Waluk, J.; Radziszewski, J. G., Vibrations of the phenoxyl radical. *Journal of the American Chemical Society* **2001,** *123* (45), 11253-11261.

57. Barry, B. A.; Chen, J.; Keough, J.; Jenson, D.; Offenbacher, A.; Pagba, C., Proton-Coupled Electron Transfer and Redox-Active Tyrosines: Structure and Function of the Tyrosyl Radicals in Ribonucleotide Reductase and Photosystem II. *J. Phys. Chem. Lett.* **2012,** *3* (4), 543-554.

58. Pagba, C. V.; McCaslin, T. G.; Veglia, G.; Porcelli, F.; Yohannan, J.; Guo, Z.; McDaniel, M.; Barry, B. A., A Tyrosine-Tryptophan Dyad and Radical-Based Charge Transfer in a Ribonucleotide Reductase-Inspired Maquette. *Nat. Commun.* **2015,** *6*, 10010.

59. Vassiliev, I. R.; Offenbacher, A. R.; Barry, B. A., Redox-Active Tyrosine Residues in Pentapeptides. *J. Phys. Chem. B* **2005,** *109* (48), 23077-23085.

CHAPTER 5. SUMMARY

5.1 Summary and Future Directions

To summarize the work presented in this thesis, I have investigated the structure and function of the internal hydrogen-bonding network in PSII in three different ways. In the first (Chapter 2), I used an infrared signal from a protonated water cluster in the S_2 state of the OEC.[1] When trapped at 190 K, solvent isotope exchange confirmed the spectral assignment to the internal water network. This signal then became a novel and effective probe of the effects of hydrogen bond disruption, calcium depletion and replacement, and pH change on the network. In the second (Chapter 3), I used EPR spectroscopy at 190 K to investigate the effects of these treatments on the EPR signal and decay rate of YZ radical.[2] The radical was trapped in the S_2 state and decayed by coupled proton and electron transfer through recombination with Q_A^-. A correlation was discovered between the intensity of the protonated water cluster and conditions that altered YZ radical decay rates. In the third (Chapter 4), I used reaction induced FT-IR spectroscopy to obtain structural information concerning YZ radical and YZ singlet in the S_2 state. Calcium depletion and replacement was employed. This third approach provides a new high-resolution method to define the structure of the radical and singlet state in the presence of an intact metal cluster. These three findings and future suggested directions are discussed below.

In Chapter 2, I utilized cryogenic spectroscopic methods to investigate the internal water clusters and hydrogen-bonding networks during photosynthetic oxygen evolution. At 190 K, the S_1 to S_2 state transition is blocked.[3] Using cryogenic reaction-induced FT-IR spectroscopy combined with isotope editing, we assigned a broad IR band centered at

2900/2740 cm^{-1} to an internal water cluster acting as a proton actor during S_1-to-S_2 transition. The center of this broad IR band was ionic strength sensitive. Using this band as a probe for the internal environment, we found that the signal amplitude is calcium dependent at pH 7.5, but not at pH 6.0. Strontium was able to support the signal at pH 6.0, but not pH 7.5. We attributed those results to a change in position of the internal water cluster. At pH 7.5, it was proposed to be closer to the calcium site; but at pH 6.0, it was proposed to move further down the proton exit pathway toward the lumen.

A future direction for this project is to reconcile these results with predictions from DFT calculations, which predict that the protonated water cluster will be sensitive to anion replacements at the PSII chloride site.[4] Similar experiments should be performed at two different pH values, i.e. pH 6.0 and pH 7.5, at 190 K on chloride-depleted and anion-substituted PSII preparations. Chloride can be replaced by bromide and nitrate, which maintain activity.[5] The effect on the protonated water cluster signal at low temperature is of interest and can be compared to studies at 283 K, which were performed only at pH 7.5. At 190 K, changes in pH can be used to investigate the effect of protonation of amino acid side chains on the trapped signal in the OEC network.

To explain the effect of pH, we proposed that at two different pH values, the position of the cluster differs. It may be possible to use site-directed mutagenesis to define a position of the water cluster. First, it is important to confirm that the signal is observed in cyanobacterial PSII. An additional challenge is that many site-directed mutations in PSII are inactive or fail to assemble a metal cluster. However, one proposed target residues might be His337 in D1 subunit. This is based on previous observations in which both H337R and H337F mutants were able to evolve oxygen about 51% and 37% of the wild-

type, respectively. The apparent PSII content of H337F mutant is about the same as the wild-type and H337R mutant is 84% of the wild-type.[6] Changing the His337 side-chain will change hydrogen-bonding properties in the network. When coupled with theoretical calculations, this approach will help to define the location of the protonated water cluster signal.

Other important experiments are to evaluate the effects of pH, ionic strength, and cryoprotectant on the frequency and amplitude of the trapped band in spinach PSII in more detail. For example, the ionic strength and pH dependence can be measured with more points. Note that in the current literature, the proton release to lumen side pattern during each S state transition is not clearly defined for all the conditions. Different sample preparation methods have been reported to yield different proton release patterns.[7] Even when the samples are prepared in the same way, different pH conditions have been reported to promote different proton release patterns, for example, PSII-enriched membranes of spinach has been reported to have a 1.0:0.5:1.0:1.5 pattern at pH 7.5, but a 1.7:0:1.0:1.3 pattern at pH 5.5.[8] It would be beneficial to conduct measurements of proton release patterns for these conditions and samples: spinach vs. cyanobacteria; different cryoprotectant, sucrose vs. trehalose vs. glycerol; different pHs, 6.0 vs. 7.5; different cations, Ca^{2+} vs. Sr^{2+}; different anions, Cl^- vs. Br^- vs. NO_3^-; different ionic strengths at room temperature. The proton release pattern during the S_1-to-S_2 transition should be evaluated at cryogenic temperature too. Multiple approaches could be taken to perform this study: 1) absorption changes using either a hydrophilic pH-indicating dyes[9] or amphiphilic dye[10]; 2) unique IR bands from protonate and deprotonated MES band combined with an isotopic editing method[11].

In Chapter 3, I used EPR spectroscopy to study the YZ radical. At 190 K, P_{680} oxidizes YZ to generate tyrosyl radical, but YZ radical cannot oxidize the OEC.[12] Using EPR methods to monitor the decay of the radical, we found that ammonia increases the half-life of YZ radical in all conditions except in Ba-PSII. This is attributed to a role for the hydrogen-bonding network in proton transfer to YZ radical. In addition, the YZ radical half-life was found to be calcium dependent at pH 7.5, but not at pH 6.0. To explain this result, we proposed that there are two competing proton donors, His190 in D1 subunit and calcium-bound water (Figure 5.1), participating in the YZ radical decay process. At pH 6.0, His190-D1 is the dominating proton donor. And at pH 7.5, the calcium-bound water acts as a dominating proton donor. The interesting ammonia-insensitivity noted in Ba-PSII suggests that barium disrupts the hydrogen-bonding network around the OEC. Tyrosine plays an important role in PCET reaction of many enzymatic systems, such as photosystem II,[13] cytochrome c oxidase,[14] ribonucleotide reductase,[15] galactose oxidase,[16] and others. The redox potential of tyrosine is sensitive to its local pH and its hydrogen-bonding partners.[17] Obtaining more information concerning the competing proton donor at different pH values will offer a general way to fine-tune the redox potential of the tyrosine radical during reactions.

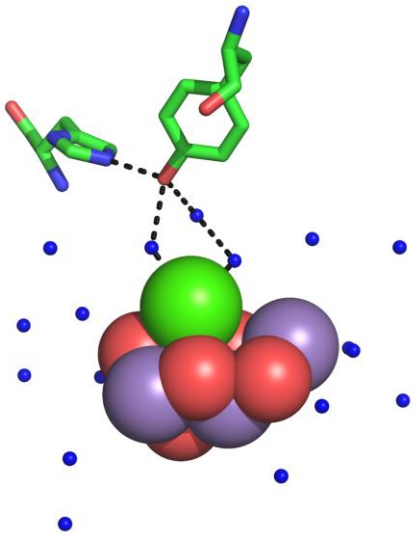

Figure 5.1 YZ (Y161 in D1 subunit) and its local hydrogen-bonding network from high resolution crystal structure. Calcium is shown in green spheres, oxygen in red, manganese in purple and water in blue. PDB ID: 4UB6.[18]

An important future direction for this project is to focus on the hypothesis that there may be a chloride effect on the tyrosyl radical decay. It has been proposed that Cl^- is essential for maintaining the hydrogen bonding network in photosystem II.[4, 19-21] The anion effect on the tyrosyl radical decay in photosystem II is an open question. We could incorporate activating anions such as Br^-, NO_3^- into PSII sample and test the impact on the tyrosyl radical decay. The effects of pH will help to test the localization model proposed above to explain the effects of calcium depletion.

In Chapter 4, I applied cryogenic reaction-induced FT-IR spectroscopy to gain more information about the radical decay process. This work relies on the measurement of the YZ radical decay time in the previous chapter. Using reaction-induced FT-IR spectroscopy, we identified a band position for the C-O stretching mode of the tyrosyl radical and the υ7a stretching mode of singlet in one hydrogen-bonding state. We found that at pH 6.0, the C-O stretching band of the tyrosyl radical state is at 1512 cm^{-1} in Ba-PSII. And another band

centered around 1260 cm^{-1}, which is assignable to the υ7a stretching band of the tyrosine singlet state, is also observed. The frequencies of these bands were sensitive to divalent cation substitution. The finding that the vibrational spectra of YZ radical and YZ singlet are sensitive to calcium substitution in the S_2 state is important, because no structural study to date has addressed the S_2 state or the radical state. By analyzing the peptide backbone C=O stretching region, we proposed that we have trapped different conformers of the tyrosine radical and singlet state. From analysis of the data, we proposed that calcium restricts backbone dynamics more than other divalent ions.

As a future direction, the project could construct a theoretical model predicting the frequency of different vibrational modes and their conformational dependence. DFT calculations on small models of the OEC will help to assign the vibrational bands to a specific conformer.[22] By comparing the theoretical predictions to the spectra, we will be able to gather valuable information about the backbone conformer change induced by different divalent ions. Second, in order to confirm the assignment of tyrosine and tyrosyl radical bands to specific vibration modes, it would be advantageous to incorporate isotope-labeled amino acids into PSII to shift bands away from their original position. The proposed amino acids we could use are L-tyrosine-(phenyl-d_4), L-tyrosine-(phenyl-3,5-d_2), L-tyrosine-1-^{13}C and other tyrosine derivatives. Third, since there is pH and calcium dependence of tyrosyl radical decay rate, the sensitivity of the spectrum to divalent ion exchange or calcium depletion as a function of pH can be defined. Even though we already have results at pH 7.5, more data in between pH 6.0 and 7.5 would give us a detailed view of how pH and calcium act together to affect the backbone conformational dynamics. Any chloride effect on the tyrosyl radical decay should also be defined. Finally, histidine could

be labeled with stable isotopes.[23] This will shift the bands of the histidine proton donor, which may be contributing to the spectrum at pH 6.0.

PSII stands as a model of sustainable energy conversion, using only light and water and producing reducing equivalents in the form of quinols. The study of the biological water oxidizing mechanism will help to open new avenues in artificial solar conversion. New strategies will address the global need for novel, sustainable energy sources.

5.2 References

1. Guo, Z.; Barry, B. A., Cryogenic Trapping and Isotope Editing Identify a Protonated Water Cluster as an Intermediate in the Photosynthetic Oxygen-Evolving Reaction. *J. Phys. Chem. B* **2016,** *120* (34), 8794-8808.

2. Guo, Z.; Barry, B. A., Calcium, Ammonia, Redox-Active Tyrosine YZ, and Proton-Coupled Electron Transfer in the Photosynthetic Oxygen-Evolving Complex. *J. Phys. Chem. B* **2017,** *121* (16), 3987-3996.

3. Styring, S.; Rutherford, A. W., Deactivation Kinetics and Temperature Dependence of the S-State Transitions in the Oxygen-Evolving System of Photosystem II Measured by EPR Spectroscopy. *Biochim. Biophys. Acta* **1988,** *933* (2), 378-387.

4. Brahmachari, U.; Gonthier, J. F.; Sherrill, C. D.; Barry, B. A., Chloride Maintains a Protonated Internal Water Network in the Photosynthetic Oxygen Evolving Complex. *J. Phys. Chem. B* **2017,** *121* (45), 10327-10337.

5. Wincencjusz, H.; Yocum, C. F.; van Gorkom, H. J., Activating Anions that Replace Cl^- in the O_2-Evolving Complex of Photosystem II Slow the Kinetics of the Terminal Step in Water Oxidation and Destabilize the S2 and S3 States. *Biochemistry* **1999,** *38* (12), 3719-3725.

6. Chu, H. A.; Nguyen, A. P.; Debus, R. J., Amino-Acid-Residues That Influence the Binding of Manganese or Calcium to Photosystem II: 2. The Carboxy-Terminal Domain of the D1 Polypeptide. *Biochemistry* **1995,** *34* (17), 5859-5882.

7. Lavergne, J.; Junge, W., Proton Release during the Redox Cycle of the Water Oxidase. *Photosynth. Res.* **1993,** *38* (3), 279-96.

8. Rappaport, F.; Lavergne, J., Proton Release during Successive Oxidation Steps of the Photosynthetic Water Oxidation Process: Stoichiometries and pH Dependence. *Biochemistry* **1991,** *30* (41), 10004-12.

9. Saphon, S.; Crofts, A. R., Protolytic Reactions in Photosystem-II - New Model for Release of Protons Accompanying Photooxidation of Water. *Z. Naturforsch C.* **1977,** *32* (7-8), 617-626.

10. Auslander, W.; Junge, W., Neutral Red, a Rapid Indicator for pH-Changes in Inner Phase of Thylakoids. *Febs Lett.* **1975,** *59* (2), 310-315.

11. Suzuki, H.; Sugiura, M.; Noguchi, T., Monitoring Proton Release during Photosynthetic Water Oxidation in Photosystem II by Means of Isotope-Edited Infrared Spectroscopy. *J. Am. Chem. Soc.* **2009,** *131* (22), 7849-7857.

12. Ioannidis, N.; Zahariou, G.; Petrouleas, V., The EPR Spectrum of Tyrosine Z* and Its Decay Kinetics in O_2-Evolving Photosystem II Preparations. *Biochemistry* **2008,** *47* (24), 6292-6300.

13. Barry, B. A.; Brahmachari, U.; Guo, Z., Tracking Reactive Water and Hydrogen-Bonding Networks in Photosynthetic Oxygen Evolution. *Acc. Chem. Res.* **2017,** *50* (8), 1937-1945.

14. Kaila, V. R. I.; Verkhovsky, M. I.; Wikstrom, M., Proton-Coupled Electron Transfer in Cytochrome Oxidase. *Chem. Rev.* **2010,** *110* (12), 7062-7081.

15. Minnihan, E. C.; Nocera, D. G.; Stubbe, J., Reversible, Long-Range Radical Transfer in E-coli Class la Ribonucleotide Reductase. *Acc. Chem. Res.* **2013,** *46* (11), 2524-2535.

16. Whittaker, J. W., Free Radical Catalysis by Galactose Oxidase. *Chem. Rev.* **2003,** *103* (6), 2347-2363.

17. Harriman, A., Further Comments on the Redox Potentials of Tryptophan and Tyrosine. *J. Phys. Chem. B* **1987,** *91* (24), 6102-6104.

18. Suga, M.; Akita, F.; Hirata, K.; Ueno, G.; Murakami, H.; Nakajima, Y.; Shimizu, T.; Yamashita, K.; Yamamoto, M.; Ago, H.; Shen, J. R., Native Structure of Photosystem II at 1.95 A Resolution Viewed by Femtosecond X-Ray Pulses. *Nature* **2015,** *517* (7532), 99-103.

19. Lindberg, K.; Vanngard, T.; Andreasson, L. E., Studies of the Slowly Exchanging Chloride in Photosystem-II of Higher-Plants. *Photosynth. Res.* **1993,** *38* (3), 401-408.

20. Cooper, I. B.; Barry, B. A., Azide as a Probe of Proton Transfer Reactions in Photosynthetic Oxygen Evolution. *Biophys. J.* **2008,** *95* (12), 5843-50.

21. Amin, M.; Pokhrel, R.; Brudvig, G. W.; Badawi, A.; Obayya, S. S. A., Effect of Chloride Depletion on the Magnetic Properties and the Redox Leveling of the Oxygen-Evolving Complex in Photosystem II. *J. Phys. Chem. B* **2016,** *120* (18), 4243-4248.

22. Offenbacher, A. R.; Burns, L. A.; Sherrill, C. D.; Barry, B. A., Redox-Linked Conformational Control of Proton-Coupled Electron Transfer: Y122 in the Ribonucleotide Reductase beta 2 Subunit. *J. Phys. Chem. B* **2013,** *117* (28), 8457-8468.

23. Campbell, K. A.; Peloquin, J. M.; Diner, B. A.; Tang, X. S.; Chisholm, D. A.; Britt, R. D., The tau-Nitrogen of D2 Histidine 189 is the Hydrogen Bond Donor to the Tyrosine Radical YD of Photosystem II. *J. Am. Chem. Soc.* **1997,** *119* (20), 4787-4788.